2013

C-Bouton Coverage of Alpha-motoneurons Following Peripheral Nerve Injury

Esra Salah Shermadou
Wright State University

C-Bouton Coverage of Alpha-motoneurons Following Peripheral Nerve Injury

A thesis submitted in partial fulfillment of the requirements for the degree of Master of Science

By

Esra Salah Shermadou
B.S., Wright State University, 2011

2013
Wright State University

WRIGHT STATE UNIVERSITY

GRADUATE SCHOOL

June 18, 2013

I HEREBY RECOMMEND THAT THE THESIS PREPARED UNDER MY SUPERVISION BY Esra Shermadou ENTITLED C-Bouton coverage on Alpha-Motoneurons Following Peripheral Nerve Injury BE ACCEPTED IN PARTIAL FULFILLMENT OF THE REQUIREMENTS FOR THE DEGREE OF Master of Science

Robert E.W. Fyffe, Ph.D.
Thesis Director

Timothy C. Cope, Ph.D.
Department Chair

Committee on
Final Examination

Robert E.W. Fyffe, Ph.D.

Adrian M. Corbett, Ph.D.

Larry J. Ream, Ph.D.

R. William Ayres, Ph.D.
Interim Dean, Graduate School

ABSTRACT

Shermadou, Esra M.S., Department of Neuroscience, Cell Biology, and Physiology, Wright State University, 2013. C-Bouton Coverage of α-motoneurons Following Peripheral Nerve Injury

Peripheral nerve injuries (PNI) cause alternations in central synapses leading to loss of function. The C-bouton synapses onto α-motoneurons in the ventral horn, and has a role in regulating motor output. Following tibial nerve ligation, the somatic C-bouton coverage is depleted (Alvarez et al., 2011), however, it is unknown what happens following crush type injuries. PNI causes neuroglia activation and proliferation that contribute to synaptic alterations, a response that has not been well-characterized in the ventral horn, where motoneurons are located. **Therefore, I hypothesize that glia activation following peripheral nerve injury correlates to the degree of depletion of synaptic coverage of C-boutons.** To test, I performed Immunohistochemical analysis of rat spinal cord to characterize C-bouton coverage, and activation of glia following two types of PNI. Our results indicate less C-bouton depletion following tibial nerve crush than ligation injuries. In addition, we found less glia activation following crush than ligation injuries.

Table of Contents

List of Figures

Acknowledgments

I would like to first express my gratitude to Dr. Robert Fyffe for granting me the wonderful opportunity of working in his lab. I have truly enjoyed this experience and have gained much more than I anticipated.

I would, also, like to thank Jackie Sisco for coming to the rescue with all of my computer, microscope and software complications. This project surely could not have been completed with you! Thank you, also, for being a constant source of positive energy! It always brightened my day, especially after spending all day in the dark analysis room!

Adam Deardorff and Shannon Romer—thank you for everything! Thank you for all of your help, support and guidance throughout this entire year. I truly could not have asked for better lab members!

Shannon, I want to especially thank you for developing this project into what it has become! Your pursuit to learn more is aspiring. I have learned so much from you, in the scope of research and beyond. I cannot express how much I appreciate all of your help and support this year. Thank you!

Finally, I would like to thank Lori Goss for doing the injury surgeries for all of our rats. Also, to everyone on the second floor of Biological Sciences II, thank you for creating an exciting and motivating work environment. I have really enjoyed getting to know everyone throughout this past year!

I. Introduction

Peripheral nerve injuries affect thousands of Americans every year. Peripheral nerves consist of sensory, motor and sympathetic components, so nerve damage in the periphery affects all three neural components. Unlike nerve injuries in the central nervous system, injuries in the periphery are better able to undergo regeneration and reinnervation of the peripheral targets. Differences exist between the environments in the CNS and the PNS that limit regeneration in the CNS. Overall, the peripheral nervous system contains a larger number of growth factors and fewer inhibiting factors, all of which favor a regenerative environment. While the success of regeneration and reinnervation is critical to functional recovery, complete functional recovery seldom occurs (Cope et al., 1994; Haftel et al., 2005; Alvarez et al., 2011). The scope of this project is to determine if a relationship exists between the stripping of synapses from lumbar motoneurons, specifically looking at the cholinergic C-bouton, and the glial response observed following peripheral nerve injury. While the response of glia after peripheral nerve injury has been well-characterized in the dorsal horn of the spinal cord, little has been reported about glia in the ventral horn. This project hopes to better characterize the response of glia in the ventral horn of the spinal cord following tibial nerve crush and ligation. The effect of peripheral nerve injury on C-boutons is also

studied after tibial n. crush and ligation. Finally, this project observes the effect on C-boutons if the glial response is inhibited after peripheral nerve injury.

II. Background

A. Spinal Cord

The spinal cord is one of the two structures comprising the central nervous system. It is located within the vertebral column, protected by three meningeal layers: the innermost pia mater, intermediate arachnoid mater, and outermost dura mater. Cerebrospinal fluid in the subarachnoid space also provides protection and nutrients to the spinal cord. The spinal cord receives sensory information from the limbs and viscera, relays that information to the brain, and carries out the brain's intended actions via motor neurons.

The spinal cord is divided into grey and white matter. The white matter is located externally, forming the outer layer on a transverse section of the spinal cord. It surrounds the grey matter and consists of ascending and descending tracts traveling up and down the spinal cord, respectively. Axons carrying similar information form organized tracts and funiculi.

The grey matter of the spinal cord mostly consists of the cell bodies of neurons of many different functions. Cell bodies of axons with similar functions are often organized together, forming various nuclei. The grey matter is divided structurally into dorsal and ventral horns. Sensory information from the body enters the spinal cord via sensory

neurons through the dorsal horn, while responses are carried out through motor neurons that leave the spinal cord through the ventral horn.

The grey matter in the rat spinal cord is further organized into ten laminae, based on its cytoarchitecture along the length of the spinal cord, as defined by Rexed's laminae. Lamina I-VI make up the posterior aspect of the spinal horn, with laminae V and VI making up the largest components of the dorsal horn. The dorsal horn is responsible for receiving all types of sensory information, including proprioceptive, nociceptive, and somatosensory afferent fibers.

Lamina IX (Figure 1) is located in the ventral horn and contains large cell bodies of motoneurons, most notably those of α-motoneurons. Small cell bodies of gamma motoneurons that innervate muscle spindles also originate in lamina IX, though these are found in smaller concentrations. This study focused on the affects of injury to the medial and lateral gastrocnemius (MG/LG) muscles in the rat. These muscles are innervated by motoneurons originating in lamina IX of the ventral horn.

B. Motoneurons

Alpha motoneurons are large, multipolar neurons with cell bodies originating in lamina IX. Gamma motoneurons, which are smaller than α-motoneurons, are found in fewer concentrations in lamina IX. Most neurons consist of four main parts: cell body (soma), dendrites, an axon and a presynaptic terminal. The cell body, or soma, contains the nucleus and functions as the integrative body of the cell. The soma gives rise to the multiple dendrites and a single axon that characterize motoneurons. Dendrites receive information from other neurons, via synapses, and relay this information to the cell body

for processing. The single axon of a motoneuron carries information away from the cell body and transmits it to other nerve cells, muscles or viscera by way of action potentials.

Although they play a minor role in the generation of action potentials, dendrites serve an important role in receiving synaptic contacts, making up 95% of the membrane surface area onto which synapses can occur. In contrast to the somatotopic organization of neuronal cell bodies within the grey matter, dendrites extend into the ventral horn and white matter of the spinal cord. The numerous excitatory and inhibitory synapses received by the dendrites provide currents that accumulate at the initial segment of the axon, where action potentials may be initiated.

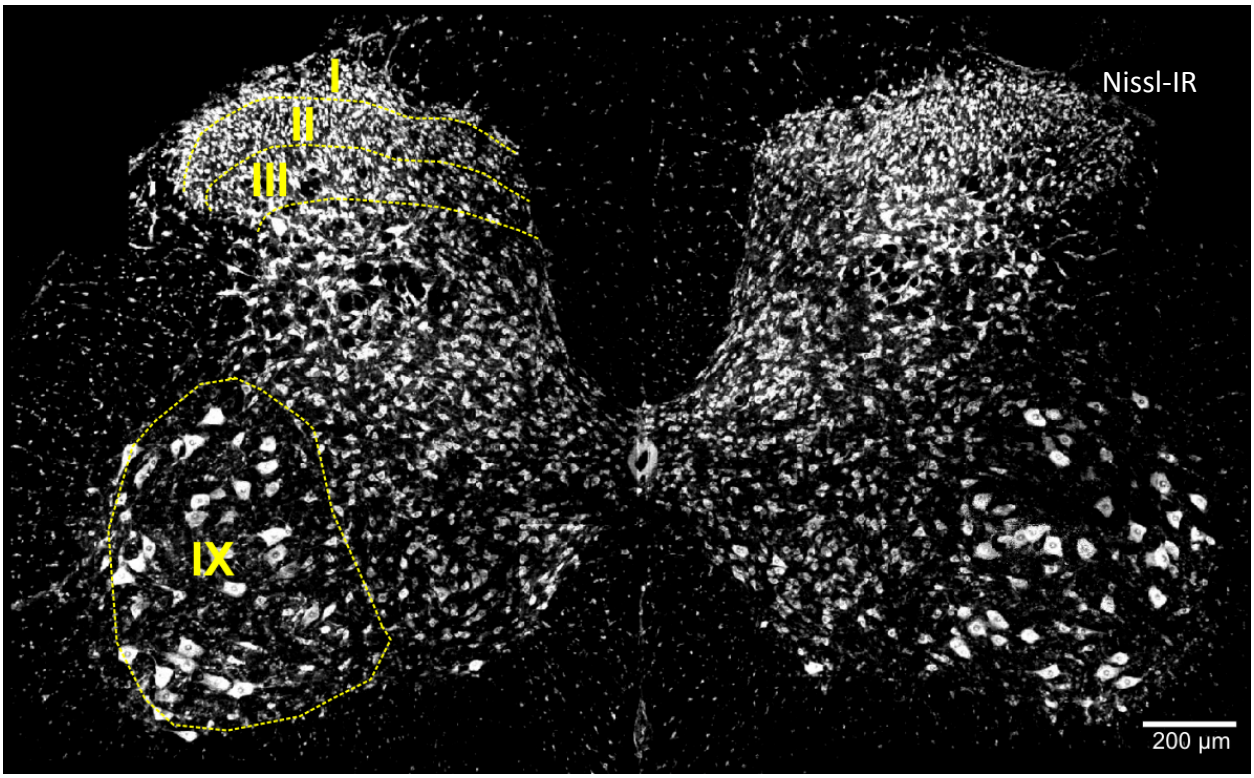
I
II
III
IX
Nissl-IR
200 µm

Figure 1. Laminar distribution of L5 lumbar spinal cord in the rat. Outlined sections represent the regions of interest in this study. Nissl (white) staining is used to label the neurons. Laminae I-III in the dorsal horn contain the synaptic terminals of neurons conveying proprioceptive and cutaneous information from the skin and muscles. Lamina IX in the ventral horn contains the large α-motoneurons that are the focus of this project. Notice the large size of the α-motoneurons, relative to the other neurons in the spinal cord. Montaged image taken at 10X magnification (10 optical sections, at 2 μm z-steps. Scale bar represents 200 μm).

C. Synapses

Synapses allow for interneuronal communication and for communication between neurons and the target tissue. Neurotransmitters located in the synaptic vesicles within the presynaptic terminal are released into the synaptic cleft where they bind to receptors on the post-synaptic membrane. Approximately 50,000 different synapses make contact with α- motoneurons. With only 1-2% of these occurring on the soma, the majority of the synapses occur on the dendrites. Proximal dendrites typically contain the same percent of synapses, or higher, as the soma. The percentage of synapses on the dendrites, however, decreases with distance away from the soma, such that proximal dendrites are covered by more synapses than distal dendrites (Rose & Neuber-Hess, 1991; Brannstrom, 1993). The soma of gamma motoneurons also receives synapses, though to a lower extent, with 20-40% somatic membrane coverage (Brannstrom, 1993).

Four main types of synapses are known to occur onto α-motoneurons. These synapses are distinguished based on the shape of the synaptic vesicles within the bouton, the size of the terminal, and the post-synaptic densities at the synaptic cleft. The percentage of these contacts onto motoneuron dendrites and soma differs among the different synapse types. These synapses have been named S-, F-, C-, and M- type boutons (Conradi *et al.*, 1979).

The small S-type boutons make up a class of boutons found to synapse onto α-motoneurons. These boutons make up 20-30% of the boutons on the soma of the α-motoneuron and can range from 0.5 to 3.0 μm in diameter. Unlike other synapses, which decrease in number with distance from the soma, S-type boutons increase from 30% on proximal dendrites to 60% on distal dendrites (Rose & Neuber-Hess, 1991; Brannstrom,

1993). S-type boutons form asymmetric junctions and are excitatory in nature, often expressing the neurotransmitter glutamate (Ornung *et al.*, 1998).

F-type boutons are the most numerous of the synapses contacting motoneurons, comprising 50-60% of the synapses on both the soma and proximal dendrites, but declining with distance from the soma. F-type boutons contain elongated or flattened synaptic vesicles and form symmetrical synapses (Conradi & Skoglund, 1969). F-type boutons arise from inhibitory interneurons and correspondingly, have been found to contain glycine-like immunoreactivity (Destombes *et al.*, 1992; Ornung *et al.*, 1996; Ornung *et al.*, 1998).

C-type boutons (Figure 2), or C-terminals, contain large spherical vesicles (Conradi & Skoglund, 1969) and are often characterized as a subtype of the large S-type bouton. C-boutons are identified by the presence of a unique post-synaptic subsurface cistern that is continuous with the rough endoplasmic reticulum, and is directly associated with the synapse (Hellstrom et al., 2003). C- boutons make up less than 10% of the total number of synapses on α-motoneuron. Due to their large size, however, C-boutons comprise 20% of the synaptic surface area on the soma of α-motoneurons. C-boutons are also found on proximal dendrites but are less associated with distal dendrites (Conradi, 1969; Nagy *et al.*, 1993; Li *et al.*, 1995). These terminals invaginate into the cell bodies of the motoneurons (Conradi & Skoglund, 1969). C-boutons release acetylcholine from their synaptic vesicles and oppose muscarinic type 2 (m2) acetylcholine receptors on the post-synaptic membrane (Welton *et al.,* 1999). Ultrastructural studies of gamma motoneurons in the cat revealed that these motoneurons do not contain C-boutons (Lagerback, 1983; Johnson, 1986; Lagerback *et al.*, 1986). C-boutons are believed to

activate m2 acetylcholine receptors and decrease excitability of motoneurons (Welton *et al.,* 1999).

Another classification of boutons, M-type boutons, resemble the large S-type bouton in their adjacent location to the smaller P-type boutons. The large spherical vesicles of the M-type (as well as the S-type) contain within their convex ends, the smaller vesicles of the P-bouton (Conradi & Skoglund, 1969). M-type boutons differ from S-type boutons in that they have a large, irregularly-shaped synaptic complex, covered by postsynaptic dense bodies (Conradi & Skoglund, 1969). These boutons appear mostly on proximal dendrites (Conradi & Skoglund, 1969). Unlike the other classes of boutons which are present at birth, the M-type bouton does not appear until the third postnatal week (Conradi & Skoglund, 1969).

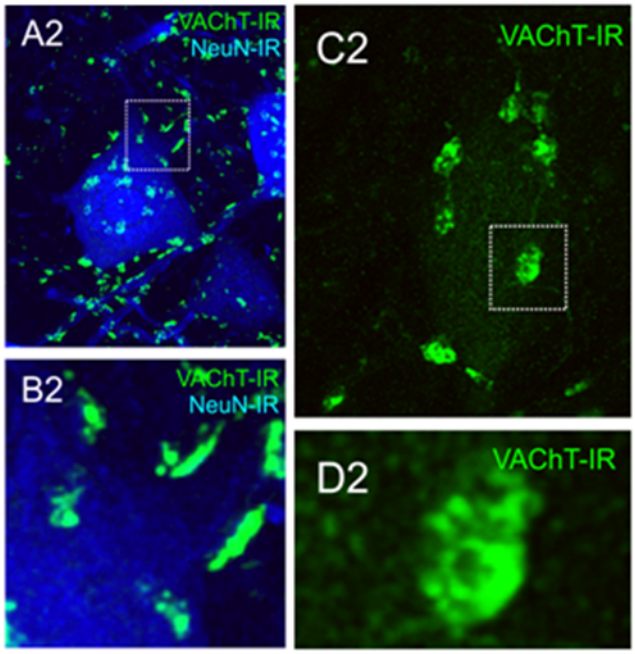
A2
VAChT-IR
NeuN-IR
C2
VAChT-IR
B2
VAChT-IR
NeuN-IR
D2
VAChT-IR

Figure 2. Expression of cholinergic C-bouton synapses on rat lumbar α-motoneurons. *A2*, represents a 60X image of α-motoneurons labeled with NeuN-IR (blue) and vesicular acetylcholine transporter (VAChT)-IR (green) (23 optical sections, 1 μm z-step). The outlined area in *A2* is shown at higher magnification in B2-*D2*, emphasizing the large size of the cholinergic C-boutons (VAChT-IR) (green). The location of C-boutons on the somatic membrane can be seen at higher magnification in *B2* (23 optical sections, 1 μm z-step). *C2*, large VACht-IR contacts along the soma of the α-motoneurons (23 optical sections, 1 μm z-step). *D2*, high magnification of VAChT-IR contact (3 optical sections; scale bar represents 2.5 μm). *Figure modified from Deardorff et al., 2013.*

D. C-boutons

Interneurons regulate certain aspects of motor behavior through modulating inhibitory and excitatory neural circuits (Miles *et al.*, 2007). Cholinergic interneurons are frequent methods of regulation in the central nervous system, and can lead to a diverse array of outcomes (Winkowski and Knudsen, 2008; Zagoraiou et al., 2009). One such cholinergic source is the C-bouton (Figure 2). The C-bouton is believed to function as a modulator of certain locomotive movements. It acts on α-motoneurons to reduce the peak of the after-hyperpolarization of the action potential, thereby increasing the firing rate and frequency of motoneurons in a state-dependent fashion (Zagoraiou *et al.*, 2009).

Alpha-motoneurons receive cholinergic input from two terminals. One cholinergic source comes from the small axon collaterals of motoneurons, which mostly make contact with the distal dendrites. The second cholinergic source onto motoneurons is larger and originates from C-boutons (Hellstrom *et al.*, 2003). This cholinergic source mostly inputs onto the soma and proximal dendrites of the motoneuron (Muennich and Fyffe, 2004; Wilson et al., 2004; Zagoraiou et al., 2009; Deardorff et al., 2013). Motoneurons innervating fast-twitch muscles, such as the medial gastrocnemius (MG) muscle are contacted by a significantly greater number of C-boutons than those innervating slow-twitch muscles, including the SOL muscle (Hellstrom *et al.*, 2003).

C-boutons contain large spherical vesicles and are often thought to be a subtype of the S-type bouton (Conradi & Skoglund, 1969). C- boutons make up less than 10% of the total number of synapses on α-motoneurons, but because of their large size, they comprise 20% of the synaptic surface area on the soma of α-motoneurons. C-boutons are

also found on proximal dendrites but are less associated with distal dendrites (Nagy *et al.*, 1993; Li *et al.*, 1995).

C-boutons are identified by the presence of a unique post-synaptic subsurface cistern (SSC) that is continuous with the rough endoplasmic reticulum of the post-synaptic cell, and is directly associated with the synapse (Bodian, 1966; Conradi, 1969). This feature is not common in the CNS (Nagy *et al.,* 1993). While the function of the SSC has yet to be determined, it is thought to play a role in calcium storage. The SSC has been identified in various cells of the central and peripheral nervous system, including the outer hair cells of the organ of Corti (Engstrom, 1958), sensory cells (Fisher and Goldman, 1975), the rat spinal cord and cerebral cortex (Rosenbluth, 1962), as well as many other cells. Muscarinic type 2 (m2) receptors were discovered on α-motoneurons, specifically in the membrane area directly associated with C-bouton terminals (Nagy *et al.,* 1993). Although the role of m2 receptors is not fully understood, they are known to be involved in the inhibition of voltage-gated calcium channels, in the activated state. Colocalized to m2 receptors is the sigma-1 receptor, a receptor found beneath the plasma membrane, in the area of the endoplasmic reticulum (Hayashi and Su, 2007; Mavlyutov and Ruoho, 2007). The sigma-1 receptor is believed to regulate various ion channels (Mavlyutov et al., 2010). The colocalization of these receptors supports the speculated function of the SSC in regulating movement by modulating various ion channels of α-motoneurons.

C-boutons are one of two cholinergic inputs onto motoneurons (Hellstrom et al., 2003), and they arise from spinal interneurons located in lamina X, lateral to the central canal. Specifically, C-boutons originate from a subset of cholinergic VO (VO_C)

interneurons that contain the Pitx2 transcription factor, and express VAChT (vesicular acetylcholine transporter) and CHAT (cholinergic acetyl transferase). Additionally, these spinal interneurons are positioned rostrally and coincide with the ventral projections of the C-bouton. (Miles et al., 2007; Zagoraiou et al., 2009). The C-bouton is thought to release acetylcholine onto motoneurons and bind to post-synaptic muscarinic type-2 receptors, resulting in a decrease in after-hyperpolarization (AHP) and increase in the firing frequency of action potentials (Miles *et al.,* 2007). While the exact mechanism by which this occurs is unknown, it is thought to occur by way of calcium-activated potassium channels (K_{Ca}), which have been found in clusters apposing C-boutons (Wilson et al., 2011; Deardorff et al., 2013). Confocal analysis of motoneurons shows colocalization between m2 receptors and C-bouton terminals on α-motoneurons (Hellstrom et al., 2003; Wilson et al., 2004). Antibodies to ChAT (Connaughton *et al.,* 1986; Ruggiero *et al.,* 1990; Nagy *et al.,* 1993; Li *et al.,* 1995), VAChT (Glimor *et al.,* 1996; Roghani et al., 1988) and VAMP-2 (Hellstrom *et al.,* 1999) have repeatedly been used to identify C-boutons as cholinergic.

As previously mentioned, m2 receptors inhibit the release of calcium from voltage-gated channels (Hellstrom et al., 2003). Experiments using the m2 recepetor agonist muscarine, as well as the m2 receptor blocker methoctramine, have shown that a decrease in potassium conductance due to a reduced influx of voltage-activated calcium via activation of C-boutons and m2 receptors leads to a reduction in the AHP (Miles *et al.,* 2007). SK channels, a class of calcium-dependant-postassium channels, are found to cluster post-synaptically to C-boutons (Deardorff et al., 2013). SK channels modulate mAHP and firing frequency, and have been found to colocalize with m2 receptors on

motoneurons, possibly suggesting an association between m2 receptors and SK channels in modulating the mAHP and firing frequency through the regulation of voltage-gated calcium channels.

III. Peripheral Nerve Injury

A. Introduction

Peripheral nerves are the nerves that extend from the brain (cranial nerves) and spinal cord (spinal nerves), and ganglia located throughout the body. Peripheral nerves relay information between the brain and spinal cord, and the rest of the body. In the spinal cord, the spinal nerves split into dorsal and ventral rami which give rise to the peripheral nerves that innervate the muscles and organs of the body. Although nerves can be classified functionally as either motor or sensory, they never consist of purely motor or sensory fibers. All nerves consist of sensory, motor and sympathetic fibers. Peripheral nerve injury brings about changes to the axonal components of the nerve bundle, the myelin surrounding the nerve and to nonneuronal cells in the environment, primarily the Schwann cells. Peripheral nerve injury also brings about major changes to the CNS, which will be discussed later. Damage to the Schwann cells or myelin surrounding the axon impairs nerve conduction, but can be easily repaired by remyelination by the Schwann cells. Injury to the axon itself, however, can be difficult to repair (Waller, 1850). Unlike nerves in the CNS, nerves in the PNS are capable of regrowth and muscle reinnervation; however, the process is slow and often fails to result in full functional recovery of the end organ (Evans, 2001). The role and timing of Schwann cells,

macrophages, cytokines, and other factors greatly influence the ability and capacity to which axons can be regenerated and reinnervate their targets.

Several degrees of nerve injury exist, and the extent of regeneration and repair can differ for each. As mentioned previously, this project will focus on two types of nerve injury: tibial nerve crush, in which the axon remains in tact, and tibial nerve ligation, where the peripheral axon is completely transected. Axonal regeneration following nerve crush is more likely to occur; nerve ligation, however, prevents nerve regeneration and reinnervation of the muscle. A critical factor that allows for regeneration is the motoneuron basal lamina, which contains many extracellular matrix proteins that play a significant role in guiding axons during regrowth. The basal lamina remains intact following a crush injury, but not after a ligation (Schlaepfer and Bunge, 1973; George et al., 1995).

The axonal repair process for both sensory and motor nerves in the periphery is very similar. Following nerve injury, the proximal segment of the axotomized peripheral nerve degenerates to the previous node of Ranvier, or further, and the cell body undergoes chromatolysis. During this, the rough endoplasmic reticulum fragments and the nucleus migrates to the periphery, and the entire soma hypertrophies. These alterations to the soma lead to changes in mRNA and gene expression of the proximal segment, transforming the function of the axotomized nerve from one of transportation of proteins to that of regrowth.

Physiological changes in the proximal segment also aid in axonal regrowth. Such changes include an upregulation of cytokines and other regeneration associated genes (RAGS) that stabilize growth cones in the proximal stump, guidance molecules and the

overall sprouting process. The concurrent downregulation of cytoskeletal proteins and other genes also aid in the regrowth of the axon. Further, corresponding neurotropic factors and receptors are upregulated in the proximal and distal stumps, allowing for communication between the growth cones in the proximal stump and the Schwann cells in the distal stump. The expression, for example, of neuregulin by both growth cones and Schwann cells upon contact with each other contributes to signaling for the proliferation of Schwann cells.

Additional axonal changes also occur at the distal segment with the upregulation of Schwann cells and macrophages, a process known as Wallerian Degeneration (WD) (Waller, 1850; Schlaepfer and Bunge, 1973; George et al., 1995). During this calcium-mediated process, the axon and its surrounding myelin beyond the injury point begin to degenerate, and an environment for nerve regrowth is established (Waller, 1850; Schlaepfer and Bunge, 1973; George et al., 1995)). Within two days, Schwann cells begin to remove some of the myelin debris surrounding the axon of injured neuron by fragmenting it into ovoids. Myelin debris contains proteins such as myelin-associated glycoprotein, which prevents axonal growth; therefore, removal of the debris is critical to axonal regeneration (Filbin, 1995, 1996; Tang et al., 1997). Schwann cells in the distal end release cytokines and other factors including the essential cytokine tumor necrosis factor-α (TNF-α**)**. These molecules attract macrophages, which play a critical role in establishing a growth-supportive environment. Macrophages appear between day two and week two, and remove the majority of axonal debris by phagocytosis, allowing axons to grow and lengthen (Stoll et al., 1989; Liu et al., 1995; Bruck, 1997).

Macrophages also function to induce the dedifferentiation of the Schwann cell phenotype from myelinating to nonmyelinating (Martini and Schachner, 1989; Johnson et al., 1990). In response to their loss of contact with axons, Schwann cells also undergo mitotic division, reaching a maximum cell count by day 3 post-axotomy (Stoll et al., 1989). The proliferation of Schwann cells allows them to continue to produce the molecules necessary for regeneration. Schwann cells arrange themselves to form tube-like Bunger bands within the basal lamina and express surface molecules to help guide the regenerating proximal segment towards its peripheral target in a process called sprouting (Fugleholm et al., 1994).

In addition, non-myelinating Schwann cells in the distal segment express cytokines and neurotropic factors to aid in guiding axonal fibers of the proximal segment towards the distal segment. Such factors include nerve growth factor (NGF), brain-derived neurotropic factor (BDNF), glial cell-derived neurotropic factor (GDNF), and the cytokines interleukin-6 and leukeumia inhibitory factor. Dennervated Schwann cells also express several receptors for neurotropic factors, including truncated trk receptors and the p75 neurotropic factor (Boyd & Gordon, 2003).

Time after injury plays a major factor in determining extent of regrowth and restoration. The upregulation of regenerative associated genes (RAGS) is essential to axonal outgrowth; however, this declines over time. Even after immediate nerve repair, the number of axotomized motoneurons that regenerate their axons declines by one-third. This is masked, however, by the ability of axotomized motoneurons to reinnervate up to five times the number of previously denervated muscle fibers. The increased capacity of

their reinnervation of the muscle fibers allows for full functional restoration and size recovery of the muscle, in a time-dependent manner (Fenrich & Gordon, 2004).

Schwann cells in the distal nerve stump undergo rapid changes after axotomy. With time post-axotomy, these cells atrophy and their growth supportive phenotype declines. Recent studies have shown that denervated Schwann cells can be reactivated over time by the inflammatory cytokine TGF-beta to support a regenerative environment. Many Schwann cells also die after injury; despite this, however, the remaining atrophic cells are able to remyelinate the growing axons (Fenrich & Gordon, 2004).

B. Motoneurons

i. Physiological Changes

As the proximal segment elongates, it eventually reaches and reinnervates its peripheral target. Peripheral nerves are mixed, containing sensory and motor fibers going to muscles, organs and to the skin. Often, full functional recovery after peripheral nerve injury is difficult to establish due to motor and sensory neurons reinnervating the wrong targets. Muscle weakness, abnormality in motor coordination and the absence of stretch reflexes result even after peripheral reinnervation. Sensory dysfunction also occurs following reinnervation, including hyperalgesia, loss of proprioception, and mechanoallodynia (Cope & Clark, 1993; Cope et al., 1994; Stoll and Muller, 1999; Haftel et al., 2005; Alvarez et al., 2011; Bullinger et al., 2011; Prather et al., 2011).

Peripheral reinnervation occurs with high specificity, especially for motoneurons (Fenrich & Gordon, 2004; Madison et al., 1996). A study using the rat femoral nerve showed that motoneurons preferentially reinnervate nerve branches going to muscle rather than to skin receptors, a phenomenon known as preferential motor reinnervation

(PMR). When motoneurons are presented with an opportunity to equally innervate the cutaneous or muscular branch of the femoral nerve, they initially send axon collaterals into each branch, but quickly dissociate from those branches going into the cutaneous branch (Madison et al., 1996).

Despite nerve regeneration, changes in the properties of motoneurons are still evident after muscle reinnervation. Furthermore, motoneurons supplying fast-twitch muscle fibers (F-type) require greater time for recovery than those innervating slow-twitch muscle fibers (S-Type) (Foehring, Sypert and Munson, 1986). Three to five weeks after axotomy of the motoneurons supplying the soleus and medial gastrocnemius muscles in the cat, no reinnervation was observed. Low and medium reinnveration were reported at 5-6 weeks and 9-10 weeks, respectively. Complete reinnervation was observed by 9 months following axotomy (Foehringet et al., 1986). Motoneurons supplying fast-twitch muscle fibers were affected more than those innervating slow-twitch muscle fibers and even undergo changes after axotomy to resemble S-type motor units (Gustafsson and Pinter, 1984; Foehring et al., 1986).

A decrease in fast-fatiguing motor units and increase in slow oxidative muscle fibers was observed with reinnervation. Muscle-unit tetanic tension and contractile properties also increased with time after reinnervation, as did motoneuron electrical properties (Foehring et al., 1986).

ii. Motoneuron Survival

Despite the growth supportive environment of the peripheral nervous system, axotomized motoneurons may still fail to regenerate, or may not regenerate to their initial capacity. Motoneuron survival is dependent on many factors, including distance from the

peripheral target, age and reinnervation. Motoneuron survival decreases with distance from the end organ or muscle. A proximal nerve injury, farther from the peripheral target, is more likely to cause motoneuron cell death versus a distal nerve injury that is closer to the peripheral target. Recovery after nerve injury depends on regeneration, as without muscle reinnervation, the motoneuron will not survive (Dai et al., 2000; Burnett and Zager, 2004)). A proximal injury indicates a longer time for the regenerating proximal axonal fibers to reinnervate the end organ, thereby resulting in motoneuron death. Proximal injuries also result in a greater loss of Schwann cells, and the supportive molecules they release, than distal injuries.

Time until reinnervation also affects motoneuron survival. Studies by Dai et al., on the facial motoneuron revealed the greatest loss in motoneurons in the facial motor nucleus (FMN) occurred at day 15 post-axotomy (31.56%), in comparison to day 3 (1.11%). The loss of motoneurons at days 30 and 60 decreased just slightly, with only a few motoneurons recovering from degeneration (Dai et al., 2000). The functional support of denervated Schwann cells decreases with time post-axotomy, so the neurotrophic factors and growth-supportive environment, critical for motoneuronal regrowth, cannot be maintained (Dai et al., 2000; Fenrich & Gordon, 2004). Age also affects the survival of motoneurons, as the survival rate of motoneurons in newborns is lower than that of motoneurons in adults (Y.M. Chan et al., 2002).

In addition to the release of cytokines and other molecules from macrophages and Schwann cells after nerve injury, motoneurons also produce tropic factors that aid in their regeneration. In the proximal segment, the cell body undergoes changes in gene expression, upregulating production of regeneration associated genes (RAGs), and

downregulating those involved in transmitting proteins and molecules in uninjured motoneurons. Important RAGs include tubulin, actin, growth associated proteins (GAP-43), cytoskeleton-associated proteins (CAP-23) (Strittmatter et al., 1994; Igarashi et al., 1995; Bomze et al., 2001).

As axonal regrowth is achieved and peripheral targets are reinnervated, many of the post-injury events are reversed. Schwann cells make contact with regrowing axons and the myelinating phenotype of Schwann cells is reacquired. Myelinating genes are re-expressed, while those involved in regrowth are downregulated. Chromatolysis in the proximal segment is also reversed, as the nucleus returns to the center, the rough endoplasmic reticulum reforms, and transmitting genes are re-expressed (Stoll and Muller, 1999).

Motoneuron regrowth in the cat occurs at a rate of 3-4 mm/day after nerve crush and 2-3 mm/day following ligation (Fugleholm & Schmalbruch, 1994). The slower regeneration rate following ligation is a consequence of the complete separation of the basal lamina. This inhibits the formation of bands of Bunger, tubes formed from proliferating dennervated Schwann cells that become enclosed within the basal lamina of the endoneurium. The bands of Bunger are essential in guiding axonal sprouts from the proximal segment towards the distal segment and to their preferred peripheral targets (Fugleholm & Schmalbruch, 1994).

C. Synaptic Stripping

The removal of synapses from the soma and dendrites of motoneurons is a phenomenom that occurs after peripheral nerve injury and is commonly referred to as "synaptic stripping." Dendrites retract, and microglia and astrocytes become associated

with the swelling soma (Sumner and Sutherland, 1973; Sumner, 1975a; Sumner 1975a; Sumner, 1976). Synaptic stripping has been studied in, and varies, among different motoneurons and different animals (Brannstrom and Kellerth, 1998; Blinzinger and Kreutzberg, 1968; Kerns and Hinsman, 1973; Sumner and Sutherland, 1973; Chen, 1978). The degree of stripping also differs depending on the synapse type, and whether or not muscle reinnervation occurs (Delgado-Garcia et al., 1988; Brannstrom and Kellerth, 1998).

Permanent axotomy the cat medial gastrocnemius (MG) α-motoneuron resulted in a transient increase in the number of bouton contacts on the motoneuron at 3 weeks and 6 weeks post-axotomy, but decreased to half of its normal value by 12 weeks post-axotomy (Brannstrom and Kellerth, 1998). The percent synaptic coverage on the motoneuron soma fell from the 3-week time point and continued in this trend until 12 weeks post-axotomy (Brannstrom and Kellerth, 1998). The increase in the number of contacts at the two early time points is attributed to the increase in the number of F-type (flattened vesicles) boutons associated with the motoneuron soma, which increased by 53% at 3 weeks and by 68% at 6 weeks post-axotomy. By 12 weeks post-axotomy, the number of boutons had decreased to 53% of its normal contacts, resulting in an 85% decrease in synaptic coverage (Brannstrom and Kellerth, 1998).

Pertaining to the other boutons studied on the cat α-motoneuron, the S-type bouton increased just slightly by 3 weeks, returned to normal values by 6 weeks, and greatly decreased in number by 12 weeks post-axotomy (Brannstrom and Kellerth, 1998). The percent coverage of the S-type bouton (containing spherical vesicles) decreased from the initial time point and continued to do so through 12 weeks post-axotomy (Brannstrom

and Kellerth, 1998). The percent synaptic coverage, as well as the number of bouton contacts on the proximal dendrites (within 100 μm) decreased throughout the time course studied (Brannstrom and Kellerth, 1998).

The loss of synapses from motoneuron membranes has also been well-studied in the rat hypoglossal nucleus (Sumner, 1975a; Sumner, 1975c; Sumner, 1976; Sumner, 1977). Fifty-two to 98 days after reinnervation of the axotomized hypoglossal nerve is prevented, by implantation of the proximal stump into the already innervated ipsilateral sternocleidomastoid muscle, somatic boutons with symmetrical synapses, and those containing clear, spherical vesicles were significantly reduced, while those with asymmetrical synapses, or with subsurface boutons were not significantly reduced (Sumner, 1976). A significant reduction of symmetrical boutons with clear, spherical vesicles was also observed on dendrites as well (Sumner, 1975 a, c; Sumner, 1976). Upon reinnveration, even after prolonged axotomy, somatic and dendritic synapses eventually recover. When the hypoglossal nerve is regenerated into the sternocleidomastoid muscle, somatic boutons showed a continued significant reduction at 32 days post-operatively, but a significant recovery at 49 and 70 days post-axotomy (Sumner, 1977). These observations imply that synapse recovery is only dependent on reinnervation of the hypoglossal nerve into any muscle (Sumner, 1977).

Other reported effects following rat hypoglossal nerve axotomy include an initial increase in the number of boutons and dendrites containing inclusions, and the disappearance of subsurface cisterns. These observations were most prominent between days 7 to 14 post-axotomy; however, the reason for this response remains unexplained. The increase of inclusions and loss of subsurface cisterns are not found to be significant

and appear to return to normal by 52 to 98 days post-axotomy, with the restoration of cisterns to normal levels occurring by day 21 (Sumner, 1975b; Sumner 1976). Similar observations were reported in models in which reinnervation was allowed and prevented. This indicates that such effects are not dependent on the reconnection, or persistent lack of the axotomized nerve; they may depend only on the initial disconnection of the hypoglossal nerve (Sumner, 1976). The transient increase in inclusions may simply be an early response to axotomy (Sumner, 1975b).

The response of glia to peripheral nerve injury is discussed in detail later. Briefly, microglia are initially noted to surround the synapse-free motoneuron soma and dendrites, and later, are replaced by astrocytic sheaths (Blinzinger and Kreutzberg, 1968; Sumner and Sutherland, 1973; Sumner, 1976). Moreover, a noteworthy distinction between the recovering cisterns of motoneurons in situations preventing or permitting reinnervation, is the location of reappearing subsurface cisterns. In situations allowing regeneration, returning cisterns are initially subastrocytic, until the boutons return and they are found subsynaptically (Sumner, 1975, 1976). When reinnervation of the hypoglossal nerve was prevented and studied 52 to 98 days post-axotomy, however, the cisterns were found to be mostly subsynaptic, despite that synapses onto the soma occur at a low frequency without reinnervation. It is not known if the subastrocytic phase precedes the subsynaptic phase in this study, as the peak astrocytic response surrounding the neuron would have diminished by 52 to 98 days (Sumner, 1976).

Upon reinnervation with muscle, however, and with time, synapses appear to recover and the changes mentioned above are reversed. Recovery of synaptic boutons has been observed in different animals and in different nerve types (Sumner, 1975;

Brannstrom and Kellerth, 1998, 1999). Just as with synapse depletions, synapse recovery occurs to different degrees, depending on the synapse type. In general, inhibitory synapses, such as the F-type bouton, appear to be less affected by synaptic stripping, and they recover faster than glutamatergic synapses, even when muscle reinnervation does not occur (Brannstrom and Kellerth, 1998, 1999; Linda et al., 2000; Novikov et al, 2000)

Alvarez et al., studied the loss of synapses in rat α-motoneurons following peripheral nerve ligation and regeneration, in which the nerve was ligated and immediately resutured. In their study, VGAT-IR terminals, which label inhibitory interneurons, showed greater recovery than excitatory synapses. VGAT synapses (inhibitory) were also more resistant to depletion after peripheral nerve injury, in comparison to VGLUT2 and VGLUT1 excitatory synapses. Moreover, recovery also differs among excitatory synapses. Of the excitatory synapses examined, VGLUT2-IR synapses showed greater recovery than VAChT-IR and VGLUT1-IR, respectively. Twelve weeks following reinnvervation, VGLUT 2 terminals actually showed better recovery than VGAT terminals; this was also observed 6 months after reinnervation. Furthermore, VGLUT1 terminals never recovered and continued to become depleted. VAChT terminals behave similar to VGAT (Alvarez et al., 2011). This recovery pattern was also reported in cat α-motoneurons, where two years after nerve reinnervation is allowed—following a 12-week period of axotomy—partial recovery of synapses is observed. S-type synapses recovered to a greater extent than F-type boutons. Two years after reinnervation, the number of S-type boutons increased by 70% following axotomy, while F-type boutons increased by 13% (Brannstrom and Kellerth, 1999).

D. Role of Glia in Synaptic Stripping

i.Glia

Glia are the nonneuronal cells of the nervous system. These cells include astrocytes, microglia, oligodendrocytes, and Schwann cells (Allen & Barnes, 2009). Microglia and oligodendrocytes are found only in the central nervous system, along with astrocytes. Schwann cells make up the majority of cells in the peripheral nervous system, along with astrocytes. Glia are smaller than neurons in size, but much more numerous, making up approximately half of the volume of the CNS. In the brain, the composition of glia in an organism correlates with the size of the organism, such that the brain glial composition of smaller animals is less than that of larger animals. The greatest differentiating factor between neurons and glia is the inability of glia to generate action potentials. Unlike neurons, glia do not have axons; therefore, they cannot initiate, transmit or conduct action potentials. Instead, glia interact closely with neurons, surrounding them and the synapses they form. In doing so, glia are able to carry out many different functions, such as regulating ion and neurotransmitter concentrations and providing nutrients to neurons. Increasing research on glia disproves the misconception of their passive roles in supporting and protecting neurons.

Unlike other types of glia, which derive from the neuroectoderm, microglia are part of the immune system and are mesodermal in origin, deriving from monocytes in the bone marrow. They migrate through the blood into the CNS during development, where they acquire their unique phenotype that differentiates them from the other blood-derived monocytes.

The initial belief that the brain is deprived of immune cells originated from the protective role of the blood-brain barrier in preventing substances from leaking into the

brain. The discovery of microglia in the brain and spinal cord, however, disproved this notion. Microglia are commonly referred to as the endogenous immune cells of CNS. They primarily function as macrophages, protecting the brain and spinal cord from pathogens and toxins by phagocytosing and removing dead or damaged cells, bacteria and myelin debris (Allen & Barres, 2009). In the development of the nervous system, microglia are also involved in synaptic remodeling, or phagocytosing and removing inappropriate and supernumerary synaptic connections, allowing for the enhancement of synapses (Allen & Barres, 2009).

To perform their primary analyzing functions, microglia are constantly moving their fine processes to detect any changes in the surrounding CNS environment (Suter et al., 2007). These processes extend in all directions and also contain protrusions to further enhance the analyzing ability of microglia. Although quiescent microglial cells remain in the same location, their processes represent the fastest moving structures in the CNS, resting only briefly at synaptic sites. This enables microglia to examine the brain's environment effectively since they comprise up to 12% of the cells of the CNS (Suter et al., 2008). Upon activation by external stimuli, microglia morph into an amoeboid shape, undergo proliferation (Figure 3a) and increase their expression of surface markers, including MHC II and CD 11b (Marc R. Sutter et al, 2008). Microglia also play a role in the pathogenesis of neurodegenerative diseases. Whether they are beneficial or harmful in these instances, however, is debatable (Allen & Barnes, 2009).

Oligodendrocytes and Schwann cells are very similar in function. Both involved in myelin production around neuronal axons, oligodendrocytes are found in the central nervous system while Schwann cells are found in the peripheral nervous system. The

myelin produced by these cells allows for the rapid propagation of action potential along the length of the axon, ultimately leading to faster communication between different neurons. In addition, myelin induces ion channels, further increasing communication between neurons (Allen & Barnes, 2009). Oligodendrocytes and Schwann cells also stimulate synapse formation between neurons, though the mechanism for how this occurs remains unknown (Allen & Barres, 2009). Damage to Schwann cells or oligodendrocytes can lead to demyelination, a large factor in neurodegenerative diseases and peripheral neuropathies.

Astrocytes play a large role in the central nervous system, making up the largest population of cells in the CNS (Ji et al., 2007). Similar to neurons, astrocytes derive from the neuroectoderm and embryonically stem from radial glial cells. Astrocytes are highly heterogeneous, but can be broadly categorized into two groups: fibrous and protoplasmic astrocyctes, found in the white and grey matters, respectively. Protoplasmic astrocytes contain much more elaborate processes than fibrous astrocytes, and are involved with neuronal cell bodies and synapses in the grey matter. Fibrous astrocytes also have elaborate processes, but are mostly involved with axons in the white matter of the CNS (Allen & Barnes, 2009). Through their extensive processes, astrocytes become highly associated with blood vessels, various parts of neurons, and with the pial meningeal layer of the brain and spinal cord, forming perivascular and subpial connections with their endfeet. Fibrous astrocytes also establish perinodal endfeet, surrounding nodes of Ranvier. Astrocytes form a syncytium amongst each other, communicating with each other via gap junctions. This allows for the synchronization of activity and movement of calcium ions intercellularly (as reviewed in Ji et al., 2007; Allen & Barnes, 2009).

Astrocytes are multifunctional cells in the CNS. Through their close associations with blood vessels of the brain (Ji et al., 2007), perivascular astrocytes form one of the major components of the blood-brain barrier, responsible for maintaining homeostasis in the CNS by highly regulating blood flow into and out of the brain. (Allen & Barres, 2009). The processes extending from these glial cells form tight associations with blood vessels, allowing them to detect deficiencies of oxygen or other nutrients to the brain and regulate blood flow accordingly (Allen & Barres, 2009).

Astrocytes are closely associated with neurons and the synapses that they form, supporting the term tripartitic synapse. This refers to the three components involved in synapses: the pre- and post-synaptic membranes, and the astrocyte. Their association with the pre- and post-synaptic cells at junction sites allows them to supply those cells with nutrients and molecules that influence neuronal function. Additionally, astrocytic processes contain the same receptors found on the membrane of the post-synaptic neuron. Through this bidirectional communication with neurons at the synaptic site, astrocytes modulate and help to induce synapses by releasing and taking up the same ions and neurotransmitters (ie-glutamate, dopamine, ATP, etc.) as neuron (Ji et al., 2007; Allen & Barnes, 2009). Their association with neurons allows them to aid in neurotransmitter and ion uptake at the synaptic cleft, helping to prevent neurotoxicity. The involvement of astrocytes, for example, in the glutamate-glutamine cycle and other similar processes allows the glutamate released by neurons at the synaptic cleft to be broken down into glutamine and recycled back into the neuron for release again as glutamate. Astrocytes may also be actively involved in brain functioning and informational processing, during both development and adulthood.

Another type of glia, radial glia, are highly involved in brain development. These cells are classified as a subtype of astrocyte and give rise to neural progenitor cells. Radial glial cells are bipolar, with one process forming endfeet at the ventricular wall and the other at the subpial surface. During development, radial glial cells contain long processes that extend along the cortex and function as migratory tracts, guiding axons to their correct location. Once neurons have moved to their correct location, radial cells transform into astrocytes or other specialized supporting cells, including Muller cells of the retina and Bergmann cells of the cerebellum.

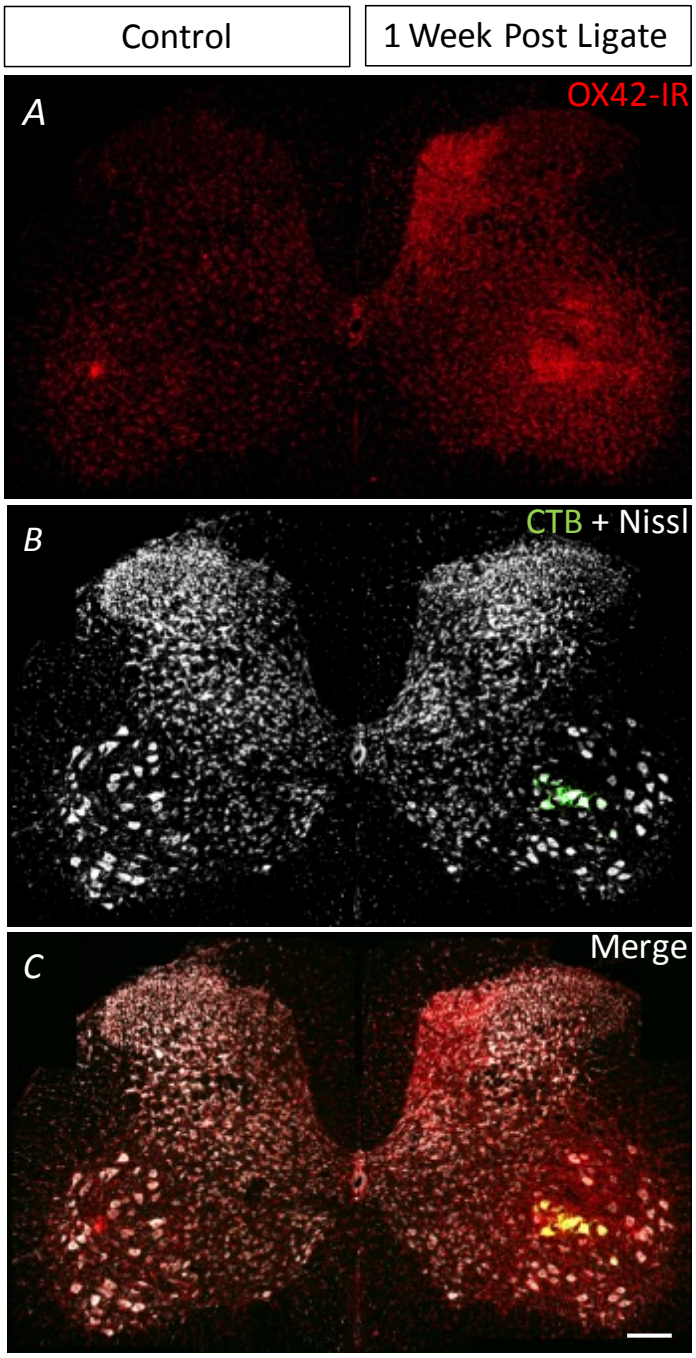
Control
1 Week Post Ligate
A
OX42-IR
B
CTB + Nissl
C
Merge

Figure 3: Microglia response in L5 lumbar spinal cord following tibial nerve injury. *A, B and C* are representative of the same images. *A,* OX42-IR (red) is labeling microglia. B, Nissl-IR (white), is labeling neurons in the spinal cord. The retrograde cholera toxin B (CTB) (green) in the right ventral horn is identifying the injured tibial n. motoneurons that innervate the medial and lateral gastrocnemius (MG/LG) muscles. CTB is injected into the MG/LG muscles 1 week prior to tibial n. injury and retrogradely travels up into the spinal cord to label the injured tibial motoneurons. *C*, is a merged image of OX42-IR, Nissl-IR and CTB. Notice the colocalization of the upregulation of OX42-IR staining with the CTB green in the left ventral horn. Images taken at 10X magnification (10 optical sections, separated by 2 μm z-steps) and montaged in CorelDRAW 12. Scale bar represents 200 μm.

ii. Glial Response after Injury

When changes in the CNS environment do occur, such as with peripheral nerve injury, microglia become activated. One of the most notable indications of activation is the transformation of microglia from the ramified to the amoeboid state, as their thin processes retract and become thicker, and their small cell bodies increase in size. A proliferation of microglia, especially well-characterized in the dorsal horn, is also a prominent change immediately observed with microglial activation (Figure 3A) (Blinzinger and Kreutzberg, 1968; Graeber et al., 1988; as reviewed in Svensoon et al., 1993; Suter et al., 2007; Ji et al., 2008; Allen & Barres, 2009; Xie et al., 2009). The once immotile microglial cells begin to move towards the injury site as their processes continue to move, surveying the environment. This movement is believed to be activated by pathological signals, including ATP, cannabinoids, chemokines, and others (Blinzinger and Kreutzberg, 1968).

Activated microglia function as the first line of defense as they begin to release second messengers and express receptors that bind to pathogens and other toxins released from the injured neurons (Reisert et al., 1984; Suter et al., 2007). An increase in the expression of microglial markers, including MHC II, CD11B and Iba1, serves as evidence of glial activation. The increase in the expression of these markers has been well-characterized in many experiments (Svensoon et al., 1993; Tanga et al., 2004; Echeverry et al., 2007; Wen et al., 2007; Ji et al., 2008). Activating microglia also take up bromodeoxyuridine (BrdU), a generic marker of mitotic cells. BrdU is incorporated into the DNA of cells undergoing S phase of the cell cycle and has been used to label actively

dividing microglia following nerve injury. In resting conditions, few glial cells actually divide (Suter et al., 2007).

Macrophaging microglia respond rapidly to peripheral nerve damage. This response has been well-characterized in the dorsal horn (Svensson et al., 1993; Tanga et. al. 2004; Echeverry et al., 2007; Suter et al., 2007; Wen et al., 2007) of many studies focusing on pain, but not well-characterized in other regions, such as the ventral horn, where motoneurons are located. Following peripheral nerve injury, microglia quickly begin phagocytosing and removing dead or damaged cells, bacteria and myelin debris, which releases molecules that can progress the development of the disease (Blinzinger and Kreutzberg, 1968; Allen & Barres, 2009). Many experiments involving damage or constriction of the sciatic nerve have reported initial responses beginning as early as 4 hours post-injury (Echeverry et al., 2007), with peak activation occurring 3 days following nerve injury. A steady decline in numbers occurs through days 7 and 14 post-injury, with populations returning to basal levels by day 61 (Echeverry et al., 2007). A similar proliferation of microglia in the spinal cord was also observed after an L5 nerve transection in rat lumbar spinal cord. In this experiment, microglial activation, marked by CD14, was observed on day 4 post-transection, was sustained through day 14, but returned to basal levels by day 28 (Tanga et al., 2004).

An increase in the growth factor neuregulin-1 (NRG-1) is observed in the dorsal horn following peripheral nerve injury. NRG-1 is released from primary afferents and contributes to the development of neuropathic pain. NRG-1 binds to erbB2, 3 and 4 receptors expressed in microglia. In vivo and in vitro studies involving treatment with NRG-1 resulted in the proliferation of microglia in the dorsal horn, and the development

of these cells into the active morphology (Calvo et al., 2010). The strong proliferation of microglia in the dorsal horn is thought to be a result of the phagocytic role of microglia in removing central presynaptic terminals of axotomized sensory neurons. Following the initial proliferation in the dorsal horn, microglia slowly migrate towards the affected motoneurons in the ventral horn (Svensson et al., 1993). In support of this migration, activated microglia show a vimentin-rich cytoskelteton (reviewed in Svensson et al., 1993), an indication of the movement of microglia

Although they play an important role following peripheral nerve injury, the astroglial reaction to injury is less characterized than that of microglia. The astrocytic reaction following peripheral nerve injury is believed to be activated by microglia. Despite the heterogeneity of astrocytes, glial fibrillary acidic protein (GFAP) is the primary identifying marker of the majority of reactive astrocytes. It is the major protein component of the glial filaments making up spinal astrocytes (Eng et al., 1971; Bignami et al., 1972; Graeber and Kreutzberg 1986; Ji et al, 2007). Although an increased expression of GFAP is evident following injury (Figure 4a), the exact function of the GFAP molecule remains unknown. In vitro experiments have reported a possible role in the stability of glial filaments (Weinstein et al., 1991; reviewed in Eddleston and Mucke, 1993). Another factor preventing the characterization of astrocytes following injury is the environment in which experiments are conducted. Many experiments testing the astrocytic response to various conditions are conducted in vitro and often generate a different response when tested in vivo. In vitro experiments can also be inconsistent, depending on whether pure astrocytic cultures are used, or if the astrocytes are cultured with microglia, neurons, or other molecules (Hatten M. E 1985; Corvalan et al., 1990;

reviewed in Eddleston and Mucke, 1993). Furthermore, the astrocytic response has been largely been obtained using in situ hybridization and immunohistochemical staining, both of which provide static images of astrocytes and prevents the observation of fast, physiological changes that may occur.

The astrocytic reaction is believed to occur in two phases, the early phase, which may last up to three weeks, and a second phase that occurs afterwards. The most common observation reported after injury is an up regulation of GFAP in the ipsilateral side of the injury during the first phase of the astrocytic reaction (Figure 4a). Although microglial proliferation is initially much greater in the dorsal horn, an increase in GFAP expression has been reported as soon as day 1 post-axotomy in several experiments (Graeber and Kreutzberg, 1988; Eriksson et al., 1993; Eriksson et al., 1997; Hajos et al., 1997; Persson et al., 1995). This is likely due to the arrangement of GFAP filaments into bundles found around the nucleus and within their cell processes. This bundle arrangement of the filaments is thought to be the cause of the very well-characterized hypertrophy of reactive astrocytes following injury (Graeber and Kreutzberg, 1986). In parallel with this, plasma and tissue levels of endothelin (ET) are greatly increased after injury. ET-1 induces hypertrophy of astrocytes (Ji et al., 2007). In addition to the well characterized hypertrophy, reactive astrocytes also retract their thickened process and are believed to morph into the fibrous-type of astrocytes (Graeber and Kreutzberg, 1988; Gilmore et al., 1990).

In the second phase of the astrocytic reaction (between weeks 2-3 post-injury), astrocytes migrate towards and form a close association with the soma and proximal dendrites of axotomized motoneurons in the ventral horn (Figure 4b) (Sumner and

Sutherland, 1973; Sumner, 1974; Sumner, 1975; Graeber and Kreutzberg, 1988; Gilmore, Sims, & Leiting), an observation not noted previously. A quantitative electron study on the injured hypoglossal nucleus showed that astrocytes replaced microglia surrounding motor nuclei two weeks after axotomy, their cell processes increasing into the synaptic cleft, forming stacks of lamellae. The development of these lamellae peaked at 5 weeks post-injury before returning to normal levels by 12 weeks post-axotomy, when the hypoglossal nerve had reinnervated the tongue (Sumner and Sutherland, 1973; Graeber and Kreutzberg, 1988). Because of this intimate relationship, astrocytes are believed to play a critical role in inhibiting synaptic transmission from axotomized motoneurons, and are likely involved in removing the presynaptic terminals from the axotomized motoneuron (Graeber and Kreutzber, 1988; W. Xie et al., 2009). Furthermore, reactive astrocyte processes contain high levels of 5'-nucleotidase, an enzyme which hydrolyzes AMP, producing ADP. ADP is believed to play a role in inhibiting synaptic transmission (Graeber and Kreutzberg, 1988).

Microglia were once thought to be involved in removing the presynaptic terminals onto motoneurons as they slowly migrated towards the axotomized motoneuron (Graeber and Kreutzberg, 1968). A closer look at these terminal sites, however, revealed that thin, sheet-like astrocytic processes actually intervene and form a barrier between the microglia at the nerve terminals and the post-cell membrane (Sumner and Sutherland, 1973; Sumner, 1974; Sumner, 1975; Svensson et al., 1993; Ji et al., 2007; Aldskogius et al., 1999). The replacement of the perineuronal microglia from the soma of motoneurons by astrocytes occurs by the end of the second week-post axotomy in studies of the sciatic (Gilmore et al., 1990) and facial nerves (Graeber and Kreutzberg, 1988). This coincides

with the initiation of the second phase of the astrocytic reaction, additionally supporting a role of microglia in activating astrocytes (Tanga et al., 2004; Svensoon et al., 1973).

A topic of great debate involving the response of astrocytes to peripheral nerve injury is the proliferation of astrocytes. While some studies indicate that a proliferation in cell number of astrocytes does not occur at all (Ji et al., 2008), others report an observed increase in cell number overtime only in chronic nerve injuries (reviewed in Eddleston and Mucke, 1993; Svensson et al., 2008; Tsuda et al., 2011), when muscle reinnervation is not allowed. Still, other studies have reported a proliferation of astrocytes following acute or chronic injury (Wohl et al., 2009). The dispute regarding proliferation can be attributed to the limited markers in studying astrocytes following peripheral nerve injury, and the conflicting results of in vivo and in vitro experiments.

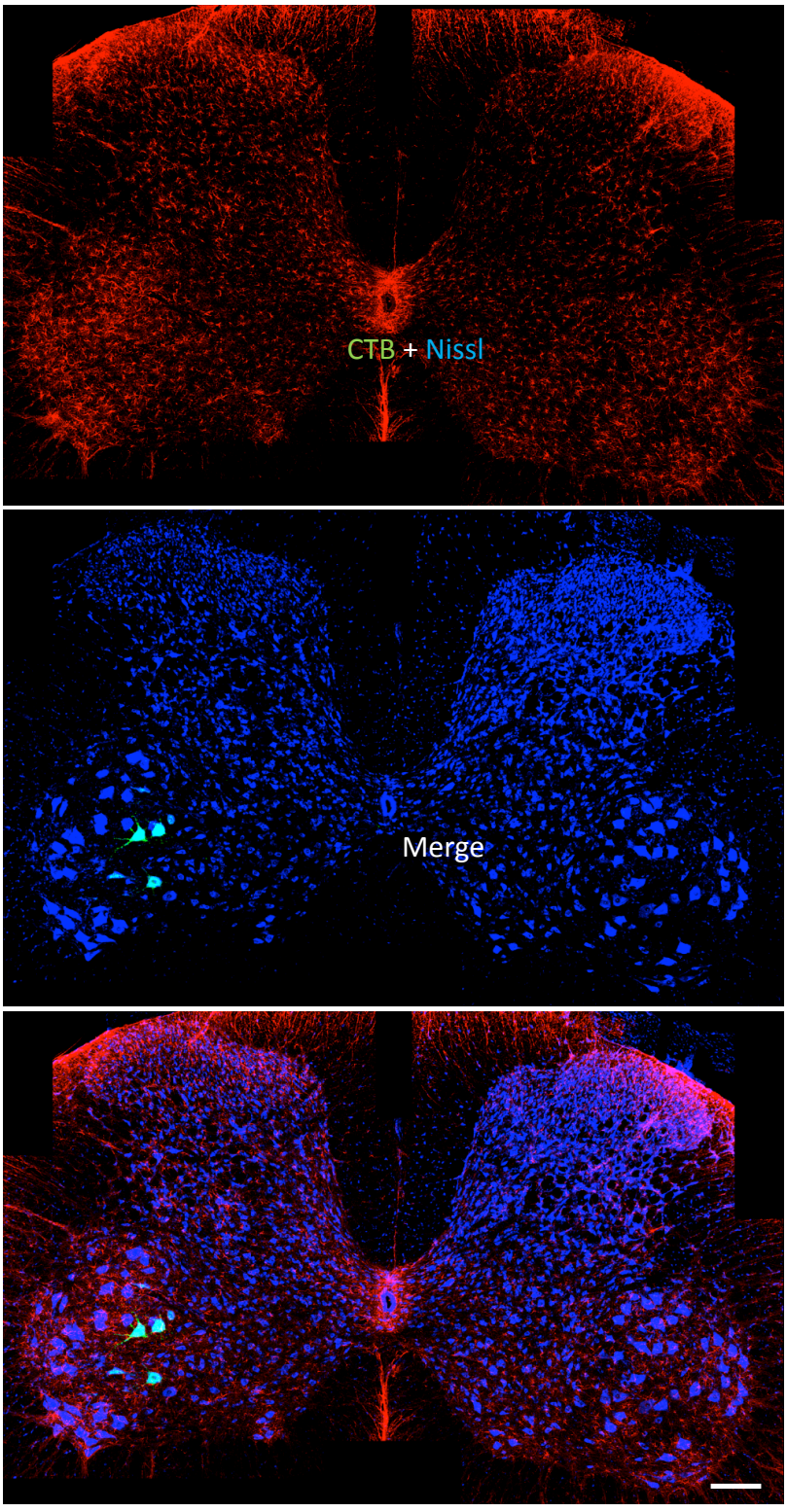
CTB + Nissl
Merge

Figure 4: Astrocytic response in L5 lumbar spinal cord following peripheral nerve injury. *A, B* and *C* are representative of the same images, labeled with *A*, Glial Fibrillary Acidic Protein (GFAP)-IR (red) to identify astrocytes, *B*, with Nissl-IR (blue) to identify all neurons and retrograde cholera toxin B (CTB) (green) to identify the injured tibial n. motoneurons. CTB is injected into the the medial and lateral gastrocnemius muscles 1 week prior to tibial n. injury and retrogradely travels up into the spinal cord to label the injured tibial n. motoneurons that innervate the LG/MG muscles. *C*, is a merged image of OX42-IR, Nissl-IR and CTB. *C*, is a merged image of GFAP-IR, Nissl-IR and CTB. Notice the colocalization of the upregulation of GFAP-IR staining with the CTB green in the left ventral horn. Image taken at 10X magnification (10 optical sections, separated by 2 μm z-steps) and montaged in CorelDRAW 12.

IV. Specific Aims

Like other synapses onto the soma and proximal dendrites of motoneurons, C-boutons are also affected after peripheral nerve injury. The degree of synaptic stripping occurring following two types of injury: peripheral nerve crush, which permits reinnervation and peripheral nerve ligation, which prevents reinnervation, have not yet been fully characterized. Furthermore, glial cells are thought to play a role in synaptic stripping. The degree and time course of glia activation and proliferation in the ventral horn, however, has also not been fully characterized following both of the types of peripheral nerve injury. Due to the glial reaction following injury and the involvement of glia in surrounding and removing synapses, **I hypothesize that glia activation following peripheral nerve injury correlates to the degree of depletion of synaptic coverage of C-boutons.** Since microglia have the quickest and most robust response following injury, and because of their potential role in activating astrocytes (Tanga et al., 2004; Svensoon et al., 1973), I believe that by using the drug, Minocycline, to inhibit microglia in the spinal cord, the glial reaction following injury will be blocked and C-boutons will continue to synapse onto motoneurons. C-boutons are believed to function as modulators of certain locomotive movements, acting on α-motoneurons to reduce the peak of the after-hyperpolarization of the action potential, thereby increasing the firing rate and frequency of motoneurons in a state-dependent fashion (Zagoraiou *et al.*, 2009). Preventing the stripping of C-boutons may have great clinical outcomes and provide insight on other synapses lost after injury.

Aim 1 characterizes the extent of the loss of C-boutons from rat motoneurons after peripheral nerve injury. *The specific hypothesis is that lumbar motoneuron C-bouton synaptic stripping occurs following tibial nerve crush as well as tibial nerve ligation.* To test this hypothesis, I used the combination of immunohistochemistry and confocal microscopy to quantify the number of C-boutons on the soma of medial and lateral gastrocnemius motoneurons following tibial nerve crush and ligation.

Aim 2 characterizes the magnitude of microglia and astrocytes in the ventral horn following peripheral nerve injury. *The specific hypothesis is that microglia and astrocytes are upregulated in the ventral horn of the lumbar spinal cord, following tibial nerve crush and ligation.* To test this hypothesis, I used the combination of immunohistochemistry and confocal microscopy to quantify the activation and proliferation of microglia and astrocytes in the mid-lateral ventral horn of the lumbar spinal cord, following tibial nerve crush and tibial nerve ligation, at different post-injury times ranging from 3 days to 3 months. To validate my results in the ventral horn of the spinal cord, I also measured glia activation and proliferation of the medial aspect of the dorsal horn, an area previously characterized.

Aim 3 observes the effect of the microglial inhibitor drug Minocycline on the stripping of cholinergic C-boutons from rat motoneurons following injury. *The specific hypothesis is that by attenuating the activation of microglia, I will suppress synaptic stripping of the C-bouton on rat lumbar motoneurons following nerve injury.* To test this hypothesis, rats received daily oral doses of Minocycline (50 mg/kg) for two

weeks, following peripheral nerve injury. I used the combination of immunohistochemistry and confocal microscopy to quantify the activation and proliferation of microglia and astrocytes in the mid-lateral ventral horn of the lumbar spinal cord following tibial nerve ligation in the presence of Minocycline. Furthermore, I quantified the number of C-boutons on the soma of medial and lateral gastrocnemius motoneurons following tibial nerve crush and ligation.

V. Materials and Methods

All procedures were carried out according to the National Institutes of Health Guidelines and approved by the Wright State University Institutional Animal Care and Use Committee. Adult female Sprague Dawley rats were used for all experimental procedures.

A. Surgical Procedures

Surgery 1. Retrograde Tracer Injection

An intramuscular injection of the retrograde tracer Cholera-Toxin B (CTB), conjugated to Alexa-555 fluorochrome, was injected into the left medial and lateral gastrocnemius (MG/LG) muscles of all Sprague-Dawley rats. The tracer is taken up by motor axon terminals at the neuromuscular junction and retrogradely travels into the spinal cord. This allows for correct identification of the injured motoneurons for *post-hoc* analysis (Figures 3b, 4b and 5). All retrograde survival surgeries were performed by Lori Goss, RVT, 7 days prior to nerve injury (crush or ligation). All animals were anesthetized with Isoflourane (2.5%) in 100% oxygen prior to surgery. The surgical site (left hind leg) was shaved and cleaned using 70% ethanol and betadine. An incision was made on the midline of the left hind leg, extending from the division of the biceps femoris muscle, rostrally, and preceded caudally. The skin overlying the muscle was carefully separated

from the biceops femoris muscle. The biceps femoris muscle was reflected and the connective tissue around the MG/LG muscles was cleared. A total of 25 ul of CTB was injected into each of the MG and LG muscles using an 18-25 gauge needle. The biceps femoris was closed using 4-O ethicon absorbable vicryl. The skin overlying the muscle was sutured close and irrigated with saline. To prevent any unforeseen distress, the analgesics Buprenorphine (0.1 mg/kg) SQ and Carprofen (5 mg/ml) SQ were injected intraperitoneally (IP) during surgery while the animal was still anesthetized. Carprofen was then again administered 24 hours later as the animals continued to be monitored for pain.

Surgery 2. Peripheral Nerve Injuries

Seven days after the retrograde tracer surgery, the tibial nerve was crushed or ligated. All rats received Isofluorane anesthesia prior to the nerve injury surgery. An incision was made in the left hind leg to expose the tibial nerve close to its entry into the MG/LG muscles. The tibial nerve was dissected and either ligated or crushed at that point. Ligation of the nerve involved transecting the nerve and ligating the proximal stump with double tie to prevent regeneration. Crushing of the tibial nerve was carried out by holding pressure on the tibial nerve for 5 seconds using jeweler forceps. To prevent any pain, Buprenorphine (0.1 mg/kg) SQ and Carporfen (0.1 ml/100 g) SQ was administered at the time of surgery. Carprofen was again administered 24 hours later.

B. Minocycline Treatment

Specific Aim 3 of this project studied the effects of the antibiotic Minocycline on glial inhibition following peripheral nerve injury in rats. These animals received a daily dose of Minocycline of 0.035 g, mixed into a 4 g ball of Pillsbury sugar cookie dough.

The Minocycline was pre-measured into individual packets and refrigerated, to be ready for use. The dough balls were also prepared ahead and refrigerated. The Minocycline was mixed into the dough ball the morning of administration (Corbett et al., 2012). Administration of the Minocycline cookie dough balls occurred between 7:30-8:00 A.M. every morning for three consecutive weeks. Animals undergoing surgery (sham and tibial nerve ligation) began their Minocycline treatment 3 days before the ligation and sham surgeries, and continued to receive Minocycline two weeks following surgery. Before receiving any Minocycline, all rats were given plain sugar cookie dough balls to acclimate them to the new food (Corbett et al., 2012). At the end of the 2-week Minocycline treatment, each animal was perfused for histological analysis of the spinal cord. The ventral horn at L4-5 was the focus of this experiment, as it contains the motoneurons of the tibial nerve, onto which C-boutons synapse.

C. Tissue Preparation for Analysis

Transcardial Perfusion

At predetermined time points, ranging from 3 days to 3 months post-injury, animals were transcardially perfused for immunohistochemical analysis. Prior to the perfusion, each animal was deeply anesthetized intraperitoneally (IP) with pentobarbital at 150 mg/kg. Anesthetic effects were tested by lack of pineal and corneal reflexes. To prevent blood clot formation during the perfusion, 0.5 mL Heparin was administered retroorbitally. The animal was then secured on a surgical board and the thoracic cavity was cut and resected. A perfusion cannula was placed into the left ventricle and the right atrium was cut to allow for drainage. A peristaltic pump was used to run vascular rinse (100-200 mL), followed by the fixative (4% paraformaldehyde in 0.1 M phosphate buffer saline (PBS)

solution) (200-300 mL). The vascular rinse clears the vascular system and the fixative stabilizes the cells from the rigors of staining and processing, preserving them in a life-like manner. The spinal cord (T9-L6) was then dissected and placed in a vial of fixative for 2-6 hours, before being transferred into a 15% sucrose solution (in 0.1 M PB) at 4 °C overnight, or until use.

Histological Sectioning

The lumbar levels of the spinal cord were identified, cut and placed into Cryoprotectant solution for 5-10 minutes. The Cryoprotecant solution was then pipetted off and replaced with OCT Freeze Medium (Tissue Tek). Lumbar levels were then assembled into frozen blocks using the OCT Freeze Medium. Spinal sections were cut into 50 um transverse sections using the Microm HM505 E cryostat and collected, free floating, into 0.01 M PBS (pH 7.4).

Immunohistochemistry

Spinal sections were washed in 0.1% PBS-T (0.01 M PBS containing 0.1% Triton-X, pH 7.3), blocked in normal horse serum (1:10 in PBS-T) for 30 minutes and incubated in primary antibodies overnight at 4 °C. All antibodies were diluted with PBS-T 0.1%, pH 7.4. OX42 primary antibody was used to label activated microglia in the dorsal and ventral horn (Figure 3a). OX42 (Mouse Anti-Rat CD11B Monoclonal Millipore; Chemicon, Temicula, CA, USA; 1:100 dilution) antibody binds to CD11b receptors on activated microglia and is commonly used to label activated microglia (Svensoon et al., 1993; Ji et al., 2008; Zheng *et al.,* 2010). Anti-Glial Fibrillary Acidic Protein (anti-GFAP) antibody (1:500) was used to label astrocytes (Figure 4a). GFAP is the primary intermediate filament protein in astrocytes and is the most common marker

targeted for labeling astrocytes (Eng et al., 1971; Bignami et al., 1972; Graeber and Kreutzberg 1986). Anti-VGLUT1 (vesicular glutamate transporters; Chemicon, Temecula, CA, USA; guinea-pig; 1:5000 dilution) antibody was used to label axons of primary afferents in the spinal cord. Anti-VAChT (vesicular acetylcholine transporter; Millipore, Billerica, MA, USA; goat, 1:5000) was used to label cholinergic contacts onto motoneurons. Nissl-blue (Invitrogen, Carlbad, CA, 1:100) was used to label all motoneurons.

Three washes in PBS-T were conducted to remove unbound primary antibodies before applying secondary antibodies. All primary antibodies were conjugated to specific anti-host secondary flourophores for visualization. OX42 and GFAP antibodies were each conjugated to FITC; the CTB to Cy3 and VAChT to Cy5. VGLUT1 was also visualized via a Cy5 secondary antibody.

Spinal cord tissues were then washed twice each, in PBS-T followed by 0.1 Phosphate Buffered Saline (PBS). The tissues were then mounted onto gelatin-coated slides and cover slipped using Vectashield with DAPI mounting medium (Vector Laboratories). DAPI-staining binds to DNA and allowed for identification of the nucleus.

D. Imaging and Analysis

The slides were imaged using a Fluoview1000 Olympus (Center Valley, PA, USA) confocal microscope using 10X and 20X objectives of the dorsal and ventral horns of the lumbar region of the spinal cord.

The proliferation of microglia and astrocytes, indicated by cell counts of microglial and astrocytic processes surrounding nissl-stained motoneurons, was determined using Fluoview software (Olympus). Regions of interest of equal size of the

medial aspect of the dorsal horn, encompassing laminae I-III (Figure 1), were measured, on both the experimental (crush or ligation) and control side. The number of glial processes surrounding motoneuron somas was counted on the experimental and control side and compared within a fixed region of interest. The same method was used to determine microglial and astrocytic counts after injury in the ventral horn, focusing on the middle and lateral aspects of the ventral horn, where motoneurons are heavily located.

The activation of microglia and astrocytes, indicated by levels of immunoreactive intensity levels of OX42-IR (identifies microglia) and GFAP-IR (identifies astrocytes), was also measured using ImagePro software. The immunoreactive intensities of areas within the dorsal and ventral horns, as described above with regards to proliferation, were measured on the experimental side, and compared to that on the control side (Figure 7). To control for the possibility of a contralateral effect due to glia activation during the sham surgeries, two naïve rats, which did not undergo any surgeries, were analyzed for cell number and intensity and compared to those of sham animals.

Statistics

Statistical analysis and graphing were conducted using SigmaPlot (Jandel). Data are expressed as the mean ± SD. The number of animals and motoneurons analyzed are indicated in the results section.

Figures

Graphs were produced using SigmaPlot (Jandel). Images were composed using Fluoview software, Image Pro Plus 5.1, Neurolucida, and CorelDraw 12.

VI. Results

Aim 1:

Characterization of the loss of C-boutons from motoneurons in the ventral horn following peripheral nerve injury

The focus of this aspect was to characterize the synaptic stripping of large, cholinergic C-bouton contacts from motoneurons, following tibial nerve crush and ligation. To carry out these studies, female Sprague Dawley rats were injected with the retrograde tracer Cholera Toxin-B (CTB) into the left MG/LG muscles. This tracer allowed for the correct identification of the injured motoneurons of the tibial nerve in the ventral horn of the spinal cord for post-*hoc* analysis. One week following the tracer surgery, the rats underwent one of two survival injury surgeries: a ligation surgery, in which the left tibial nerve was transected and ligated with double tie to prevent regeneration and reinnervation, or a nerve crush surgery, in which pressure was applied to the left tibial nerve using jeweler forceps. Two weeks following the injury surgeries, these animals were perfused and their spinal cords dissected out. The spinal tissue was prepared for histological analysis through the use of various antibodies (see materials and methods).

The following experiments in this aim were conducted at 2 weeks post tibial nerve crush or ligation. All data obtained from the injured rats were compared to sham surgery controls, animals that underwent the retrograde tracer surgery, but the tibial nerve was only exposed and did not experience nerve injury.

To characterize the stripping of C-bouton contacts from the soma, the percent coverage of C-boutons on the motoneuron soma membrane was calculated following tibial nerve crush and ligation. In 60X confocal images described above, the center of the motoneuron was determined by the presence of a clear nucleolus. Using this as the starting point, the perimeter of the motoneuron soma was measured every 2-3 μm, traveling up and down from the center and going through the entire stack of images for that motoneuron. At each of these measured points, the length of each C-bouton contact around the soma membrane was individually found in the Fluoview software (Olympus). The sum of all of the contact lengths at a particular z-step was then divided by the perimeter at that z-step to determine the percent coverage. The mean percent coverage of that motoneuron was calculated and used to find the percent depletion, as compared to sham controls (Figure 8). Our data shows that there was a significant (-29.749% membrane depletion ± 22.286 SD, 106 MNs, 2 animals, T-test P = 0.845) depletion in membrane coverage of C-boutons following 2-week tibial nerve ligation, as compared to sham controls. Following tibial nerve crush, there is not a significant depletion in soma C-bouton coverage 2 weeks after injury (11.3% membrane coverage ± 3.96 SD, 69 MNs, 2 animals, T-test P=0.845) (data not shown) when compared to Sham surgery controls (11.4% membrane coverage ± 3.42 SD, 120 MNs, 2 animals). The depletion in C-bouton

contacts was much greater following ligation than crush. As a result, the focus of our C-bouton study shifted to the ligate injury animals.

To determine the density of C-boutons, or the number of C-boutons contacting the motoneuron soma, three-dimensional reconstructions of 60X confocal images of CTB-labeled motoneuron somas (Figure 5), stained with the VAChT antibody, were created using Neurolucida software (Figure 9). The 3-D reconstructions of the motoneuron somas allowed us to analyze the entire stack of confocal images and count the number of C-bouton contacts on the motoneuron soma. At two weeks post-ligation, there was not a significant difference (0.489 VAChT-IR contacts/100 μm^2 ± 0.240, n = 11, 2 animals) in the number of C-bouton contacts synapsing onto the motoneuron soma, compared to the sham control (0.565 VAChT-IR contacts/100 μm^2 ± 0.155, n = 8, 2 animals) (Figure 10). Therefore, synaptic coverage loss is not likely the result of synapses being completely removed from the membrane.

To determine if the loss of soma synaptic coverage of C-boutons are the result of size decrease, the cross-sectional area of *en face* C-bouton clusters was also measured. Again, using the same 60X confocal images, the area of complete C-bouton clusters, on the face of the motoneuron soma, was determined using Fluoview software. A random sampling of approximately100 *en face* C-bouton clusters was analyzed from each animal sampled and the mean area was calculated. This was conducted at 2-weeks following tibial nerve ligation, where significant stripping of VACht-IR contacts from motoneurons has been reported (Alvarez et at., 2011). Our data showed a significant decrease in the area of C-bouton clusters following 2-week ligation (8.761 ± 3.340 SD, n = 200 cells, 2 animals) as compared to sham controls (12.369 ± 4367 SD, n = 165 cells, 2 animals)

(Figure 11). These data suggest that the decrease in C-bouton synaptic coverage following tibial nerve ligation may be explained by a loss in C-bouton area rather than a complete removal of synapses, which has been reported in other synapses such as VGLUT1-IR + synapses on motoneurons (Alvarez et al., 2011).

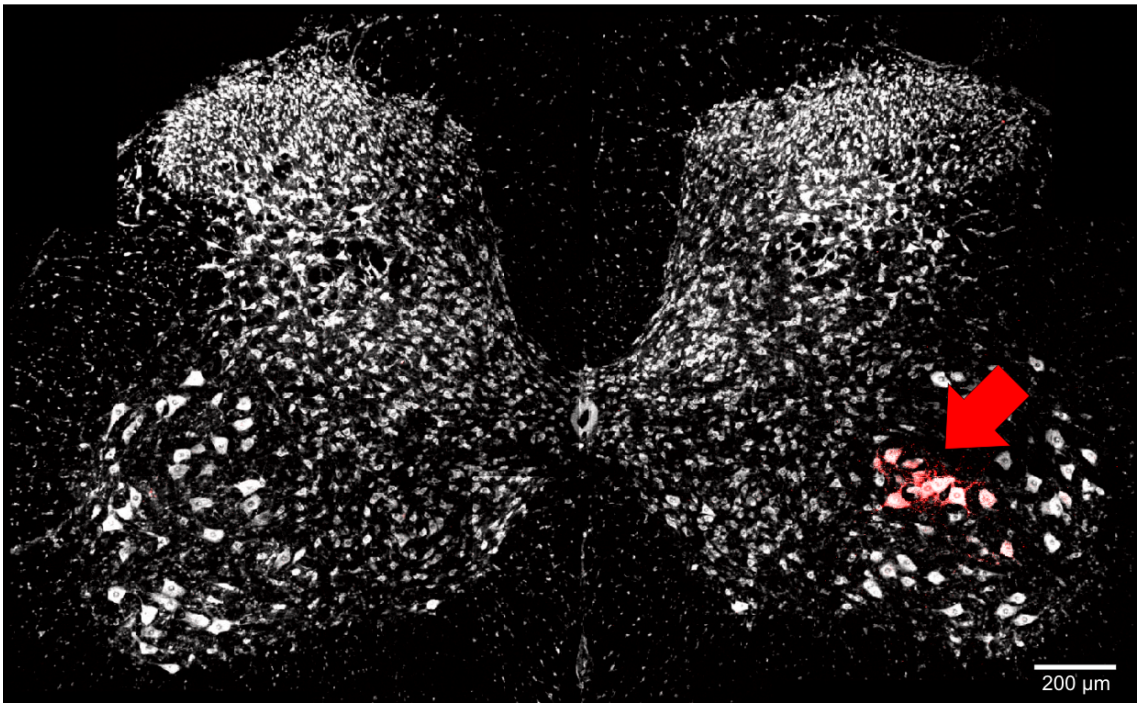
200 µm

Figure 5: L5 rat lumbar α-motoneuron, following peripheral nerve injury. The arrow is pointing to retrograde-CTB staining (red) used to identify the cell bodies of peripherally injured axons. CTB was injected into the right LG/MG muscles and retrogradedly transported back into the spinal cord by way of the axon terminals. The contralateral side, which contains no CTB labeling, is not injured and serves as an internal bilateral control. Image taken at 10X magnification (10 optical sections, at 2 μm z-steps) and montaged in CorelDRAW 12. Scale bar represents 200 μm.

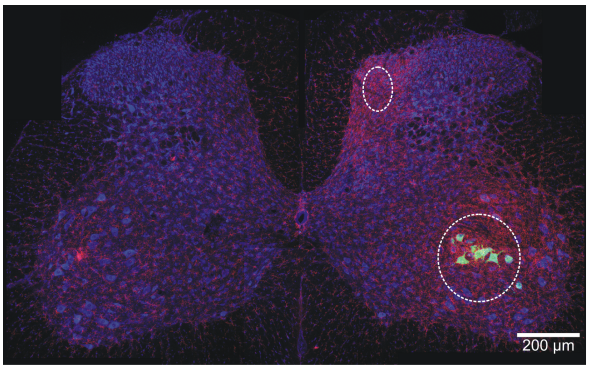
200 µm

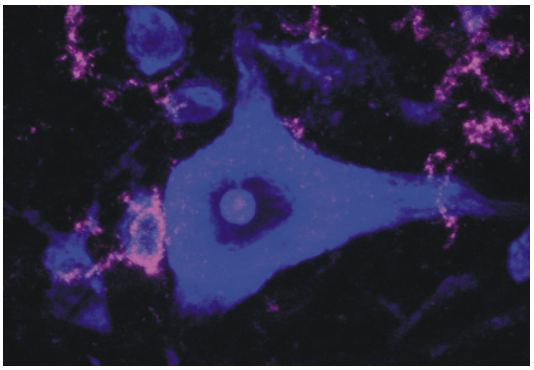

Figure 6: *(Left)* Glia proliferation was calculated in defined regions of interest (ROI) within the dorsal and ventral horns, for quantifying the number of glial cells (*right*). Glia were quantified by counting DAPI+ nuclei. Data in this project are reported as fold changes between the number of OX42-IR (microglia) and GFAP-IR (astrocyte) cells, within equal regions of interest on the ipsilateral injured side and the contralateral control side. Fold changes, between the injured and control sides, were determined by dividing the number of cells within a ROI on the injured side, by the number of cells within a ROI on the contralateral control side. The contralateral control ROI was identified as an area of equal size and mirrored location, as compared to the ROI on the injured side. *(Left)* Merged image of OX42-IR (red, microglia), Nissl-IR (blue, neurons) and CTB-green. Image taken at 10X magnification (10 optical sections, at 2 μm z-steps) and montaged in CorelDRAW 12. Scale bar represents 200 μm. *(Right)* Image taken at 60X magnification (11 optical sections, at 1 μm z-steps).

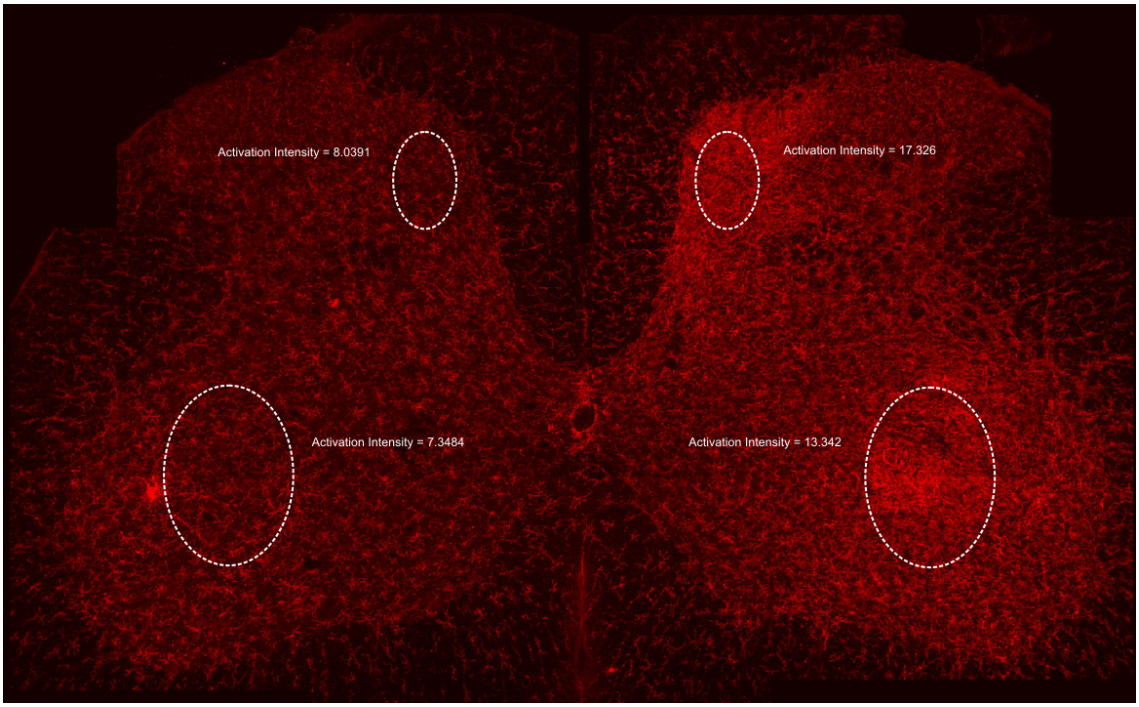
Activation Intensity = 8.0391
Activation Intensity = 17.326
Activation Intensity = 7.3484
Activation Intensity = 13.342

Figure 7. Glia activation calculated in defined regions of interest within the dorsal and ventral horns. The intensity of OX42-IR (representing microglia activation) and GFAP-IR (representing astrocyte activation) within regions of interest on the injured side, and on the contralateral control side, was determined. Intensity was measured using Image-Pro Plus 7.0. All data in this project as are reported as fold changes between the ipsilateral injured side and the contralateral control side. This was calculated by dividing the OX42- or GFAP-IR intensity on the injured side by the OX42-IR or GFAP-IR intensity on the control side.

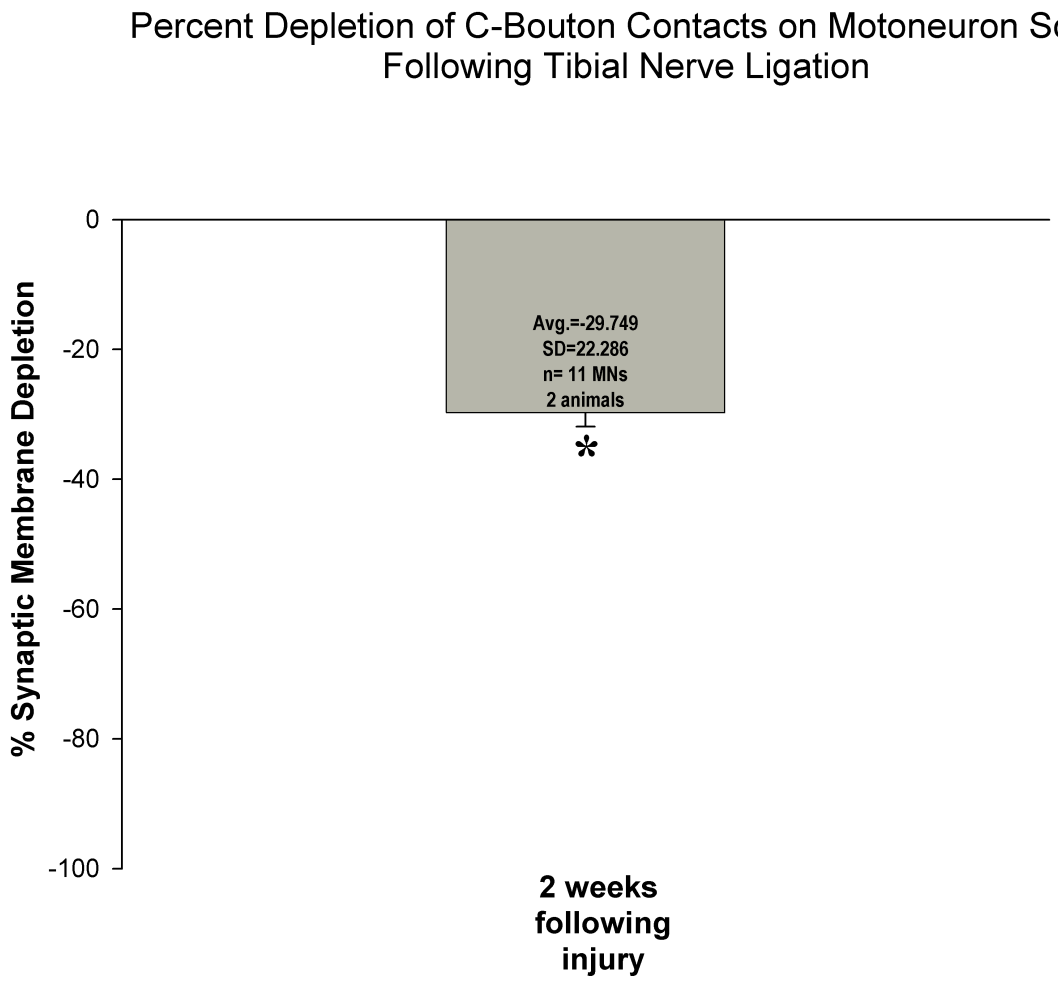
Percent Depletion of C-Bouton Contacts on Motoneuron Soma
Following Tibial Nerve Ligation
0
-20
-40
-60
-80
-100
% Synaptic Membrane Depletion
Avg.=-29.749
SD=22.286
n= 11 MNs
2 animals
*
2 weeks
following
injury

Figure 8: Percent depletion of C-boutons on the soma of rat motoneurons in L4-5 following tibial n. ligation. The x-axis identifies the time point after injury. The y-axis represents the percent depletion of VAChT-IR membrane coverage, as compared to sham surgery controls**.** C-bouton percent coverage on motoneurons is significantly (indicated with black asterisks, $p<0.001$, t-test) depleted 2 weeks following tibial n. ligation, as compared to sham surgery controls.

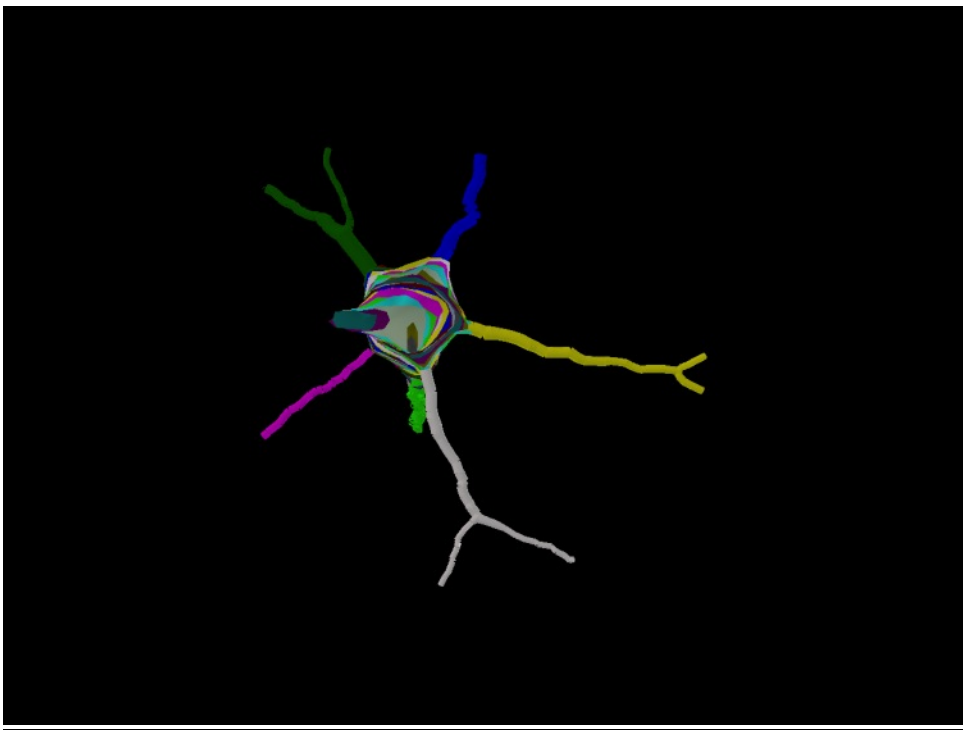

Figure 9: 3D reconstruction of a medial gastrocnemius motoneuron. Reconstructions were formed from a stack of confocal images. Reconstructions were necessary for calculating the surface area of the soma, in order to determine the density, or number, of C-boutons. Reconstructed cells were obtained from confocal stacks of 35-40 optical sections, at 0.5 μm z-steps.

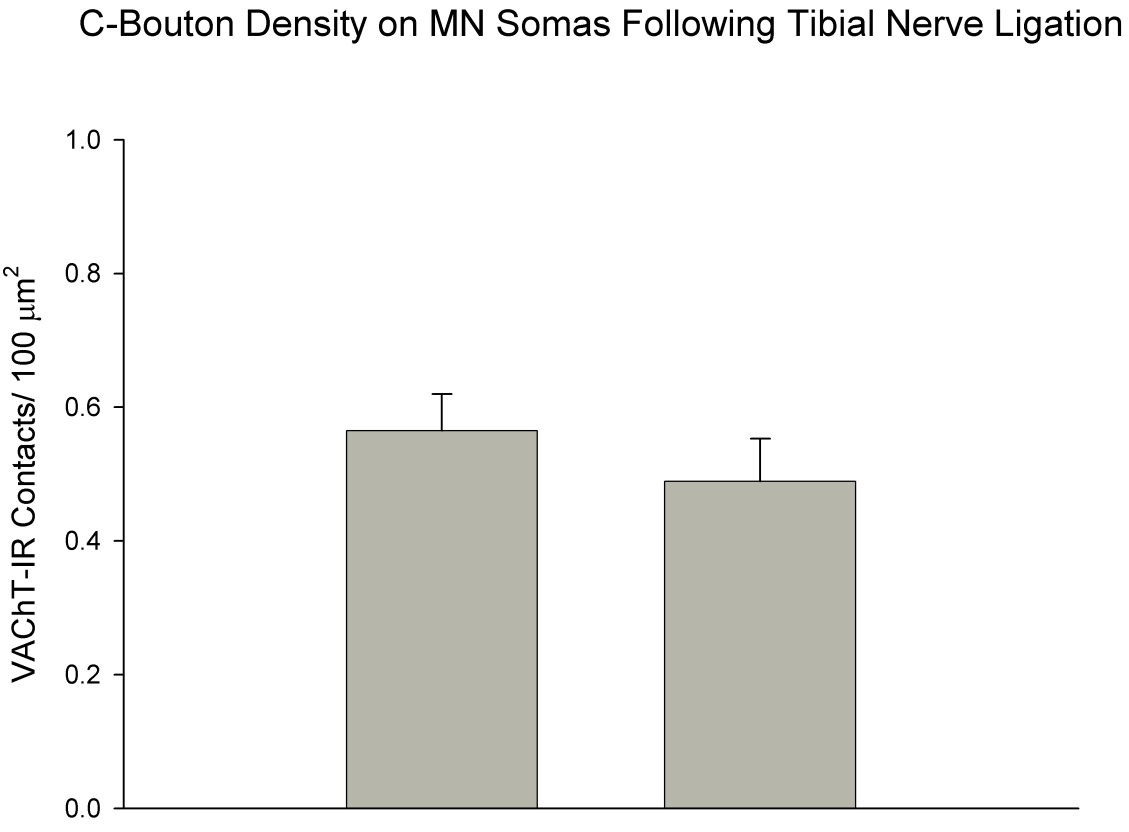
C-Bouton Density on MN Somas Following Tibial Nerve Ligation
VAChT-IR Contacts/ 100 μm2
1.0
0.8
0.6
0.4
0.2
0.0

Figure 10. Density of C-Boutons on rat lumbar motoneuron somas. The x-axis lists the different experimental groups. The y-axis represents the C-boutons (VAChT-IR contacts) per 100 μm^2. Following a 2 week ligation (0.565 ± 0.155 SD, n=11 cells, 2 animals, p=0.434, t-test) the density, or number, of C-boutons per soma surface area, is not significantly different from sham surgery controls (0.489 ± 0.240, n=8 cells, 2 animals, p=0.434, t-test).

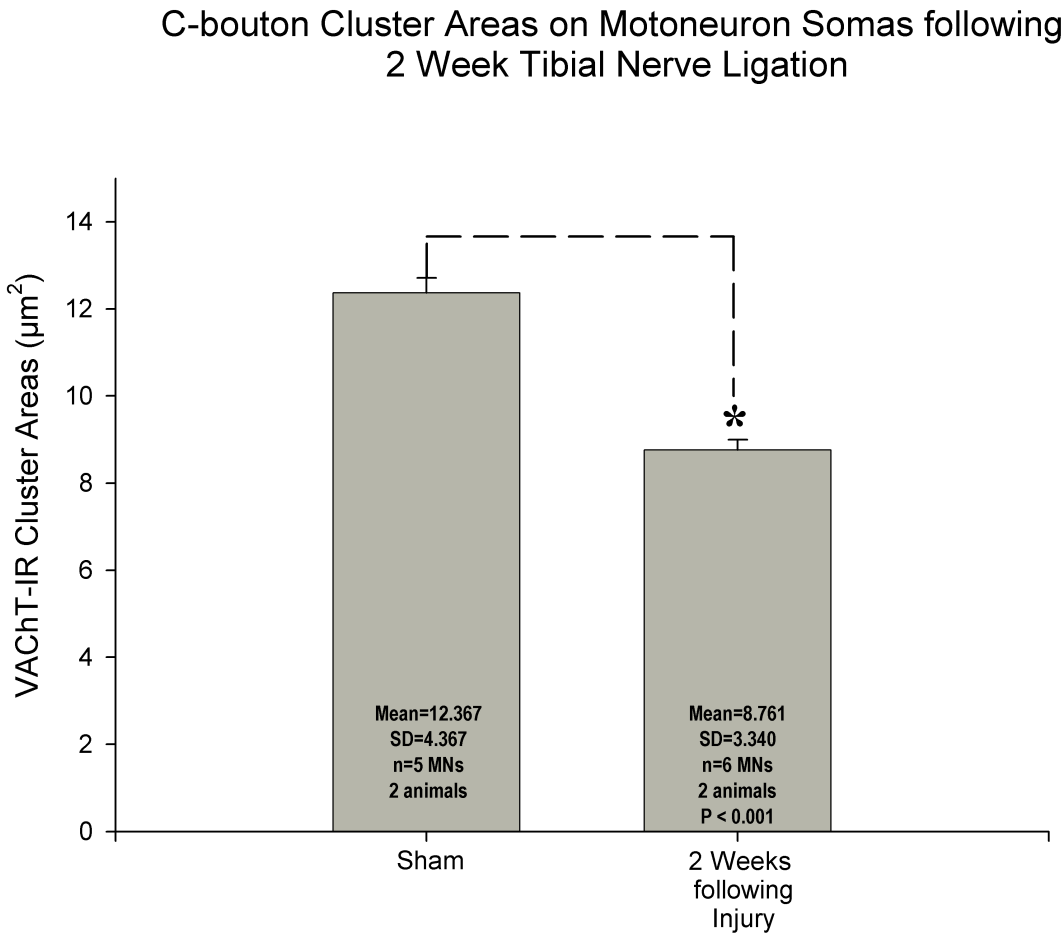
C-bouton Cluster Areas on Motoneuron Somas following
2 Week Tibial Nerve Ligation
VAChT-IR Cluster Areas (μm²)
14
12
10
8
6
4
2
0
*
Mean=12.367
SD=4.367
n=5 MNs
2 animals
Mean=8.761
SD=3.340
n=6 MNs
2 animals
P < 0.001
Sham
2 Weeks
following
Injury

Figure 11. C-bouton cluster areas (indicated by VAChT-IR) 2 weeks following tibial n. ligation. The x-axis indicates the different experimental groups. The y-axis signifies the area of VAChT-IR clusters (μm^2). The C-bouton cluster areas, 2 weeks following tibial nerve ligation, were significantly (indicated with black asterisks, $p<0.001$, t-test) smaller, as compared to sham surgery controls.

Aim 2:

Characterization of microglial and astrocytic activation in ventral horn following peripheral nerve injury

The focus of this study was to characterize the robust reaction of glia in the ventral horn of the spinal cord following tibial nerve crush, in which reinnervation of muscle is permitted, and tibial nerve ligation, in which reinnervation is prevented. The response of glia to peripheral nerve injury has already been well-characterized in the dorsal horn. Peripheral nerve injury results in many changes within the central nervous system, including the activation and proliferation of glia in the dorsal horn, as can be seen in Figures 3A and 4A. Activation of microglia occurs as these cells transform from a resting, ramified state to an amoeboid one. During this, their processes retract and get thicker, and they upregulate their immune response receptors, such as the complement receptor 3 antigen Cd11b (Zheng *et al.,* 2010; Network Glia, 2011). The Cd11b receptor is commonly used to identify activated microglia and is recognized by the OX42 antibody (Svensoon et al., 1993; Ji et al., 2008; Zheng *et al.,* 2010) (Figure 3A). The proliferative response of resident microglia has also been noted following nerve injury, as the number of microglial cells around the injury site quickly multiplies (Ajami et al., 2007; Echeverry et al., 2008; Calvo et al., 2010).

Astrocytes undergo a similar activating and proliferative response as microglia following peripheral nerve injury. Glial fibrillary acidic protein (GFAP) is the primary identifying marker of reactive astrocytes (Figure 4A). It is the major protein component of the glial filaments making up astrocytes (Eng et al., 1971; Bignami et al., 1972; Graeber and Kreutzberg 1986). An increased expression of GFAP is observed following

injury, as can be seen in Figure 4A. Astrocytes are also thought to undergo proliferation after injury (reviewed in Eddleston and Mucke, 1993; Svensson et al., 2008; Tsuda et al., 2011).

Activation of both microglia and astrocytes was determined by a significant increase in immunoreactive intensity of OX42 (OX42-IR) and GFAP (GFAP-IR), respectively, when compared to the contralateral "injury spared" side of the spinal cord (Figures 3A and 4A). The number of glia were quantified by counting the nuclei of OX42-IR and GFAP-IR glial cells within fixed regions of interest (Figure 6). For both activation (Figure 7) and proliferation, fold changes were calculated by dividing the ipsilateral injured side by the contralateral control side.

Contralateral effects have been previously described in nerve injury models (as reviewed by Koltzenburg et al., 1999; Jancalek et al., 2010). While there tends to be an increase in glia on the control side, this effect is not as robust as that which occurs on the injured side. In our models, there were subtle changes in glia numbers following injury, however, these effects were not significant (data not shown).

Glia response in rat lumbar spinal cord following peripheral nerve injury

Microglia Activation:

We first quantified a glial response, both activation and proliferation, throughout the entire lumbar spinal cord, L1-L6, in the dorsal and ventral horns, in both of our injury models. This was conducted at 2 weeks following tibial nerve injury, as we observed the greatest glial response at this time point.

Following tibial nerve crush, in which peripheral reinnervation is permitted, microglia activation, indicated by OX42-IR intensity levels, was significant from sham controls at L3-L5 in the dorsal horn (Figure 12). Increases in fold-change over the sham controls measured at 1.809 ± 0.347 SD, 1.622 ± 0.294 SD, and 1.593 ± 0.188 SD, respectively, at these spinal levels. Peak activation occurred at L3 in the dorsal horn (1.809 ± 0.347 SD). Activation levels at L4-L5 were relatively constant before dramatically decreasing at L6 (1.038 ± 0.089 SD).

Microglia activation in the ventral horn, again following tibial nerve crush, was significant from sham controls at L4 and L5, with increases in fold change of 1.446 ± 0.080 SD and 1.262 ± 0.0653 SD (Figure 12). The fold change over the sham controls remained around 1.0 in L1-L3, indicating no significant changes in microglia activation from the sham controls at these spinal levels, in the ventral horn. Peak activation of microglia occurred at L4 and steadily decreased through L6 (1.108 ± 0.111). Microglia activation at L6, in both the dorsal and ventral horns, was very similar, with a fold change of approximately 1.0. In general, the response of microglia in the dorsal horn was greater than that observed in the ventral horn, following tibial nerve crush.

Microglia activation following tibial nerve ligation, was significant from sham at L2-5, in the dorsal horn (Figure 13). Increases in fold changes measured 1.659±0.195 (L2), 1.818±0.208 (L3), 2.182±0.298 (L4), and 1.859±0.236 (L5). The microglial response steadily increased L1-4, where it peaked, with an increase of 2.182 ± 0.298 over the sham controls. A sharp decline in activation levels was observed through L5 and L6.

Following ligation in the ventral horn (Figure 13), microglia activation was significant from sham at L4 (1.763 ± 0.264) and L5 (1.806 ± 0.234) (Figure 1). Microglia

activation between spinal levels L1-L3 remained constant, with fold change values around 1.0. A dramatic increase was observed between L3-4, with a difference in fold change of approximately 0.7 between the two levels. Peak activation occurred at L5, with a slightly greater activation than that observed at L4. Microglia activation levels decreased at L6 (1.437 ± 0.304). Overall, the activation of microglia was more dramatic in the dorsal horn than in the ventral horn following tibial nerve ligation.

Microglia Proliferation:

In addition to microglia activation, the number of microglia (OX42-IR) nuclei was quantified, in both injury models. Following tibial nerve crush, significance from sham was observed at L2-L5 in the dorsal horn, with increases in fold change of 2.139 ± 0.846 (L2), 2.875 ± 0.740 (L3), 2.947 ± 0.915 (L4), and 2.269 ± (1.011) (L5) (Figure 14). A steady increase in fold change was observed from L1-L4, before decreasing at L5. The greatest increase in fold change of cell number was observed at L4. The proliferation in microglia cell numbers declines at L5, but increases at L6. The decline at L5 may be due to a limited sampling pool at this level.

In the ventral horn, following tibial nerve crush (Figure 14), significance from sham was observed at L5, with increases in fold change of 1.883 ± 0.947 (Figure 4). Very little change in microglia cell numbers, as compared to sham, was observed at L1-3, before peaking at L4 (2.975 ± 2.811). Similar to microglia cell numbers in the ventral horn, a decrease in cell number was observed at L5 before increasing again at L6 (2.967 ± 2. 387). In general, the proliferation of microglia in the dorsal horn was greater than that observed in the ventral horn in the crush injury animals.

Following tibial nerve ligation, significance from sham, in cell number was observed at L4 (2.1 ± 0.593) and L5 (2.219 ± 0.258) in the dorsal horn (Figure 15). No major increases in fold change were observed between L1-3, in comparison to sham controls. A small peak in microglia cell number was observed at L5, with a decrease in the fold change of cell number observed at L6 (1.536 ± 0.911).

In the ventral horn, following tibial nerve ligation, the number of microglia observed in L1-3 was very similar to cell numbers of sham controls at these levels, with fold change values close to 1.0 (Figure 15). This parallels the cell number response seen in the dorsal horn following ligation. A dramatic increase in cell number was observed between L3-4. The most significant increase in cell number was observed at L5, with an increase in fold change over sham controls of 3.834 ± 1.539. Again, a decrease in cell number was observed at L6 (2.747 ± 0.68), just like in the dorsal horn. Overall, the response of microglia was more significant in the ventral horn than in the dorsal horn, following tibial nerve ligation.

Astrocyte Activation:

The astrocytic response, activation and proliferation, was also studied across the lumbar spinal cord in both injury models. Activation levels were measured as GFAP-IR intensity levels, and cell number proliferation was quantified as GFAP-IR nuclei. Following tibial nerve crush, astrocyte activation was significant from sham at L2-4, with increases in fold change of 1.456 ± 0.040, 1.359 ± 0.256 and 1.538 ± 0.241, respectively (Figure 16). A slight decrease in activation was observed at L5 (1.491 ± 0.063), followed by a dramatic decline at L6. Increases in fold change from sham controls were relatively constant in the dorsal horn, remaining between 1-1.5, except for at L6 (0.846 ± 0.125).

In the ventral horn, again, following tibial nerve crush, significance from sham controls was observed at L4 (1.38 ± 0.151) and L5 (1.292 ± 0.054) spinal levels (Figure 16). Minor deviations from sham numbers were observed between L1-3, with increases in fold change remaining around 1.0 (1.020 ± 0.0893, 1.050 ± 0.155, and 0.967 ± 0.037, respectively). The most significant activation of astrocytes was observed at L4 and decreased steadily through L5-6. Overall, the response of astrocytes, following tibial nerve crush, was more significant in the dorsal horn than in the ventral horn.

Following tibial nerve ligation, the activation of astrocytes in the dorsal horn was significant only at L6 (1.256 ± 0.130) (Figure 17). Peak activation was observed at L5, with an increase in fold change of 1.442 ± 0.366 from sham controls. Astrocytic activation following ligation remained relatively constant throughout the lumbar dorsal horn, with increases in fold change ranging from 1.113 ± 0.319 to 1.442 ± 0.366, in comparison to sham controls.

Following tibial nerve ligation, the activation of astrocytes in the ventral horn was significant from sham at L4 (1.413 ± 0.460), L5 (1.483 ± 0.177) and L6 (1.385 ± 0.403) (Figure 17). Only minor increases in activation were observed between spinal levels L1-L3, with fold change values ranging from 1.023 ± 0.133 to 1.169 ± 0.296. The greatest increase in activation was observed at L5, with an increase in fold change of 1.482 ± 0.177. In general, the activation of astrocytes in the ventral horn was slightly greater than that observed in the dorsal horn.

Astrocyte Proliferation:

Following tibial nerve crush, significance from sham was observed at L1 (2.452 ± 1.378) and L4 (1.944 ± 0.419) (Figure 18), with a peak in proliferation was observed at

L1. A slight decrease in astrocyte activation was observed between L4 and L5, followed by a large decrease at L6 (0.914 ± 0.687).

In the ventral horn, following tibial nerve crush, significance from sham was observed at L2-5, with increases in fold change of 2.4 ± 1.039, 1.806 ± 0.835, 1.606 ± 0.248, and 2.222 ± 0.948 (Figure 18). Peak activation was observed at L2; however, this could be due to a limited sampling pool. A dramatic increase in the fold change of cell number over control was observed at L5, before declining at L6, with a fold change of only 1.452 ± 0.168. In general, the proliferation of astrocytes in the dorsal horn and ventral horn was very similar.

Following tibial nerve ligation, astrocyte cell number in the dorsal horn was significant from sham at L1 (1.712 ± 0.787), L2 (1.781 ± 0.953), L4 (1.655 ± 0.834) and L6 (1.855 ± 0.422) (Figure 19). Increases in fold change over the control remained relatively constant throughout the lumbar dorsal horn, ranging from 1.336 ± 0.626 to 1.855 ± 1.322. An usual peak of activation was observed at L6 (1.855 ± 1.322).

In the ventral horn, following tibial nerve ligation, significance from sham was observed at L3 (1.361 ± 0.552), L4 (2.715 ± 1.779) and L5 (2.252 ± 1.392) (Figure 19). Fold changes over sham controls remained relatively constant at L1-3, with values around 1.0. A dramatic increase in fold change was observed at L4, decreasing afterwards through L5 and L6 (1.261 ± 0.422). Overall, the response of astrocytes in the ventral horn, following ligation, was more significant than that in the dorsal horn.

Overall, the microglial and astrocytic response observed in the dorsal horn following nerve injury are consistent with published reports. The response of the glia to levels beyond that of where most tibial n. neurons are located is typical. Nerve injury is

often seen to project to spinal levels beyond those of the injured nerves (Ikeda et al., 2011). This is especially seen with sensory neurons, whose terminals can terminate at multiple levels of the spinal cord (Persson et al., 1995). The greatest amount of glia activation was generally observed in the L4 and L5 spinal levels. This data are consistent with where most of the motoneuron somas that compose the tibial nerve are known to reside. Because we have peak activation in these regions, we directed the remaining analysis in the section to just L4 and L5.

Microglia respond to nerve injury within hours, mainly thought to play a macrophaging role in removing degenerating terminals. Studies have reported microglial responses occurring within hours after injury, usually peaking between 3-7 days. The response is sustained through day 14 and generally returns to normal levels 4 weeks after injury (Echeverry et al., 2007; Tanga et al., 2004). Astrocytes are believed to be activated by microglia, but still have responses to injury as early as day 1, though the response is typically less dramatic than the microglial response in the dorsal horn (Graeber and Kreutzberg, 1988; Eriksson et al., 1993; Eriksson et al., 1997; Hajos et al., 1997; Persson et al., 1995). The glial responses observed in the dorsal horn in this study are consistent with other studies and confirm the validity of our animal models and antibodies used.

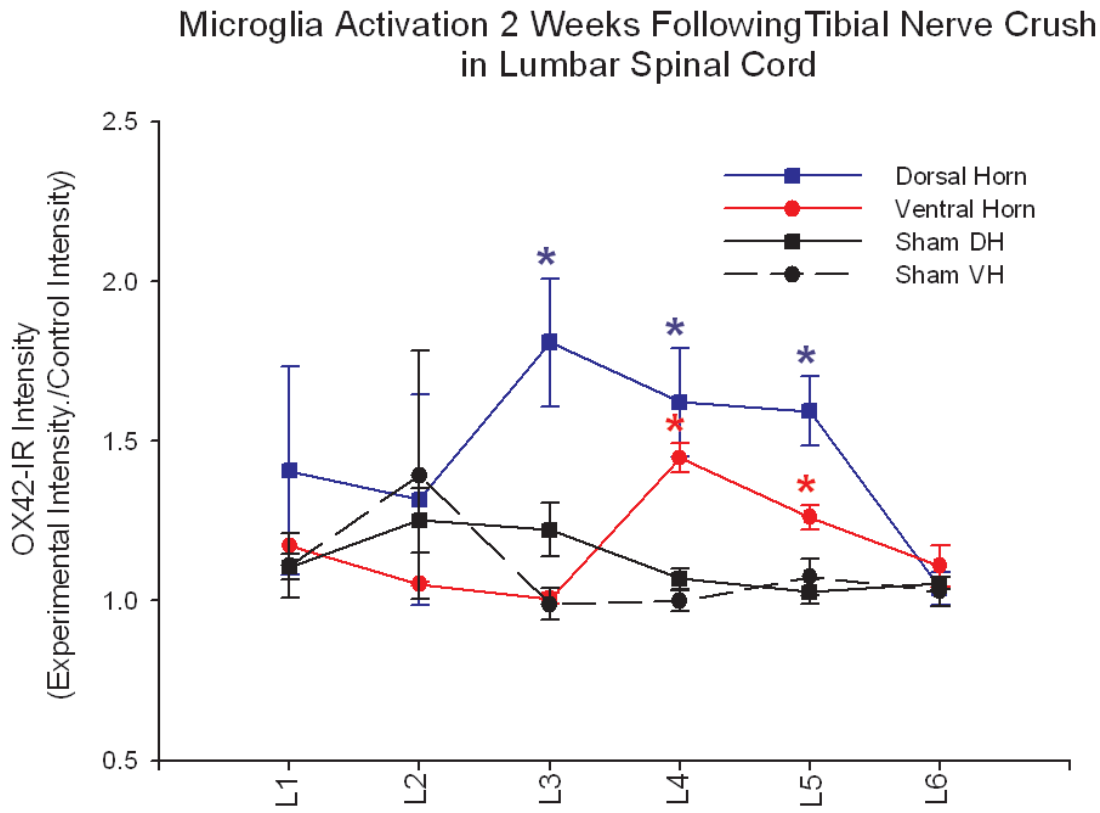
Microglia Activation 2 Weeks FollowingTibial Nerve Crush
in Lumbar Spinal Cord
OX42-IR Intensity
(Experimental Intensity./Control Intensity)
2.5
2.0
1.5
1.0
0.5
Dorsal Horn
Ventral Horn
Sham DH
Sham VH
L1
L2
L3
L4
L5
L6

Figure 12. Microglia activation, indicated as OX42-IR intensity levels, per lumbar spinal level, 2 weeks following tibial n. crush. The x-axis lists each of the spinal levels in the lumbar region of the spinal cord, L1-6. The y-axis represents the fold change in OX42-IR intensity levels (measured as experimental OX42-IR intensity/control OX42-IR intensity). In the dorsal horn significance (indicated by blue asterisks, $p<0.05$, t-test) from sham surgery controls was observed at L3-5. In the ventral horn, significance (indicated by red asterisks, $p<0.05$, t-test) from sham was observed at L4-5.

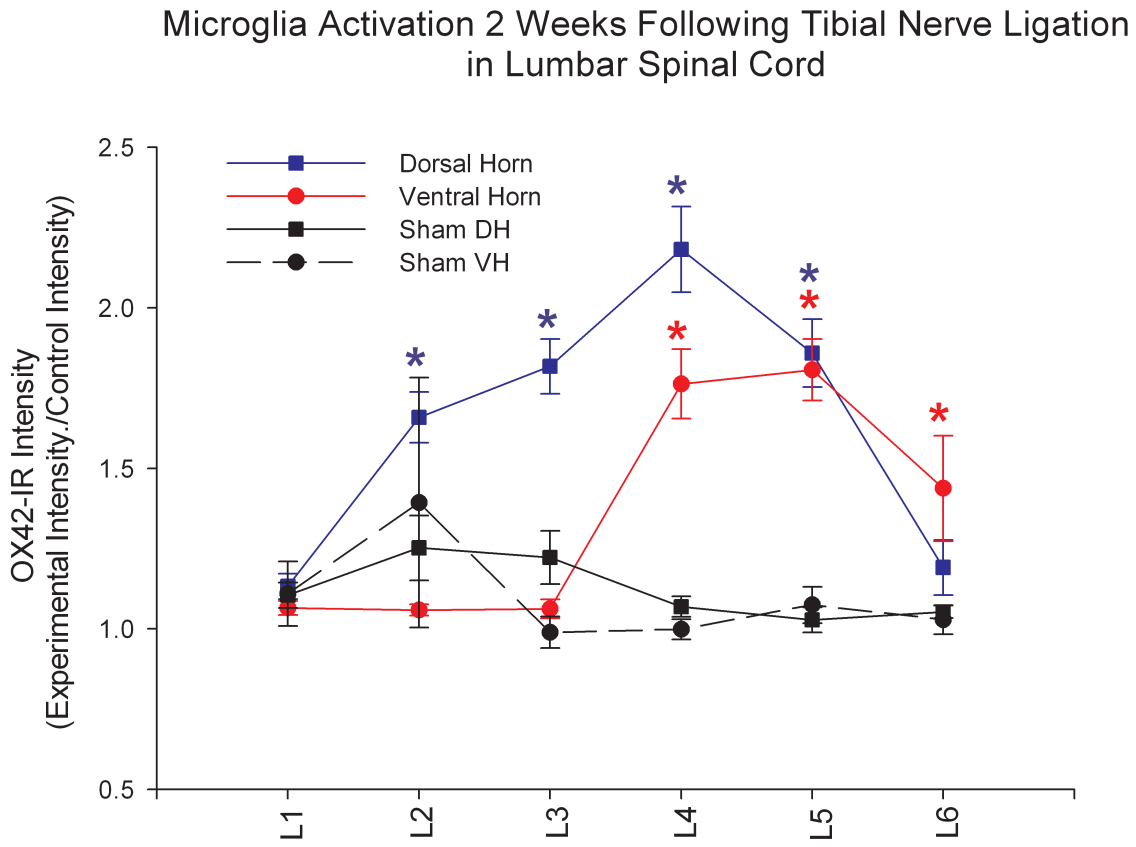
Microglia Activation 2 Weeks Following Tibial Nerve Ligation
in Lumbar Spinal Cord
OX42-IR Intensity
(Experimental Intensity./Control Intensity)
2.5
2.0
1.5
1.0
0.5
Dorsal Horn
Ventral Horn
Sham DH
Sham VH
L1
L2
L3
L4
L5
L6

Figure 13. Microglia activation, indicated as OX42-IR intensity levels, per lumbar spinal level, 2 weeks following tibial n. ligation. The x-axis lists each of the spinal levels in the lumbar region of the spinal cord, L1-6. The y-axis represents the fold change in OX42-IR intensity levels (measured as experimental OX42-IR intensity/control OX42-IR intensity). In the dorsal horn significance (indicated by blue asterisks, $p<0.05$, t-test) from sham surgery controls was observed at L2-5. In the ventral horn, significance (indicated by red asterisks, $p<0.05$, t-test) from sham was observed at L4-6.

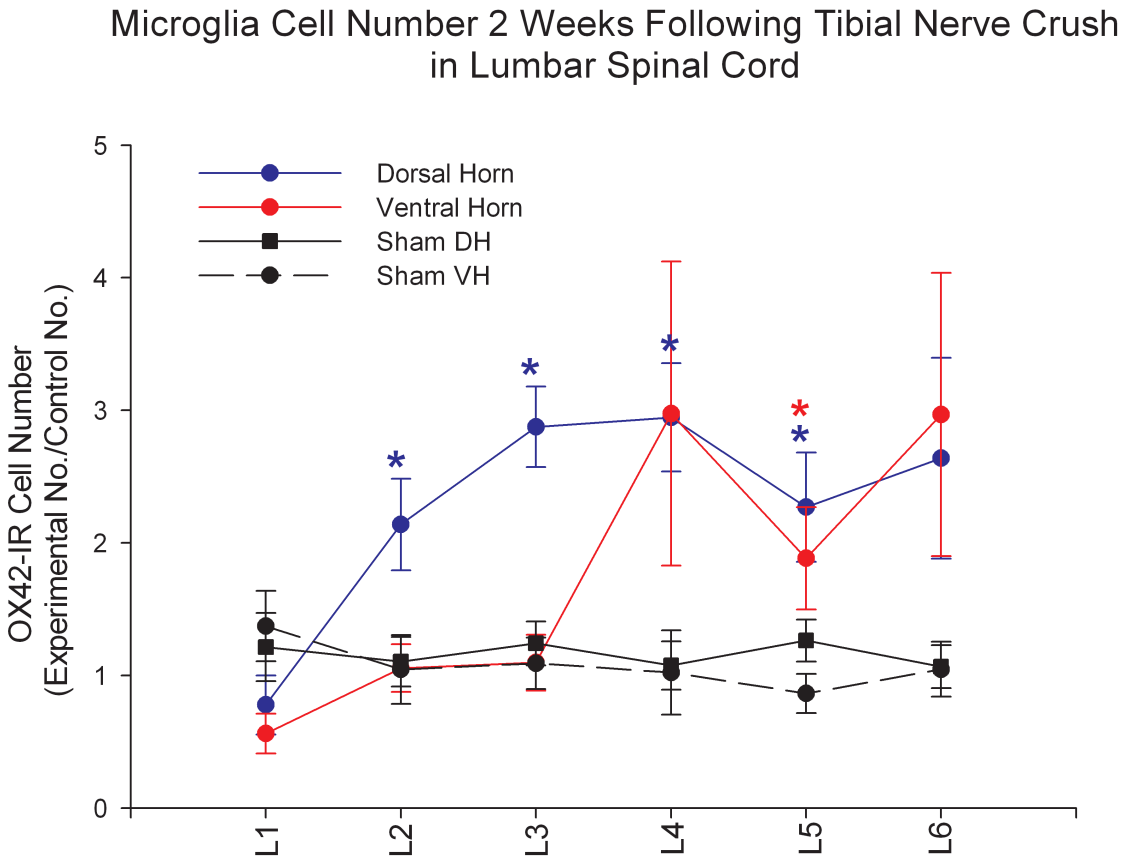
Microglia Cell Number 2 Weeks Following Tibial Nerve Crush
in Lumbar Spinal Cord
OX42-IR Cell Number
(Experimental No./Control No.)
Dorsal Horn
Ventral Horn
Sham DH
Sham VH
0
1
2
3
4
5
L1
L2
L3
L4
L5
L6
*
*
*
*
*
*

Figure 14. Microglia proliferation, indicated as OX42-IR, per lumbar spinal level, 2 weeks following tibial n. crush. The x-axis lists each of the spinal levels in the lumbar region of the spinal cord, L1-6. The y-axis represents the fold change in OX42-IR cells (measured as experimental cell number/control cell number). In the dorsal horn, there is a significant (indicated by blue asterisks, $p<0.05$, t-test) increase in the number of microglia at L2-5, in comparison to sham surgery controls. In the ventral horn, a significant (indicated by red asterisks, $p<0.05$, t-test) increase, from sham, in microglia cell numbers was observed at L5.

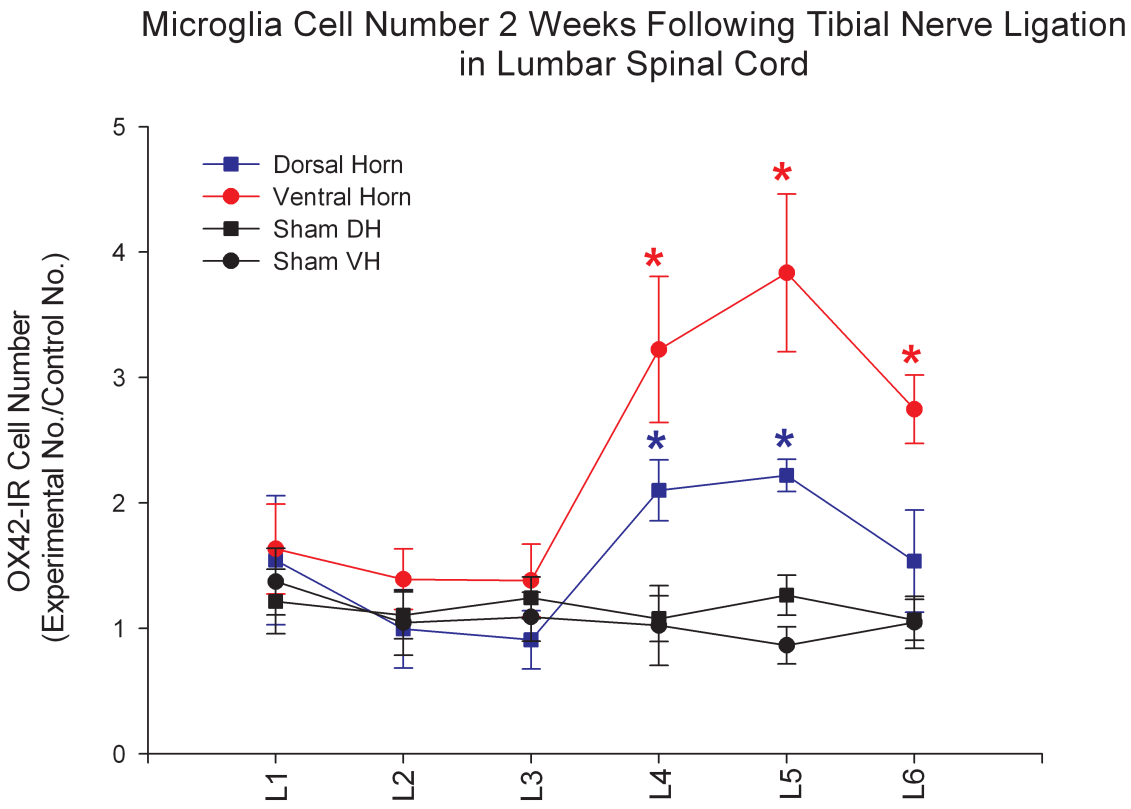
Microglia Cell Number 2 Weeks Following Tibial Nerve Ligation
in Lumbar Spinal Cord
OX42-IR Cell Number
(Experimental No./Control No.)
Dorsal Horn
Ventral Horn
Sham DH
Sham VH
0
1
2
3
4
5
L1
L2
L3
L4
L5
L6
*

Figure 15. Microglia proliferation, indicated as OX42-IR, per lumbar spinal level, 2 weeks following tibial n. ligation. The x-axis lists each of the spinal levels in the lumbar region of the spinal cord, L1-6. The y-axis represents the fold change in OX42-IR cells (measured as experimental cell number/control cell number). In the dorsal horn, there is a significant (indicated by blue asterisks, $p<0.05$, t-test) increase in the number of microglia at L4-5, in comparison to sham surgery controls. In the ventral horn, a significant (indicated by red asterisks, $p<0.05$, t-test) increase, from sham, in microglia cell numbers was observed at L4-6.

Astrocyte Activation 2 Weeks FollowingTibial Nerve Crush
in Lumbar Spinal Cord

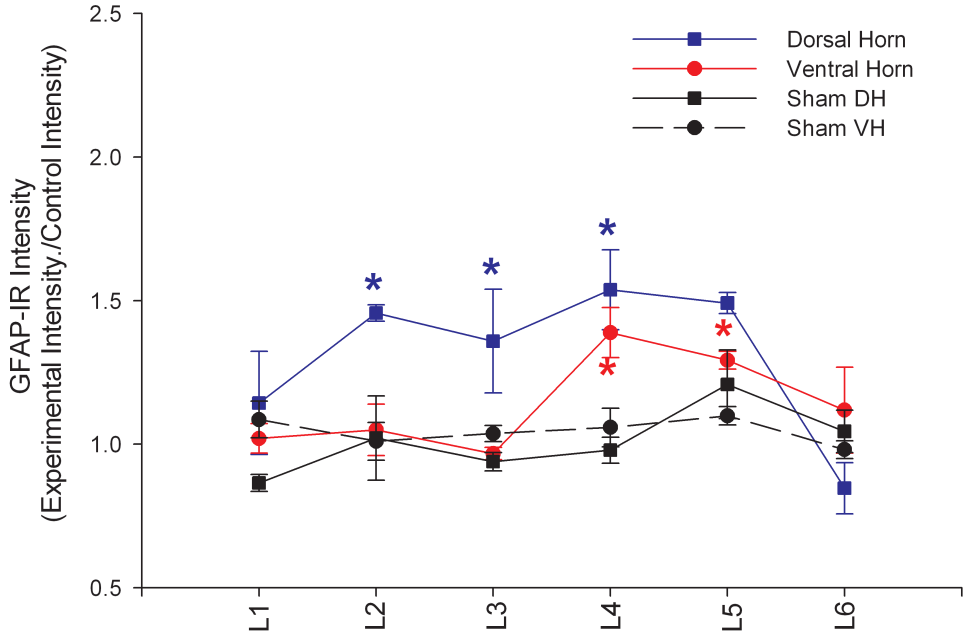

Figure 16. Astrocyte activation, indicated as GFAP-IR intensity levels, per lumbar spinal level, 2 weeks following tibial n. crush. The x-axis lists each of the spinal levels in the lumbar region of the spinal cord, L1-6. The y-axis represents the fold change in GFAP-IR intensity levels (measured as experimental GFAP-IR intensity/control GFAP-IR intensity). In the dorsal horn significance (indicated by blue asterisks, $p<0.05$, t-test) from sham surgery controls was observed at L2-4. In the ventral horn, significance (indicated by red asterisks, $p<0.05$, t-test) from sham was observed at L4-5.

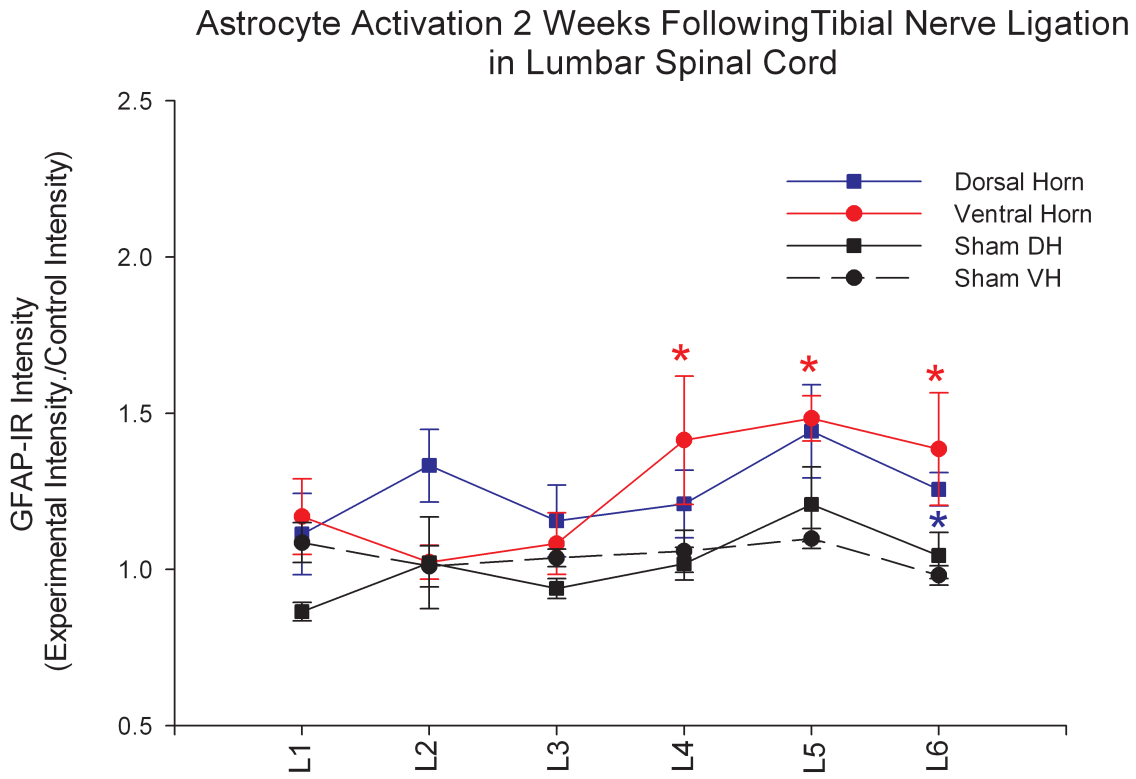
Astrocyte Activation 2 Weeks FollowingTibial Nerve Ligation
in Lumbar Spinal Cord
GFAP-IR Intensity
(Experimental Intensity./Control Intensity)
2.5
2.0
1.5
1.0
0.5
L1
L2
L3
L4
L5
L6
Dorsal Horn
Ventral Horn
Sham DH
Sham VH
*
*
*
*

Figure 17. Astrocyte activation, indicated as GFAP-IR intensity levels, per lumbar spinal level, 2 weeks following tibial n. ligation. The x-axis lists each of the spinal levels in the lumbar region of the spinal cord, L1-6. The y-axis represents the fold change in GFAP-IR intensity levels (measured as experimental GFAP-IR intensity/control GFAP-IR intensity). In the dorsal horn significance (indicated by blue asterisks, $p<0.05$, t-test) from sham surgery controls was observed at L6. In the ventral horn, significance (indicated by red asterisks, $p<0.05$, t-test) from sham was observed at L4-6.

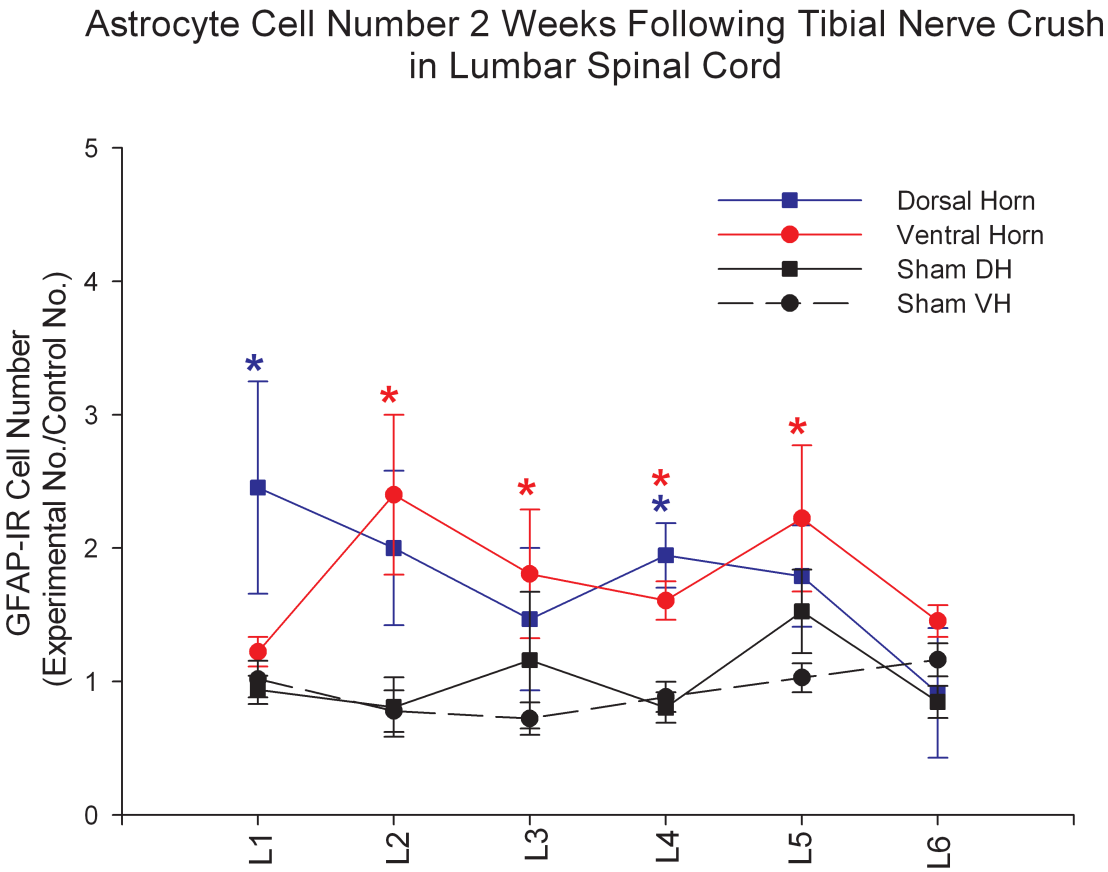
Astrocyte Cell Number 2 Weeks Following Tibial Nerve Crush
in Lumbar Spinal Cord
GFAP-IR Cell Number
(Experimental No./Control No.)
0
1
2
3
4
5
L1
L2
L3
L4
L5
L6
Dorsal Horn
Ventral Horn
Sham DH
Sham VH
*

Figure 18. Astrocyte proliferation, indicated as GFAP-IR, per lumbar spinal level, 2 weeks following tibial n. crush. The x-axis lists each of the spinal levels in the lumbar region of the spinal cord, L1-6. The y-axis represents the fold change in GFAP-IR cells (measured as experimental cell number/control cell number). In the dorsal horn, there is a significant (indicated by blue asterisks, $p<0.05$, t-test) increase in the number of astrocytes at L1 and L4, in comparison to sham surgery controls. In the ventral horn, a significant (indicated by red asterisks, $p<0.05$, t-test) increase from sham, in astrocyte cell numbers was observed at L2-5.

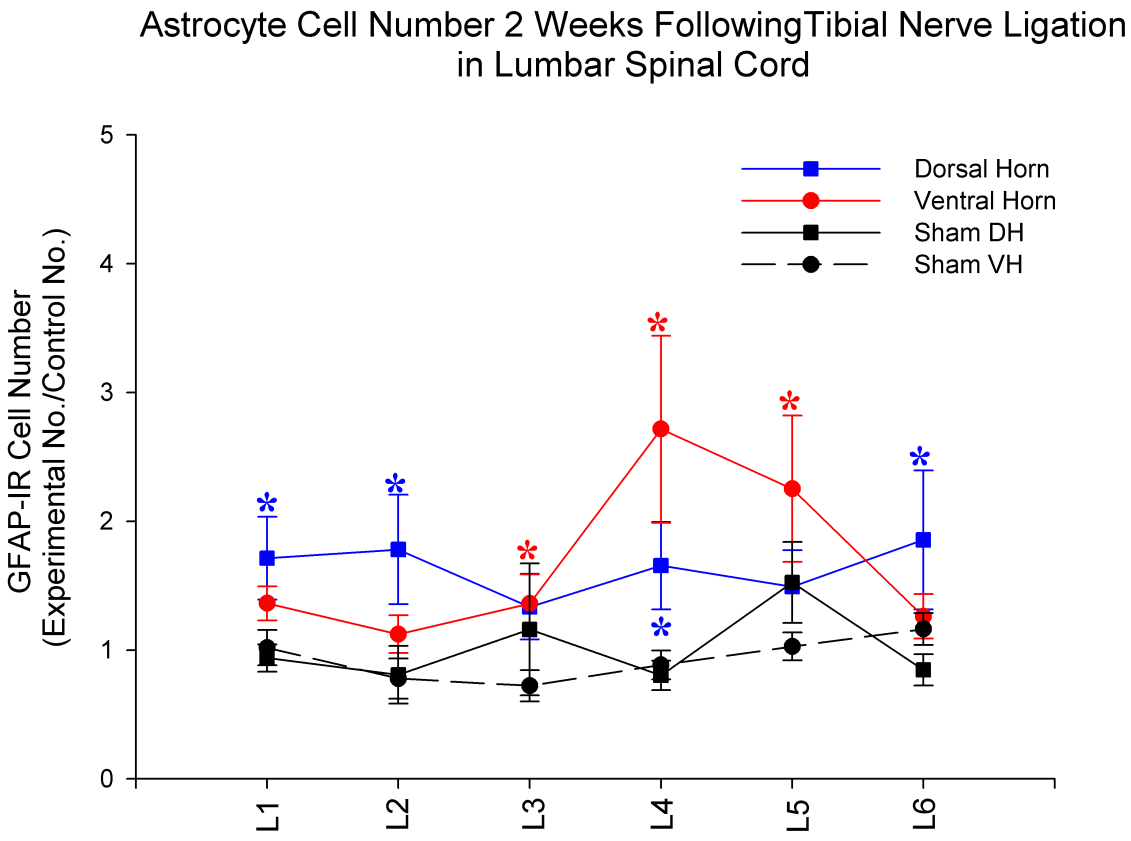
Astrocyte Cell Number 2 Weeks FollowingTibial Nerve Ligation
in Lumbar Spinal Cord
GFAP-IR Cell Number
(Experimental No./Control No.)
0
1
2
3
4
5
L1
L2
L3
L4
L5
L6
Dorsal Horn
Ventral Horn
Sham DH
Sham VH

Figure 19. Astrocyte proliferation, indicated as GFAP-IR, per lumbar spinal level, 2 weeks following tibial n. ligation. The x-axis lists each of the spinal levels in the lumbar region of the spinal cord, L1-6. The y-axis represents the fold change in GFAP-IR cells (measured as experimental cell number/control cell number). In the dorsal horn, there is a significant (indicated by blue asterisks, $p<0.05$, t-test) increase in the number of astrocytes at L1-2, L4 and L6, in comparison to sham surgery controls. In the ventral horn, a significant (indicated by red asterisks, $p<0.05$, t-test) increase from sham, in astrocyte cell numbers was observed at L3-5.

Time course of glial response in rat lumbar spinal cord following peripheral nerve injury in the Dorsal Horn

The next aim was to determine the timecourse glial response to peripheral nerve injury in the ventral horn. Since the significant glial responses were consistently occurring in the L4 and L5 regions of the spinal cord (see *Glial Response in Rat Lumbar Spinal Cord following Peripheral Nerve Injury*), we focused our time course study to these spinal levels. In doing so, the response in the dorsal horn was characterized first, as this has previously been published in many studies pertaining to neuropathic pain (reviewed in Eddleston and Mucke, 1993; Svensson et al., 2003; Echeverry et al., 2007; Tsuda et al., 2011). As such, the data we acquired from the dorsal horn was used an internal control, validating our rat models and experimental techniques.

To characterize the glial response in the dorsal horn, the activation intensity and cell number of microglia and astrocytes, following peripheral nerve injury, was determined and compared to the contralateral control dorsal horn. This was conducted in the L4-5 region of the spinal cord, following tibial n. crush and tibial n. ligation, at 3 days, 1 week, 2 weeks, 4 weeks, and 3 months. Furthermore, to ensure that a contralateral glial response was not occurring, the contralateral control side of each animal was also compared to 3-day and 1-week sham animals, as well as two naïve animals, which did not undergo any surgeries or CTB injections. No significance was detected between the contralateral control side, the sham animals or the naïve animals (data not shown).

Microglia Activation

Microglia activation in the L4-5 dorsal horn, following tibial nerve crush, indicated by OX42-IR intensity levels, was significant from sham controls (1.036 ±

0.114) at 1 and 2 weeks post-injury, with increases in fold change of 1.691 ± 0.235 and 1.608 ± 0.221 over sham, respectively (Figure 20). An increase in activation was initially observed 3 days following axotomy, with a fold change increase of 1.414 ± 0.222 over sham. The response decreased slightly at 4 weeks and almost returned to sham levels by 3 months (1.116 ± 0.088) following injury. OX42-IR intensity levels at 1-week were slightly greater than those at 2-weeks. Slight decreases in microglia activation were observed between weeks 1 and 2, and between weeks 2 and 4.

Following tibial nerve ligation, microglia activation showed significance from sham at 1, 2 and 4 weeks after nerve injury, with increases in fold change of 1.930 ± 0.388, 2.020 ± 0.305, and 1.605 ± 0.266, respectively (Figure 21). The most significant change in microglia activation occurred at 2 weeks post-ligation, only slightly greater than the activation observed at 1 week. Microglia activation was almost back to sham levels at 3 months post-ligation (1.127 ± 0.251).

Microglia Proliferation

The fold change in the number of microglia cells following tibial nerve crush was significant from sham numbers (1.247 ± 0.440) at 3 days (3.375 ± 1.046), 1 week (2.780 ± 1.052) and 2 weeks (3.113 ± 2.078) following injury (Figure 11). The number of cells returned to almost sham levels by 4 weeks post-injury (1.504 ± 0.454) and decreased below sham levels at 3 months post-axotomy (1.040 ± 0.121).

The fold change in microglial cell numbers in the dorsal horn, following tibial nerve ligation, was significant from sham at 3 days (3.150 ± 0.963), 1 week (2.814 ± 1.262) and 4 weeks (2.733 ± 1.535) post-axotomy (Figure 23). The most significant increase was observed at 3 days post-ligation. An unusual decrease was observed at 2

weeks (1.347 ± 0.836) following ligation before increasing significantly at 4 weeks. The proliferation of cells at 3 months (1.409 ± 0.534) post axotomy was slightly greater than those observed at sham.

Astrocyte Activation

The activation of astrocytes in the dorsal horn following tibial nerve crush, indicated by GFAP-IR intensities, showed significance at 1, 2 and 4 weeks post-crush, with increases in fold change over sham controls, of 1.491 ± 0.298, 1.514 ± 0.160 and 1.293 ± 0.088, respectively (Figure 24). An initial increase over sham was observed at 3 days post-crush (1.198 ± 0.206), though insignificant. Astrocyte activation levels at 1 and 2 weeks following injury are almost equal in value. Activation levels at 3 months post-axotomy (1.064 ± 0.167) are approximately similar to those of sham controls.

The activation of astrocytes in the dorsal horn following tibial nerve ligation was significant from sham at 1, 2 and 4 weeks post-ligation, with increases in fold change over the controls of 1.419 ± 0.159, 1.263 ± 0.256, and 1.317 ± 0.314, respectively (Figure 25). The most significant activation was observed at 1 week post-ligation. An initial increase in activation was observed at 3 days post-ligation, and activation levels at 2 and 4 weeks were relatively constant. The astrocytic response almost returned to basal levels (1.056 ± 0.140) at 3 months (1.141 ± 0.247). Minor deviations from sham activation levels were observed at all time points, with values of fold change ranging from 1.141 ± 0.247 to 1.419 ± 0.159.

Astrocyte Proliferation

Following tibial nerve crush in L4-5 of the dorsal horn, significance, in astrocyte cell number, from sham was observed at 2 weeks following nerve injury (1.867 ± 0.501)

(Figure 26). A small increase in fold change was observed beginning at 3 days (1.172 ± 0.399) following injury and continues until 4 weeks (1.736 ± 0.624), before returning to approximate basal levels (1.148 ± 0.686) by 3 months (1.154 ± 0.268) following injury. Gradual changes from sham were observed at all time points.

Following tibial nerve ligation, significance from sham, at L4-5 dorsal horn, was observed at 1 and 2 weeks following injury, with increases of fold change of 1.257 ± 0.488 and 2.680 ± 1.855, respectively (Figure 27). The most dramatic increase was observed at 1 week post-injury. The proliferation of astrocyte cell numbers appears to return to basal levels (1.148 ± 0.686) by 4 weeks (1.337 ± 0.653) following injury.

Overall, the microglial and astrocytic response observed in the dorsal horn following nerve injury are consistent with published reports. Microglia respond to nerve injury within hours, mainly thought to play a macrophaging role in removing degenerating terminals. Studies have reported microglial responses occurring within hours after injury, usually peaking between 3-7 days. The response is sustained through day 14 and generally returns to normal levels 4 weeks after injury (Echeverry et al., 2007; Tanga et al., 2004). Astrocytes are believed to be activated by microglia, but still have responses to injury as early as day 1, though the response is typically less dramatic than the microglial response in the dorsal horn (Graeber and Kreutzberg, 1988; Eriksson et al., 1993; Eriksson et al., 1997; Hajos et al., 1997; Persson et al., 1995). The glial responses observed in the dorsal horn in this study are consistent with other studies and confirm the validity of our animal models and antibodies used.

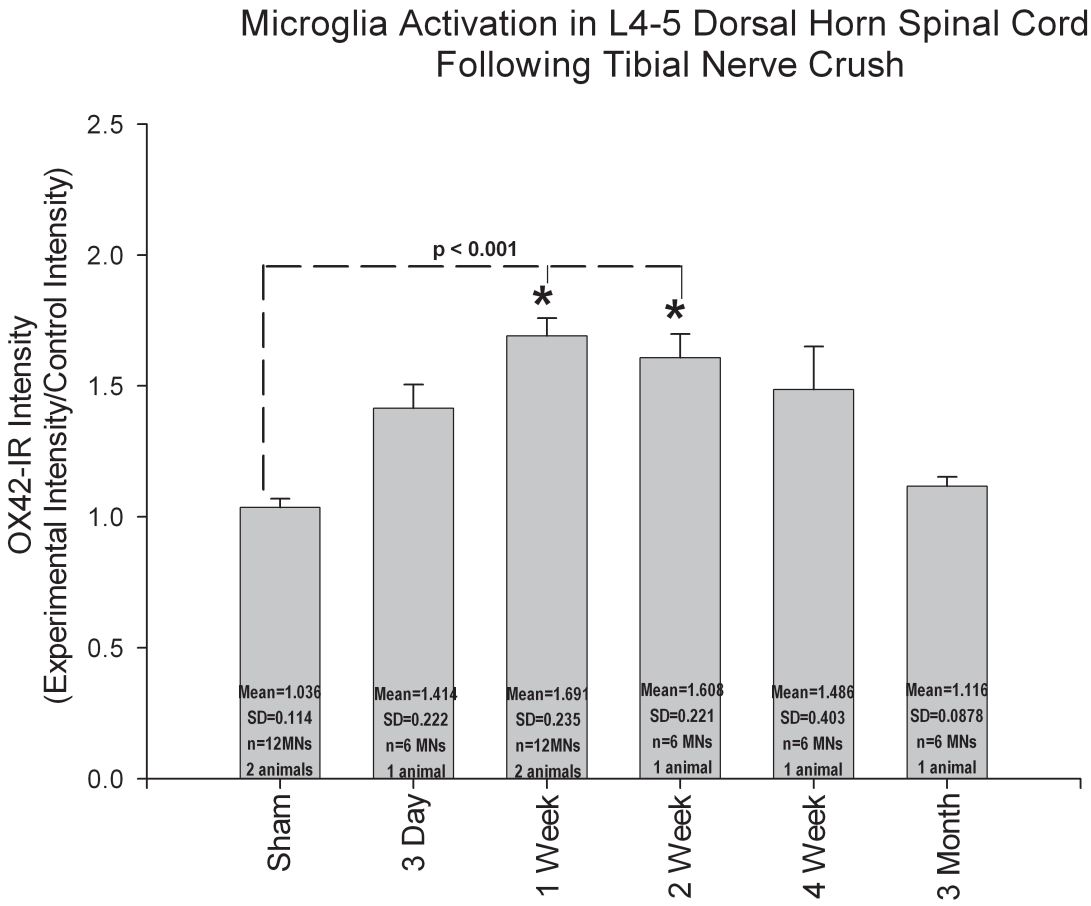
Microglia Activation in L4-5 Dorsal Horn Spinal Cord
Following Tibial Nerve Crush
OX42-IR Intensity
(Experimental Intensity/Control Intensity)
2.5
2.0
1.5
1.0
0.5
0.0
p < 0.001
*
*
Mean=1.036
SD=0.114
n=12MNs
2 animals
Mean=1.414
SD=0.222
n=6 MNs
1 animal
Mean=1.691
SD=0.235
n=12MNs
2 animals
Mean=1.608
SD=0.221
n=6 MNs
1 animal
Mean=1.486
SD=0.403
n=6 MNs
1 animal
Mean=1.116
SD=0.0878
n=6 MNs
1 animal
Sham
3 Day
1 Week
2 Week
4 Week
3 Month

Figure 20. Time course of microglia activation, indicated as OX42-IR intensity levels, in L4-5 dorsal horn of the rat spinal cord, following tibial n. crush. The x-axis represents the time course following tibial n. injury. The y-axis signifies the fold change in microglia activation (calculated as experimental OX42-IR intensity/control OX42-IR intensity). Significance (indicated with black asterisks; $p<0.001$, Anova), from sham surgery controls, was observed at 1 week and 2 weeks post tibial n. crush.

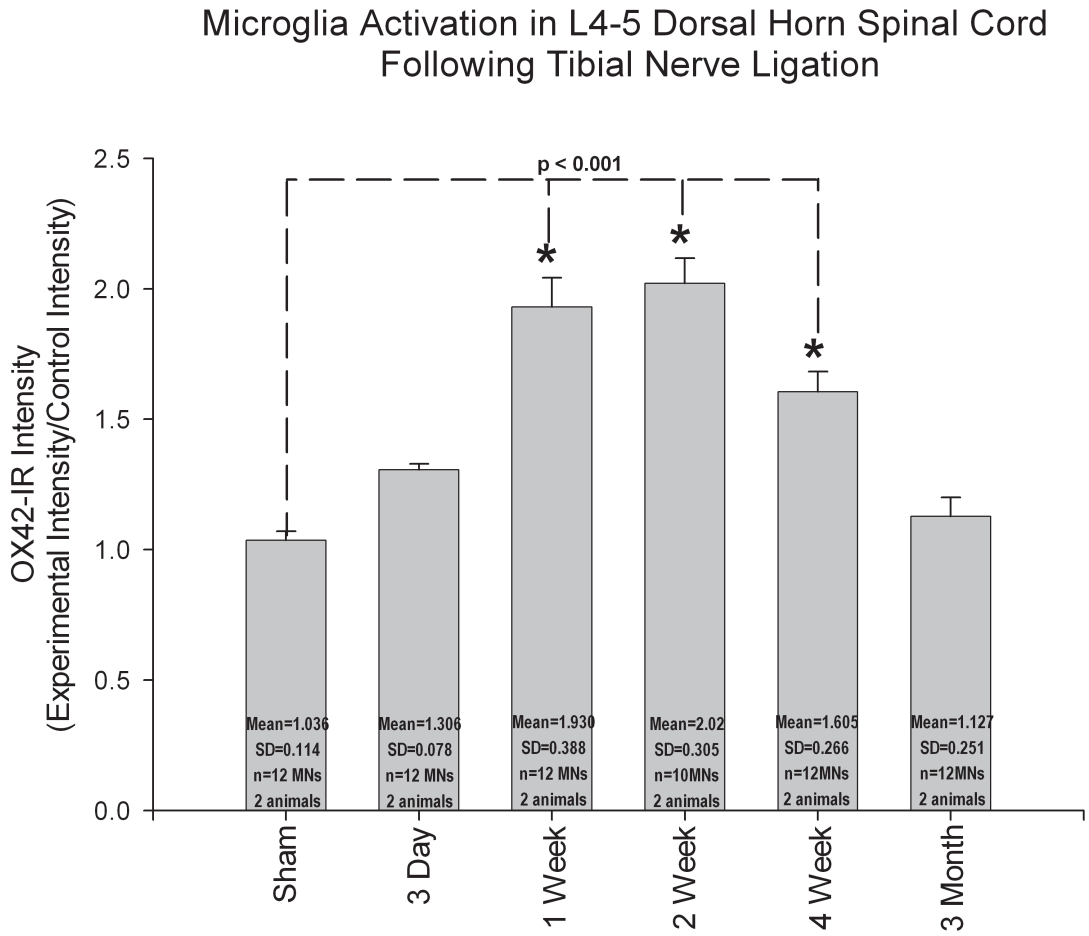
Microglia Activation in L4-5 Dorsal Horn Spinal Cord
Following Tibial Nerve Ligation
OX42-IR Intensity
(Experimental Intensity/Control Intensity)
2.5
2.0
1.5
1.0
0.5
0.0
p < 0.001
*
*
*
Mean=1.036
SD=0.114
n=12 MNs
2 animals
Mean=1.306
SD=0.078
n=12 MNs
2 animals
Mean=1.930
SD=0.388
n=12 MNs
2 animals
Mean=2.02
SD=0.305
n=10MNs
2 animals
Mean=1.605
SD=0.266
n=12MNs
2 animals
Mean=1.127
SD=0.251
n=12MNs
2 animals
Sham
3 Day
1 Week
2 Week
4 Week
3 Month

Figure 21. Time course of microglia activation, indicated as OX42-IR intensity levels, in the L4-5 dorsal horn of the rat spinal cord, following tibial n. ligation. The x-axis represents the time course following tibial n. injury. The y-axis signifies the fold change in microglia activation (calculated as experimental OX42-IR intensity/control OX42-IR intensity). Significance (indicated by black asterisks; $p<0.001$, Anova), from sham surgery controls, was observed at 1 week, 2 weeks and 4 weeks post-tibial n. ligation.

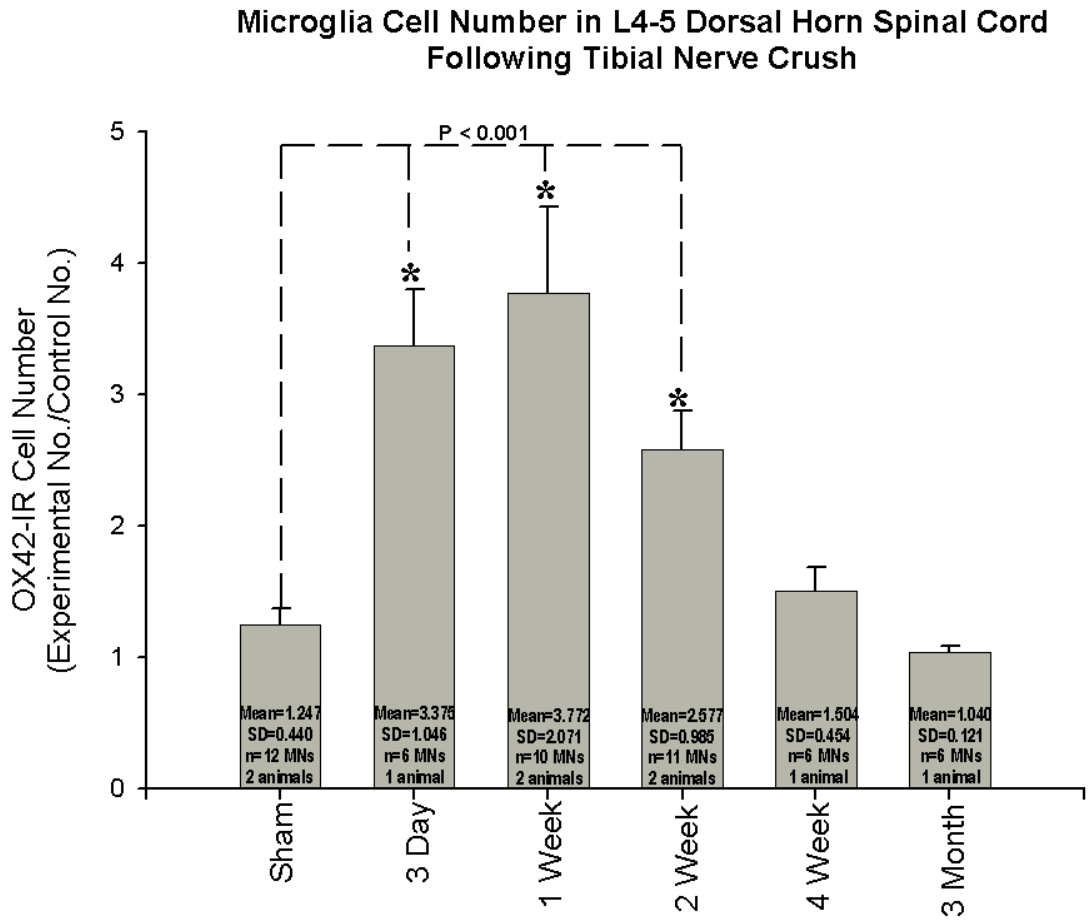
Microglia Cell Number in L4-5 Dorsal Horn Spinal Cord
Following Tibial Nerve Crush
OX42-IR Cell Number
(Experimental No./Control No.)
P < 0.001
*
*
*
Mean=1.247
SD=0.440
n=12 MNs
2 animals
Mean=3.375
SD=1.046
n=6 MNs
1 animal
Mean=3.772
SD=2.071
n=10 MNs
2 animals
Mean=2.577
SD=0.985
n=11 MNs
2 animals
Mean=1.504
SD=0.454
n=6 MNs
1 animal
Mean=1.040
SD=0.121
n=6 MNs
1 animal
0
1
2
3
4
5
Sham
3 Day
1 Week
2 Week
4 Week
3 Month

Figure 22. Time course of microglia proliferation, indicated as OX42-IR, in the L4-5 dorsal horn of the rat spinal cord, following tibial n. crush. The x-axis represents the time course following tibial n. injury. The y-axis signifies the fold change in OX42-IR cells (calculated as experimental cell number/control cell number). There is a significance (indicated by black asterisks; $p<0.001$, Anova) in the number of microglia, from sham surgery controls, at 3 days,1 week and 2 weeks following tibial nerve crush.

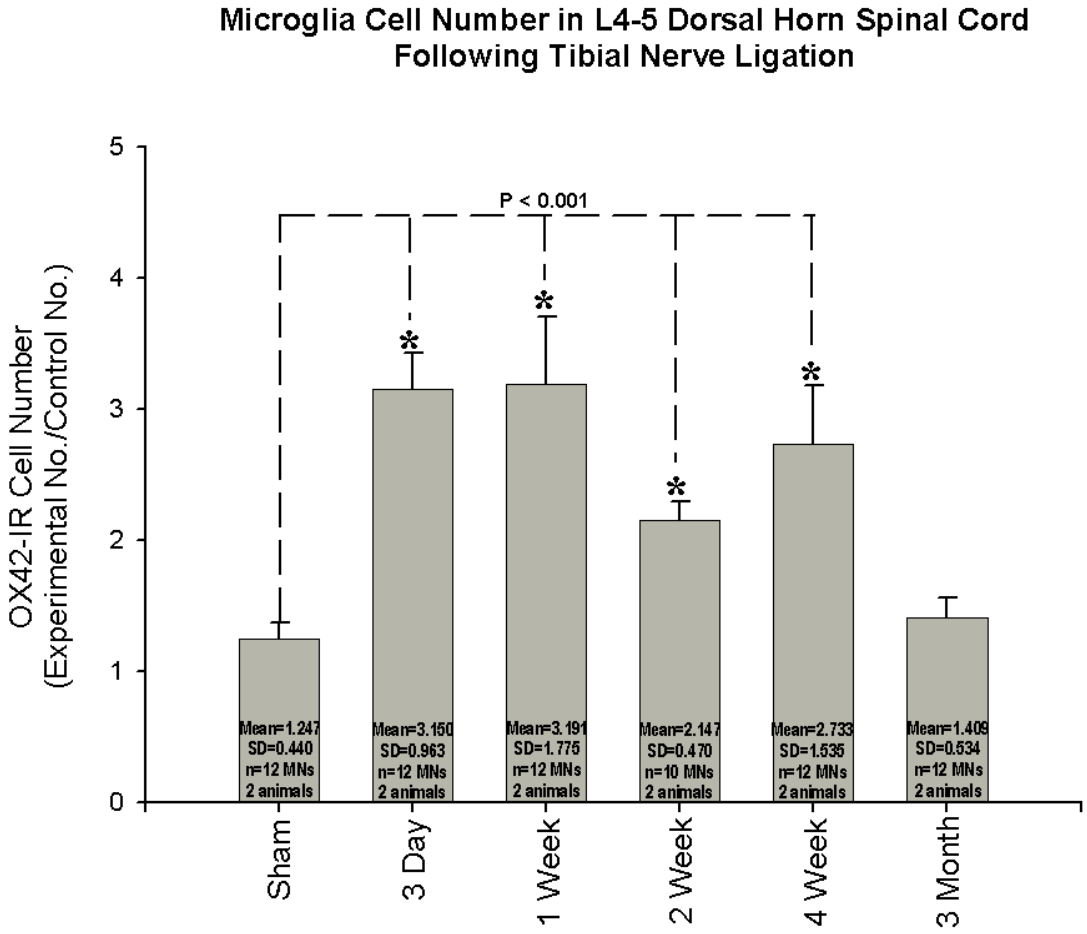
Microglia Cell Number in L4-5 Dorsal Horn Spinal Cord
Following Tibial Nerve Ligation
OX42-IR Cell Number
(Experimental No./Control No.)
P < 0.001
Mean=1.247
SD=0.440
n=12 MNs
2 animals
Mean=3.150
SD=0.963
n=12 MNs
2 animals
Mean=3.191
SD=1.775
n=12 MNs
2 animals
Mean=2.147
SD=0.470
n=10 MNs
2 animals
Mean=2.733
SD=1.535
n=12 MNs
2 animals
Mean=1.409
SD=0.534
n=12 MNs
2 animals
Sham
3 Day
1 Week
2 Week
4 Week
3 Month

Figure 23. Time course of microglia proliferation, indicated as OX42-IR, in the L4-5 dorsal horn of the rat spinal cord, following tibial n. ligation. The x-axis represents the time course following tibial n. injury. The y-axis signifies the fold change in OX42-IR cells (calculated as experimental cell number/control cell number). There is a significance (indicated by black asterisks; $p<0.001$, Anova) in the number of microglia, from sham surgery controls, at 3 days, 1 week, 2 weeks, and 4 weeks post-tibial n. ligation.

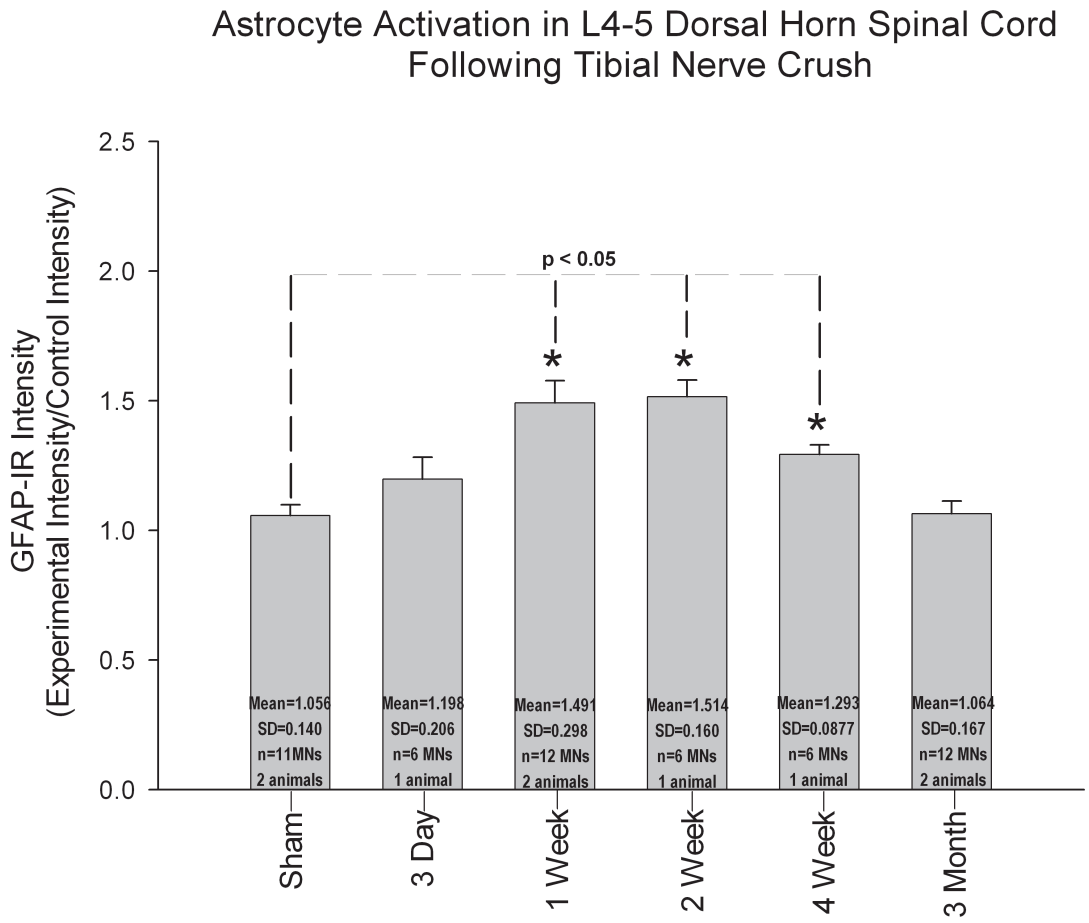
Astrocyte Activation in L4-5 Dorsal Horn Spinal Cord
Following Tibial Nerve Crush
GFAP-IR Intensity
(Experimental Intensity/Control Intensity)
2.5
2.0
1.5
1.0
0.5
0.0
p < 0.05
*
*
*
Mean=1.056
SD=0.140
n=11MNs
2 animals
Mean=1.198
SD=0.206
n=6 MNs
1 animal
Mean=1.491
SD=0.298
n=12 MNs
2 animals
Mean=1.514
SD=0.160
n=6 MNs
1 animal
Mean=1.293
SD=0.0877
n=6 MNs
1 animal
Mean=1.064
SD=0.167
n=12 MNs
2 animals
Sham
3 Day
1 Week
2 Week
4 Week
3 Month

Figure 24. Time course of astrocyte activation, indicated as GFAP-IR intensity levels, in the L4-5 dorsal horn of the rat spinal cord, following tibial n. crush. The x-axis represents the time course following tibial n. injury. The y-axis signifies the fold change in astrocyte activation (calculated as experimental GFAP-IR intensity/control GFAP-IR intensity). Significance (indicated by black asterisks; $p<0.05$, Anova), from sham surgery controls, was observed at 1 week, 2 weeks and 4 weeks post-tibial n. crush.

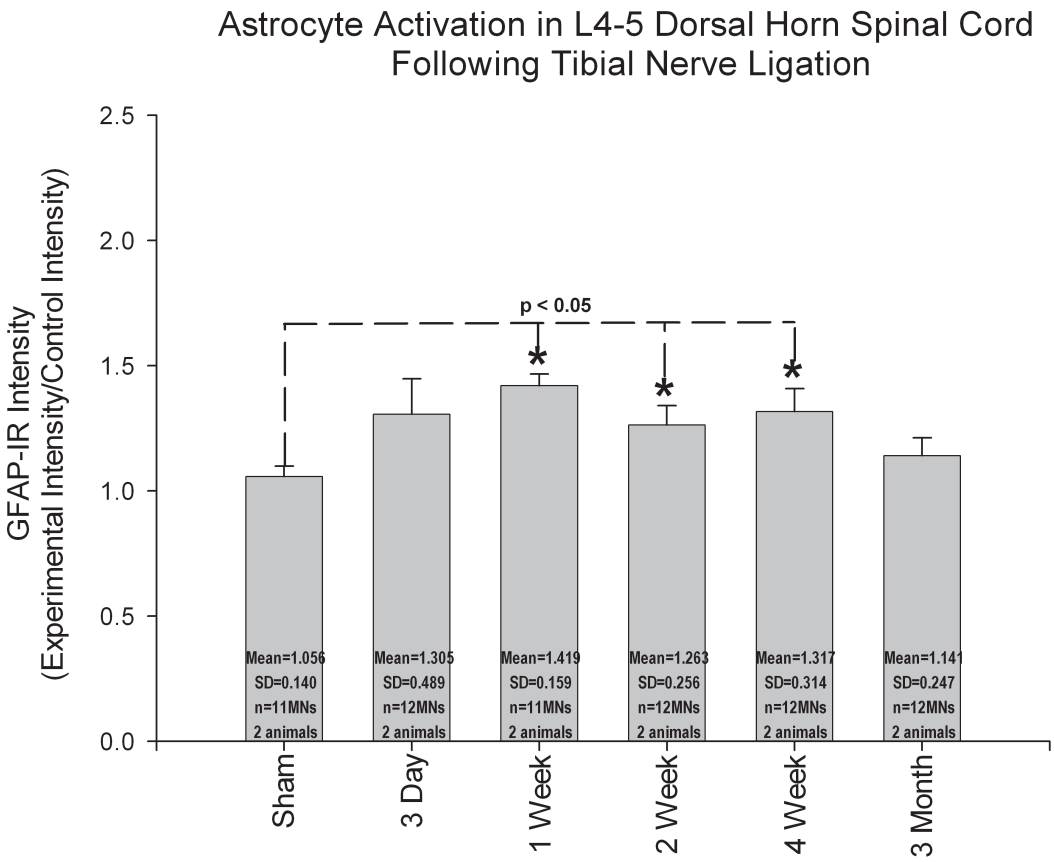
Astrocyte Activation in L4-5 Dorsal Horn Spinal Cord
Following Tibial Nerve Ligation
GFAP-IR Intensity
(Experimental Intensity/Control Intensity)
2.5
2.0
1.5
1.0
0.5
0.0
p < 0.05
*
*
*
Mean=1.056
SD=0.140
n=11MNs
2 animals
Mean=1.305
SD=0.489
n=12MNs
2 animals
Mean=1.419
SD=0.159
n=11MNs
2 animals
Mean=1.263
SD=0.256
n=12MNs
2 animals
Mean=1.317
SD=0.314
n=12MNs
2 animals
Mean=1.141
SD=0.247
n=12MNs
2 animals
Sham
3 Day
1 Week
2 Week
4 Week
3 Month

Figure 25. Time course of astrocyte activation, indicated as GFAP-IR intensity levels, in the L4-5 dorsal horn of the rat spinal cord, following tibial n. ligation. The x-axis represents the time course following tibial n. injury. The y-axis signifies the fold change in astrocyte activation (calculated as experimental GFAP-IR intensity/control GFAP-IR intensity). Significance (indicated by black asterisks; $p<0.05$, Anova), from sham surgery controls, was observed at 1, 2 and 4 weeks post-tibial nerve ligation.

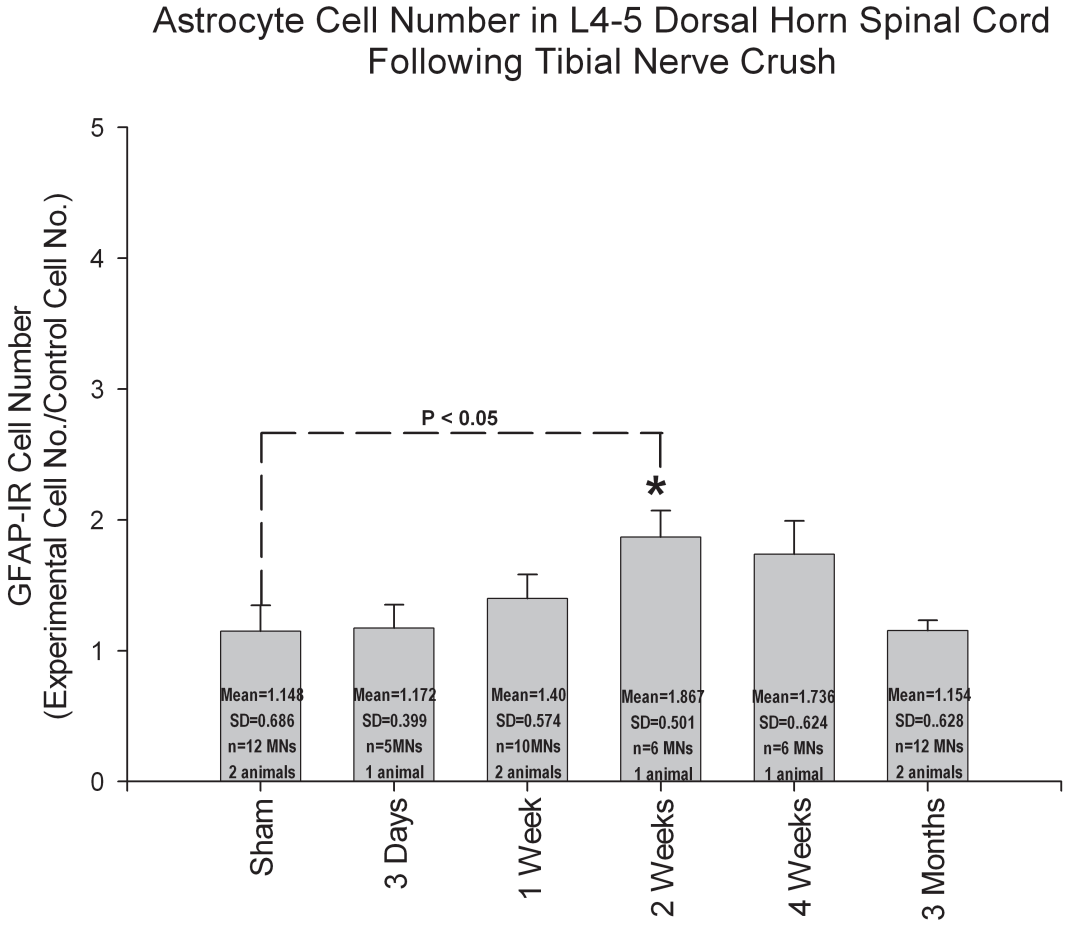
Astrocyte Cell Number in L4-5 Dorsal Horn Spinal Cord
Following Tibial Nerve Crush
GFAP-IR Cell Number
(Experimental Cell No./Control Cell No.)
5
4
3
2
1
0
P < 0.05
*
Mean=1.148
SD=0.686
n=12 MNs
2 animals
Mean=1.172
SD=0.399
n=5MNs
1 animal
Mean=1.40
SD=0.574
n=10MNs
2 animals
Mean=1.867
SD=0.501
n=6 MNs
1 animal
Mean=1.736
SD=0..624
n=6 MNs
1 animal
Mean=1.154
SD=0..628
n=12 MNs
2 animals
Sham
3 Days
1 Week
2 Weeks
4 Weeks
3 Months

Figure 26. Time course of astrocyte proliferation, indicated as GFAP-IR, in the L4-5 dorsal horn of the rat spinal cord, following tibial n. crush. The x-axis represents the time course following tibial n. injury. The y-axis signifies the fold change in GFAP-IR cells (calculated as experimental cell number/control cell number). Significance (indicated by black asterisks; $p<0.001$, Anova) in the number of astrocytes, from sham surgery controls, was observed at 2 weeks following tibial nerve crush.

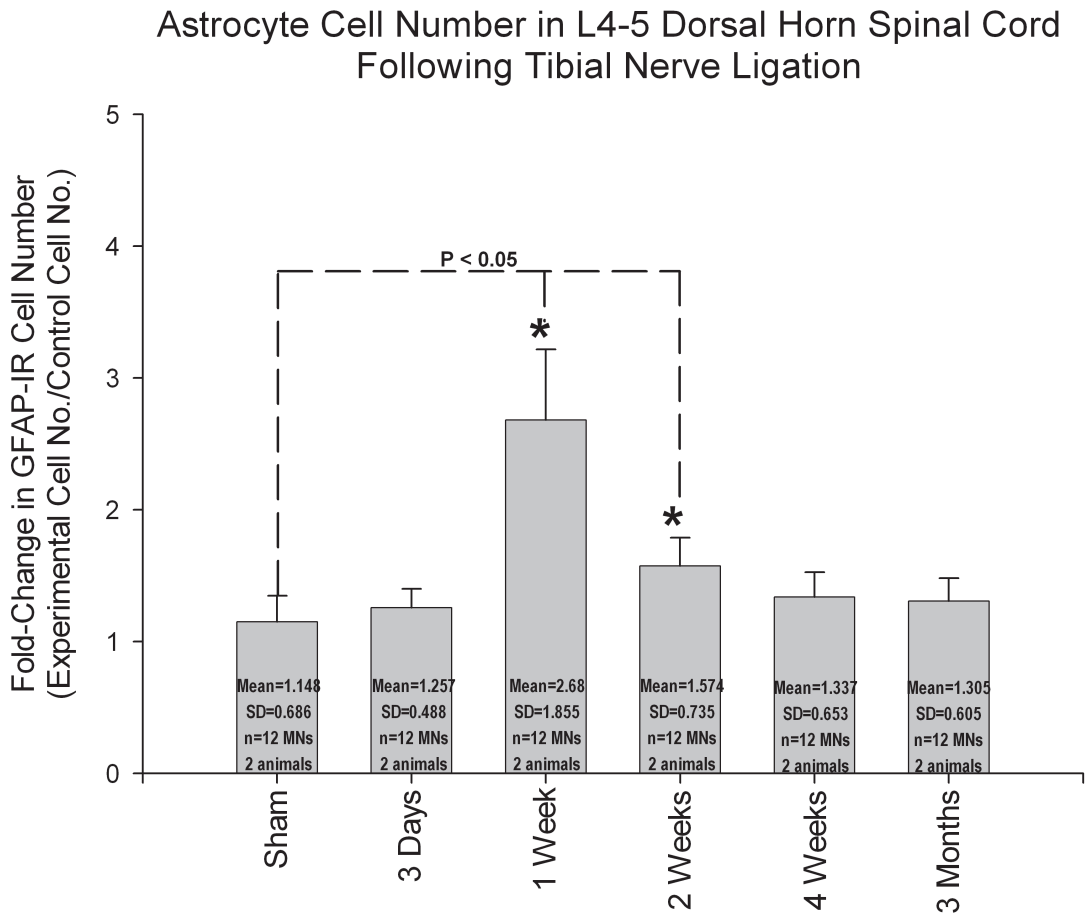
Astrocyte Cell Number in L4-5 Dorsal Horn Spinal Cord
Following Tibial Nerve Ligation
Fold-Change in GFAP-IR Cell Number
(Experimental Cell No./Control Cell No.)
5
4
3
2
1
0
P < 0.05
*
*
Mean=1.148
SD=0.686
n=12 MNs
2 animals
Mean=1.257
SD=0.488
n=12 MNs
2 animals
Mean=2.68
SD=1.855
n=12 MNs
2 animals
Mean=1.574
SD=0.735
n=12 MNs
2 animals
Mean=1.337
SD=0.653
n=12 MNs
2 animals
Mean=1.305
SD=0.605
n=12 MNs
2 animals
Sham
3 Days
1 Week
2 Weeks
4 Weeks
3 Months

Figure 27. Time course of astrocyte proliferation, indicated as GFAP-IR, in the L4-5 dorsal horn of the rat spinal cord, following tibial n. ligation. The x-axis represents the time course following tibial n. injury. The y-axis signifies the fold change in GFAP-IR cells (calculated as experimental cell number/control cell number). Significance (indicated by black asterisks; $p<0.05$, Anova) in the number of astrocytes, from sham surgery controls, was observed at 1 and 2 weeks following tibial nerve ligation.

Time course of glial response in rat lumbar spinal cord following peripheral nerve injury in Ventral Horn

Microglia Activation

The glial response in the ventral horn, where motoneurons are located, has not been studied extensively. After verifying our models through analysis of the dorsal horn, we sought to characterize the glial response to nerve injury in the ventral horn. Again, the activation intensity and cell number of astrocytes and microglia were determined after tibial nerve crush and ligation. Since most of the cell bodies of motoneurons of the tibial nerve are located in the L4-5 region of the spinal cord, our focus concentrated only in these spinal nerves.

Following tibial nerve crush, microglia activation in the ventral horn, again indicated by OX42-IR intensity levels, was significant from sham at 1 (1.395 ± 0.235) and 2 (1.354 ± 0.120) weeks post-injury in the crush model (Figure 28). The greatest activation was observed at 1 week post-axotomy, though the activation at 2 weeks was only slightly less than this. Microglia activation appeared to return to basal levels (1.036 ± 0.114) by 3 months post-injury (1.115 ± 0.186). Overall, the activation of microglia in the L4-5 ventral horn was not robust and did not show dramatic changes from sham controls.

Following tibial nerve ligation, the activation of microglia was significant from sham (1.036 ± 0.114) at 2 weeks post-ligation (1.607 ± 0.158) (Figure 29). Slight increases in fold change were observed at 3 days (1.044 ± 0.060) and 1 week (1.198 ± 0.247) post-ligation, compared to sham controls. A dramatic increase was observed at 2 weeks post-ligation. Levels of microglia activation return to sham levels by 3 months post-axotomy (1.077 ± 0.0852).

Microglia Proliferation

Following tibial nerve crush, the proliferation of microglia cells was significant from sham at 3 days (1.787 ± 1.016), 1 week (4.104 ± 1.739), 2 weeks (1.923 ± 1.171), and 4 weeks (1.235 ± 0.425) post-ligation (Figure 30). The fold change in the number of microglia at 1 week post-tibial nerve crush was approximately two-fold greater than the responses observed at 3 days and 1 week. At 3 months post-ligation (1.047 ± 0.172), the response was still greater than those of sham (0.801 ± 0.332), although not significantly.

Following tibial nerve ligation model, the proliferation of microglia cells was significant from sham at 1 week (1.395 ± 0.223), 2 weeks (1.354 ± 0.120), 4 weeks (1.231 ± 0.237), and 3 months (1.115 ± 0.186) post-ligation (Figure 20). An initial increase in cell number was observed at 3 days post-injury (1.340 ± 0.687). The most dramatic increase in fold change in the number of microglia was observed at 1 week, approximately two-fold greater than the other time points. Significance from sham was still evident at 3 months.

Astrocyte Activation

Following tibial nerve crush, the astrocytic activation in the L4-5 ventral horn, measured by GFAR-IR intenstiy, significance from sham was found at 1 (1.397 ± 0.347) and 2 (1.340 ± 0.115) weeks post-injury (Figure 32). While intensity levels at 1 and 2 weeks were almost the same, by 4-weeks (1.076 ± 0.108) post-crush, the astrocytic activation almost returned to basal levels (1.080 ± 0.112).

Following tibial nerve ligation, the activation of astrocytes in the L4-5 ventral horn was observed to be significant from sham (1.080 ± 0.112) at 2 weeks (1.567 ± 0.504) post-ligation (Figure 33). Levels of activation at 1 week (1.177 ± 0.287) and 4

weeks (1.178 ± 0.208) were just above basal levels. At 3 months post-ligation (1.078 ± 0.085), astrocyte activation was similar to those at sham levels.

Astrocyte Proliferation

Following tibial nerve crush, the proliferation of astrocytes was significant from sham at 3 days, 1 week and 2 weeks post-crush, with increases in fold change over the control of 1.561 ± 0.839, 1.403 ± 0.450, and 1.694 ± 0.897, respectively (Figure 34). The greatest increase in cell number was observed at 2 weeks post-crush and decreased steadily through 3 months post-injury. Cell numbers appeared to return to sham (0.956 ± 0.268) levels by 3 months post-injury, with a slight increase in fold change (0.986 ± 0.402).

Following tibial nerve ligation, the number of astrocytes was significant from sham (0.956 ± 0.268) at 1 week (1.594 ± 0.718) and 2 weeks (2.164 ± 1.125) post injury, with the greatest number of cells observed at 2 weeks (Figure 35). A small increase in cell number was observed at 3 days (1.104 ± 0.389) post-injury. At 3 months (1.239 ± 0.467) post-injury, the number of astrocytes remained slightly greater than those of sham controls, although not significantly.

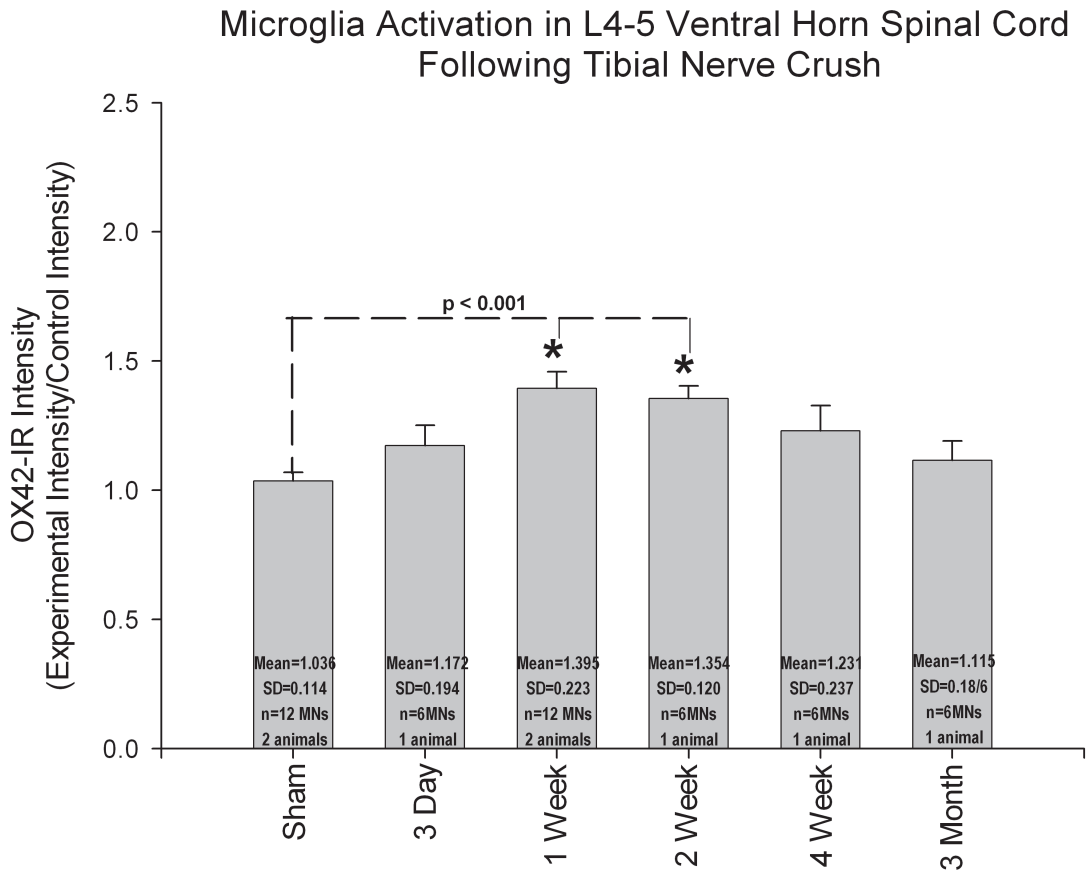
Microglia Activation in L4-5 Ventral Horn Spinal Cord
Following Tibial Nerve Crush
OX42-IR Intensity
(Experimental Intensity/Control Intensity)
2.5
2.0
1.5
1.0
0.5
0.0
p < 0.001
*
*
Mean=1.036
SD=0.114
n=12 MNs
2 animals
Mean=1.172
SD=0.194
n=6MNs
1 animal
Mean=1.395
SD=0.223
n=12 MNs
2 animals
Mean=1.354
SD=0.120
n=6MNs
1 animal
Mean=1.231
SD=0.237
n=6MNs
1 animal
Mean=1.115
SD=0.18/6
n=6MNs
1 animal
Sham
3 Day
1 Week
2 Week
4 Week
3 Month

Figure 28. Time course of microglia activation, indicated as OX42-IR intensity levels, in the L4-5 ventral horn of the rat spinal cord, following tibial n. crush. The x-axis represents the time course following tibial n. injury. The y-axis signifies the fold change in microglia activation (calculated as experimental OX42-IR intensity/control OX42-IR intensity). Significance (indicated by black asterisks; $p<0.001$, Anova), from sham surgery controls, was observed at 1 and 2 weeks post-tibial nerve crush.

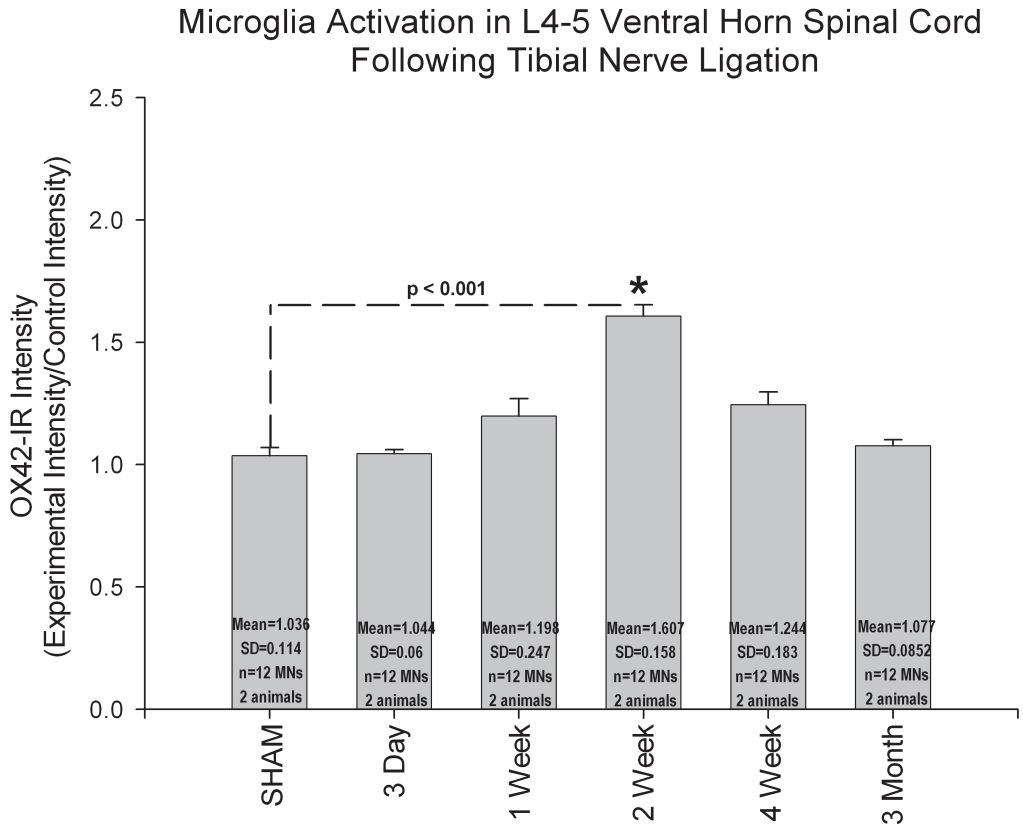
Microglia Activation in L4-5 Ventral Horn Spinal Cord
Following Tibial Nerve Ligation
OX42-IR Intensity
(Experimental Intensity/Control Intensity)
2.5
2.0
1.5
1.0
0.5
0.0
p < 0.001
*
Mean=1.036
SD=0.114
n=12 MNs
2 animals
Mean=1.044
SD=0.06
n=12 MNs
2 animals
Mean=1.198
SD=0.247
n=12 MNs
2 animals
Mean=1.607
SD=0.158
n=12 MNs
2 animals
Mean=1.244
SD=0.183
n=12 MNs
2 animals
Mean=1.077
SD=0.0852
n=12 MNs
2 animals
SHAM
3 Day
1 Week
2 Week
4 Week
3 Month

Figure 29. Time course of microglia activation, indicated as OX42-IR intensity levels, in the L4-5 ventral horn of the rat spinal cord, following tibial n. ligation. The x-axis represents the time course following tibial n. injury. The y-axis signifies the fold change in microglia activation (calculated as experimental OX42-IR intensity/control OX42-IR intensity). Significance (indicated by black asterisks; $p<0.001$, Anova), from sham surgery controls, was observed at 2 weeks post-tibial nerve ligation.

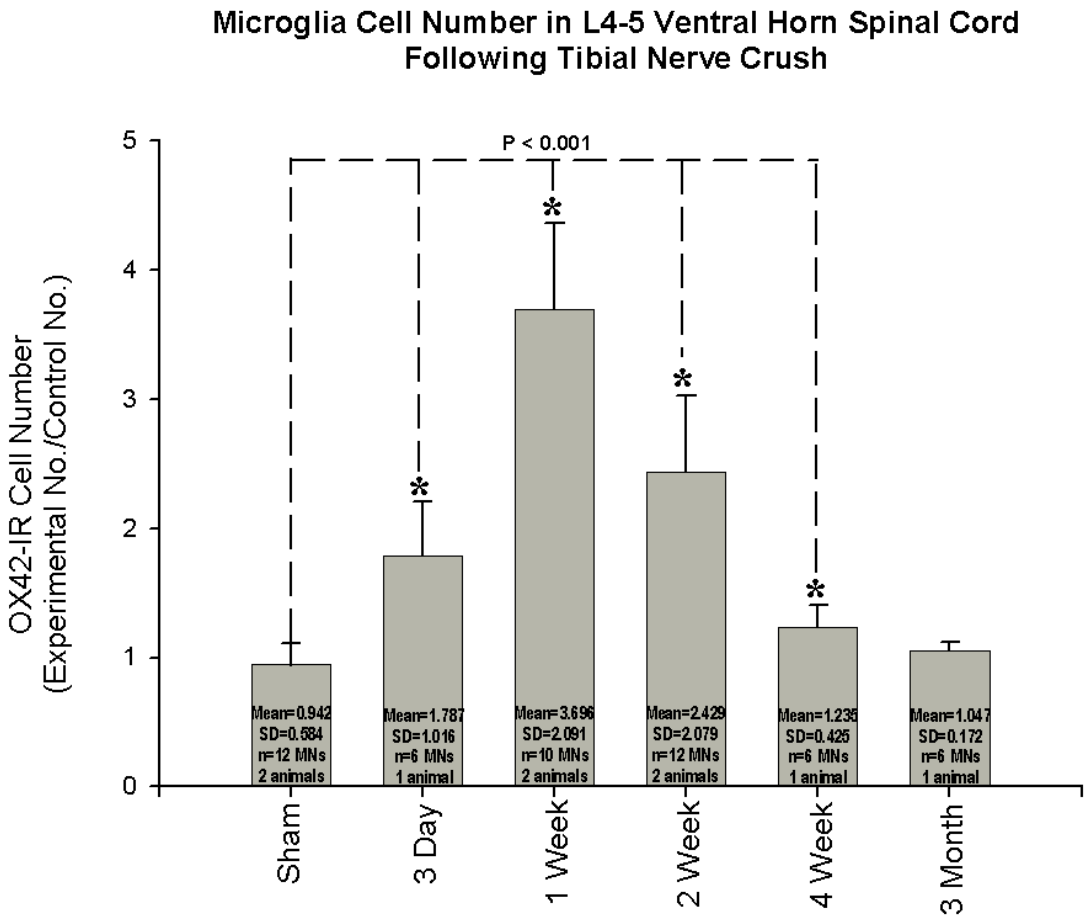
Microglia Cell Number in L4-5 Ventral Horn Spinal Cord
Following Tibial Nerve Crush
OX42-IR Cell Number
(Experimental No./Control No.)
P < 0.001
Mean=0.942
SD=0.584
n=12 MNs
2 animals
Mean=1.787
SD=1.016
n=6 MNs
1 animal
Mean=3.696
SD=2.091
n=10 MNs
2 animals
Mean=2.429
SD=2.079
n=12 MNs
2 animals
Mean=1.235
SD=0.425
n=6 MNs
1 animal
Mean=1.047
SD=0.172
n=6 MNs
1 animal
Sham
3 Day
1 Week
2 Week
4 Week
3 Month

Figure 30. Time course of microglia proliferation, indicated as OX42-IR, in the L4-5 ventral horn of the rat spinal cord, following tibial n. crush. The x-axis represents the time course following tibial n. injury. The y-axis signifies the fold change in OX42-IR cells (calculated as experimental cell number/control cell number). Significance (indicated by black asterisks; $p<0.001$, Anova) in the number of microglia, from sham surgery controls, was observed at 3 days, 1 week, 2 weeks, and 4 weeks, following tibial nerve crush.

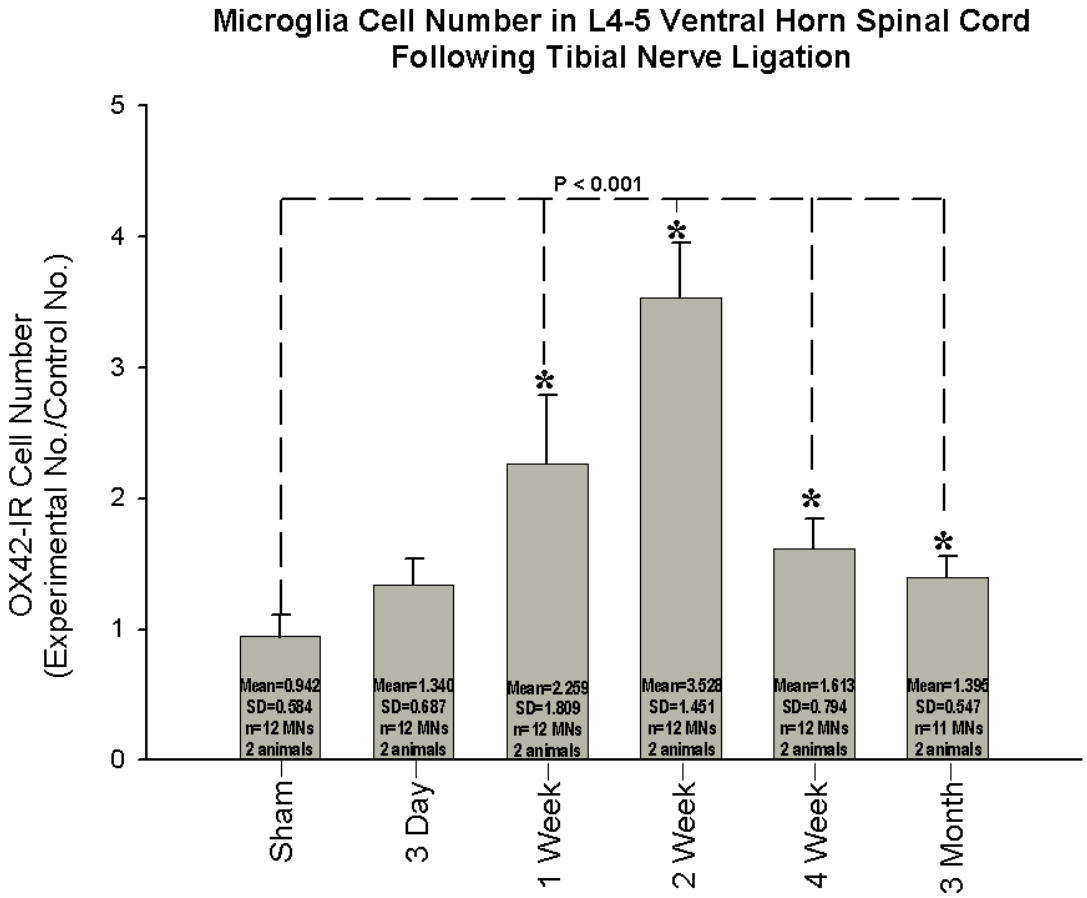
Microglia Cell Number in L4-5 Ventral Horn Spinal Cord
Following Tibial Nerve Ligation
OX42-IR Cell Number
(Experimental No./Control No.)
P < 0.001
Mean=0.942
SD=0.584
n=12 MNs
2 animals
Mean=1.340
SD=0.687
n=12 MNs
2 animals
Mean=2.259
SD=1.809
n=12 MNs
2 animals
Mean=3.528
SD=1.451
n=12 MNs
2 animals
Mean=1.613
SD=0.794
n=12 MNs
2 animals
Mean=1.395
SD=0.547
n=11 MNs
2 animals
Sham
3 Day
1 Week
2 Week
4 Week
3 Month

Figure 31. Time course of microglia proliferation, indicated as OX42-IR, in the L4-5 ventral horn of the rat spinal cord, following tibial n. ligation. The x-axis represents the time course following tibial n. injury. The y-axis signifies the fold change in OX42-IR cells (calculated as experimental cell number/control cell number). Significance (indicated by black asterisks; $p<0.001$, Anova) in the number of microglia, from sham surgery controls, was observed at1 week, 2 weeks, 4 weeks, and 3 months, following tibial nerve ligation.

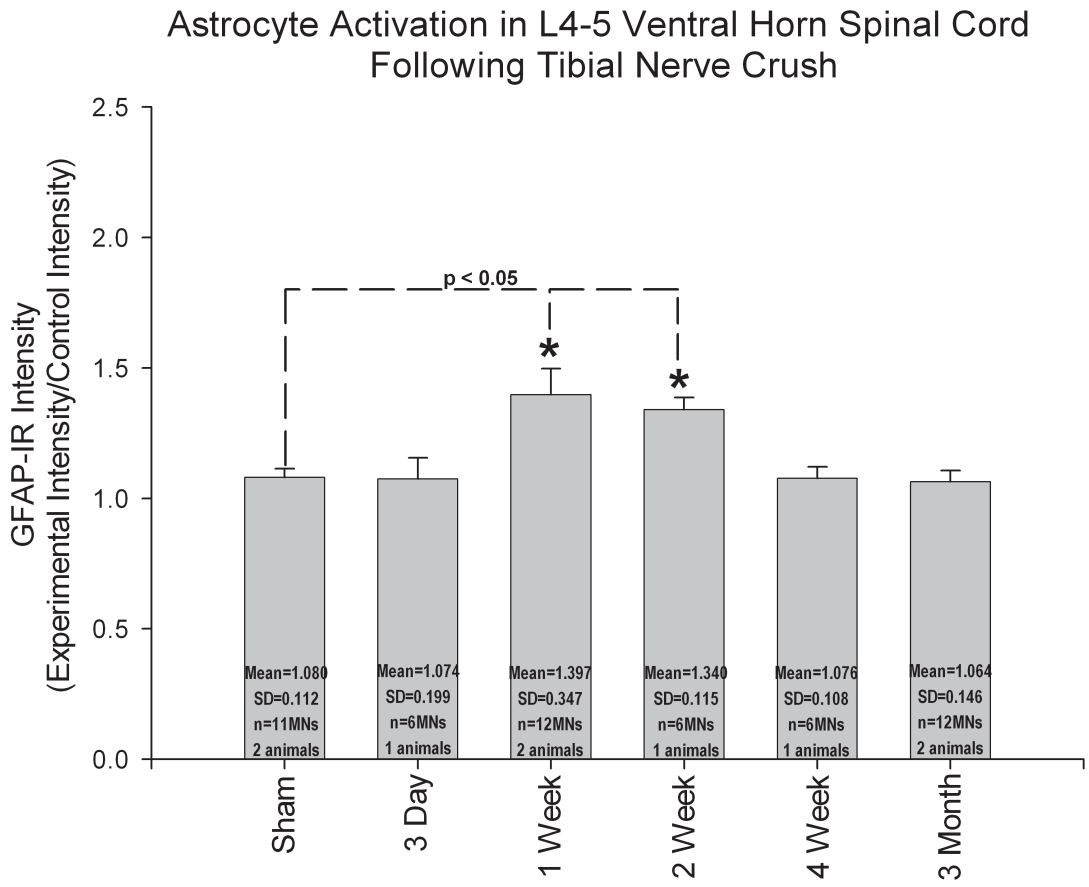
Astrocyte Activation in L4-5 Ventral Horn Spinal Cord
Following Tibial Nerve Crush
GFAP-IR Intensity
(Experimental Intensity/Control Intensity)
2.5
2.0
1.5
1.0
0.5
0.0
p < 0.05
*
*
Mean=1.080
SD=0.112
n=11MNs
2 animals
Mean=1.074
SD=0.199
n=6MNs
1 animals
Mean=1.397
SD=0.347
n=12MNs
2 animals
Mean=1.340
SD=0.115
n=6MNs
1 animals
Mean=1.076
SD=0.108
n=6MNs
1 animals
Mean=1.064
SD=0.146
n=12MNs
2 animals
Sham
3 Day
1 Week
2 Week
4 Week
3 Month

Figure 32. Time course of astrocyte activation, indicated as GFAP-IR intensity levels, in the L4-5 ventral horn of the rat spinal cord, following tibial n. crush. The x-axis represents the time course following tibial n. injury. The y-axis signifies the fold change in astrocyte activation (calculated as experimental GFAP-IR intensity/control GFAP-IR intensity). Significance (indicated by black asterisks; $p<0.05$, t-test), from sham surgery controls, was observed at 1 and 2 weeks post-tibial nerve crush.

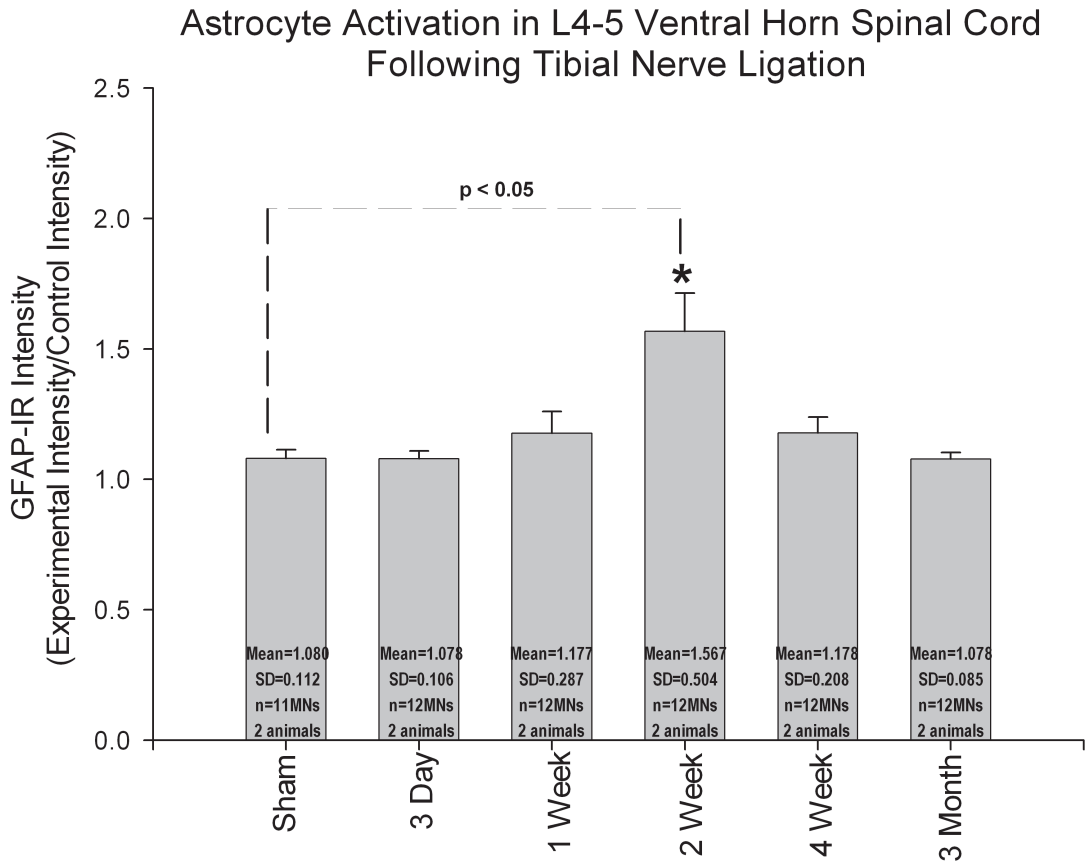
Astrocyte Activation in L4-5 Ventral Horn Spinal Cord
Following Tibial Nerve Ligation
GFAP-IR Intensity
(Experimental Intensity/Control Intensity)
2.5
2.0
1.5
1.0
0.5
0.0
p < 0.05
*
Mean=1.080
SD=0.112
n=11MNs
2 animals
Mean=1.078
SD=0.106
n=12MNs
2 animals
Mean=1.177
SD=0.287
n=12MNs
2 animals
Mean=1.567
SD=0.504
n=12MNs
2 animals
Mean=1.178
SD=0.208
n=12MNs
2 animals
Mean=1.078
SD=0.085
n=12MNs
2 animals
Sham
3 Day
1 Week
2 Week
4 Week
3 Month

Figure 33. Time course of astrocyte activation, indicated as GFAP-IR intensity levels, in the L4-5 ventral horn of the rat spinal cord, following tibial n. ligation. The x-axis represents the time course following tibial n. injury. The y-axis signifies the fold change in astrocyte activation (calculated as experimental GFAP-IR intensity/control GFAP-IR intensity). Significance (indicated by black asterisks; $p<0.05$, t-test), from sham surgery controls, was observed at 2 weeks post-tibial nerve ligation.

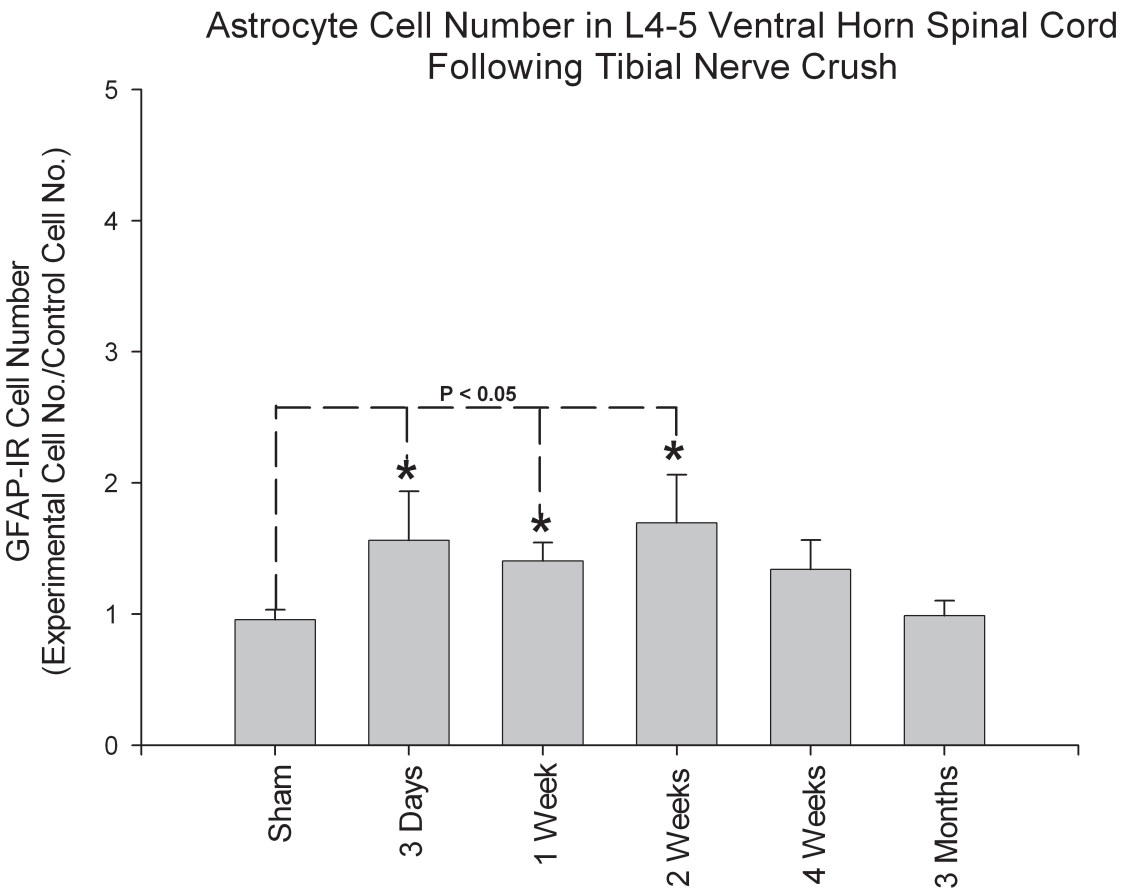
Astrocyte Cell Number in L4-5 Ventral Horn Spinal Cord
Following Tibial Nerve Crush
GFAP-IR Cell Number
(Experimental Cell No./Control Cell No.)
5
4
3
2
1
0
P < 0.05
*
*
*
Sham
3 Days
1 Week
2 Weeks
4 Weeks
3 Months

Figure 34. Time course of astrocyte proliferation, indicated as GFAP-IR, in the L4-5 ventral horn of the rat spinal cord, following tibial n. crush. The x-axis represents the time course following tibial n. injury. The y-axis signifies the fold change in GFAP-IR cells (calculated as experimental cell number/control cell number). A significant increase (indicated by black asterisks; $p<0.05$, t-test) in the number of astrocytes, from sham surgery controls, was observed at 3 days, 1 week and 2 weeks, following tibial nerve crush.

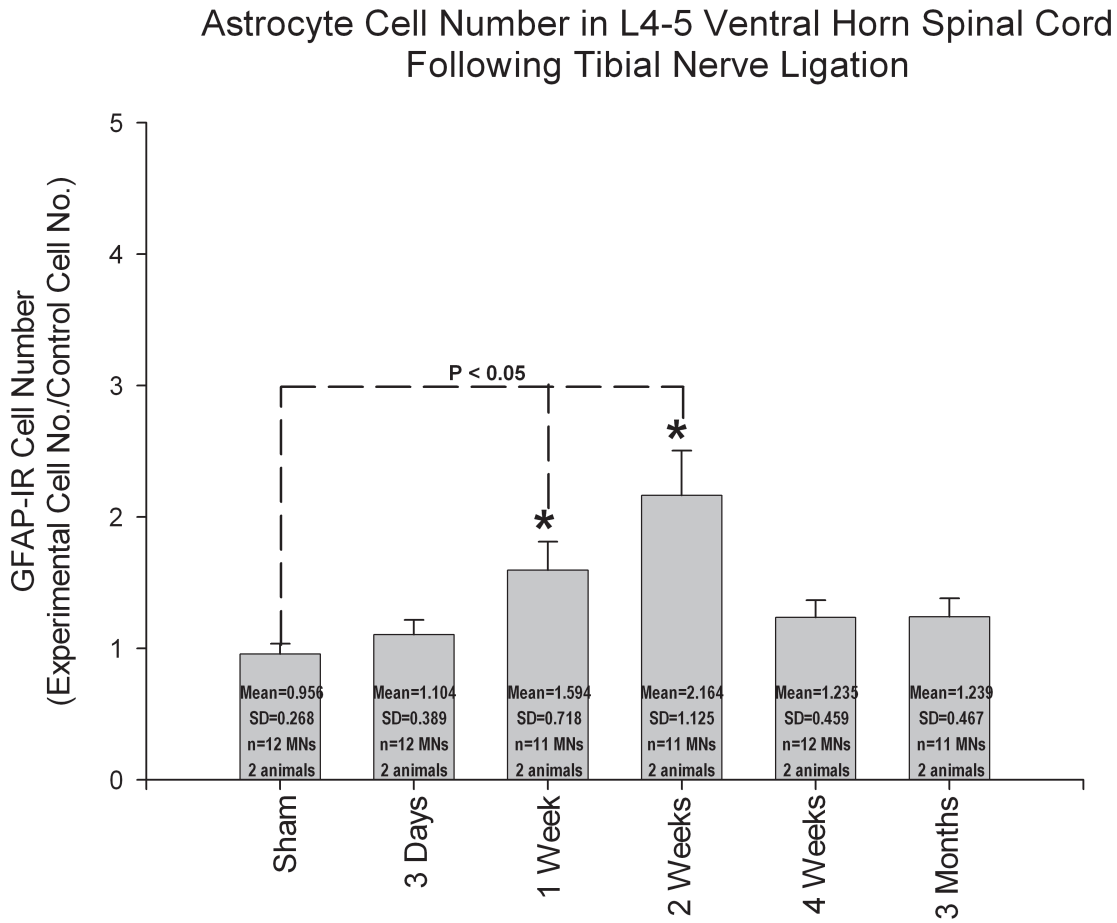
Astrocyte Cell Number in L4-5 Ventral Horn Spinal Cord
Following Tibial Nerve Ligation
GFAP-IR Cell Number
(Experimental Cell No./Control Cell No.)
5
4
3
2
1
0
P < 0.05
*
*
Mean=0.956
SD=0.268
n=12 MNs
2 animals
Mean=1.104
SD=0.389
n=12 MNs
2 animals
Mean=1.594
SD=0.718
n=11 MNs
2 animals
Mean=2.164
SD=1.125
n=11 MNs
2 animals
Mean=1.235
SD=0.459
n=12 MNs
2 animals
Mean=1.239
SD=0.467
n=11 MNs
2 animals
Sham
3 Days
1 Week
2 Weeks
4 Weeks
3 Months

Figure 35. Time course of astrocyte proliferation, indicated as GFAP-IR, in the L4-5 ventral horn of the rat spinal cord, following tibial n. ligation. The x-axis represents the time course following tibial n. injury. The y-axis signifies the fold change in GFAP-IR cells (calculated as experimental cell number/control cell number). A significant increase (indicated by black asterisks; $p<0.05$, t-test) in the number of astrocytes, from sham surgery controls, was observed at 1 week and 2 weeks, following tibial nerve ligation.

Differences in Crush and Ligate Injury Animals

This project studied the glial response to a peripheral nerve injury in two types of injury. Following a tibial nerve crush, regeneration of the axon occurs and the muscle is reinnervated. Following tibial nerve ligation, axonal regeneration fails to occur since the proximal stump of the nerve is tied off with suture to prevent regeneration and reinnveration.

Microglia activation across the entire lumbar spinal cord showed similar results after tibial nerve crush and ligation with peaks around L4 and L5 (Figures 12 and 13). The activation of microglia was greater following ligation than crush, in both the dorsal and ventral horns. In the ventral horn of both injuries, an increase in fold change from sham controls was not typically evident in L1-3. Peak activation of microglia was observed at L4 after both types of injury, and a decline in activation occurred at L6. The activation of microglia was greater in the dorsal horn than in the ventral horn, following both tibial nerve crush and ligation.

The proliferation of microglia cells in the lumbar spinal cord resulted in many differences between the crush and ligate injury animals (Figures 14 and 15). Following tibial nerve crush, the proliferation of microglia cells in the dorsal horn was significant at L2 and increased steadily through L4. After ligation, however, the proliferation of microglia was constant and insignificantly different from sham from L1-3 before it dramatically increased at L4 -5. Overall, the proliferation of microglia in the dorsal horn was greater following tibial nerve crush than ligation. On the other hand, microglia proliferation was greater in the ventral horn following ligation compared to crush

Astrocyte activation across the entire lumbar region also showed differences in activation following crush and ligation (Figure 16 and 17). The activation of astrocytes in the dorsal horn was greater following nerve crush than ligation. Like microglia, the activation of astrocytes in the ventral horn, however, was greater following ligation than crush. The activation of astrocytes in the ventral horn was similar at L1-3, following both types of injury, showing no major changes from sham controls at theses spinal levels. Increases in fold change from sham in both injury types remained between 1-1.5.

The proliferation of astrocytes resulted in a greater cell number in the dorsal horn following tibial nerve crush than ligation (Figures 18 and 19). The response in the ventral horn, however, was greater following ligation than crush. The range in the number of astrocyte cells across the L1-6 was relatively constant following crush injury. In the ligation animals, however, the proliferation of astrocytes was more variable across the lumbar spinal cord. Following both types of injury, the response of astrocytes in the ventral horn was greater than the astrocytic response in the dorsal horn at the 2-week time point.

In general, the activation and proliferation of astrocytes and microglia was more significant following tibial nerve ligation than crush. At times, however, crush injury animals resulted in a more significant response. Differences between the crush and ligate injury animals were also observed in the spinal levels indicated as significant from sham, and in the general trend across the lumbar spinal cord. All of this is evidence that crush and ligate injuries evoke different responses that extend beyond the allowing or preventing of reinnervation, Each injury appears to induce distinctive mechanisms within the central nervous system that activate different cytokines and molecules, and to various

extents. Ligation of a nerve is a quick, but severe injury that likely generates a strong release of molecules, resulting in the observed robust response of glia. In contrast, the slow-occurring crush injury might cause the slow release of molecules, generating a weaker, but more widespread response. These data reveal that the central differences between these injuries must be further studied.

Aim 3

Determining the effect of the microglia inhibitor Minocycline on the stripping of cholinergic C-boutons from motoneuron somas two weeks following tibial n. ligation

Characterization of Glial Response following Minocycline Treatment

The focus of this aim was to determine if the proliferation of microglia observed following peripheral nerve injury plays a role in the stripping of cholinergic C-boutons that occurs after injury. Since a significant depletion in C-bouton membrane coverage was observed 2 weeks following tibial nerve ligation (see *Aim 1*), only ligate injury animals were the focus of this aim. In order to study this, the microglia inhibitor Minocycline was orally administered to female Sprague-Dawley rats, every morning for two weeks.

Minocycline is a widely used tetracycline antibiotic commonly used to treat acne. Minocycline has been found to inhibit microglial proliferation in the early days following peripheral nerve injury (Liu et al., 2011; Ikeda et al., 2012). Minocycline is highly lipophilic; it can be easily absorbed from the gut after ingestion, and is capable of crossing the blood-brain-barrier (Liu et al., 2011). Minocycline has also shown to provide neuroprotection against certain neurodegenerative diseases. Though the exact mechanism of how Minocycline works is unknown, it is thought to act on many targets. Possible

mechanisms of action in the attenuation of microglia include inhibition of p38 mitogen-activated protein (MAP) kinase pathway (Suter et al., 2007), inhibition of matrix metalloproteinases (MMPs) (Suter et al., 2007), and reduction of inflammatory cytokines (Liu et al., 2011).

Six rats were used in this experiment. Two rats served as vehicle controls and received Minocycline for two weeks. These rats did not undergo any surgeries, nor did they receive retrograde CTB labeling. Two rats served as sham surgery control animals and also received Minocycline for two weeks following sham surgeries. These rats received retrograde CTB labeling in the left LG/MG muscles to label tibial n. motoneurons in the ventral horn of the spinal cord (see *Aim 1*). The last two rats received retrograde CTB labeling injections into the LG/MG muscle, underwent tibial n. ligations and received Minocycline for two weeks following nerve surgeries. Sham control and ligate injury animals initially began their Minocyline treatment 3 days prior to injury (or sham) surgeries, and continued the treatment for 2 weeks following surgeries.

The tissue slices of all of the animals were immunolabed for C-boutons (VAChT), astrocytes (GFAP) and microglia (OX42). Just as in Specific Aim 2, the activation intensity of GFAP-IR and OX42-IR and the cell number of each glial cell were analyzed (Figures 36-39).

Following 2-week ligation, as shown in SA2, microglia activation in L4-5 ventral horn, observed an increase in fold change of 1.785 ± 0.239 over sham controls (1.036 ± 0.114) (Figures 29, 36). Microglia activation, 2 weeks following ligation plus a 2-week treatment of Minocycline, also observed activation levels significant from sham, with an increase in fold change of 1.652 ± 0.372, over the sham controls (Figure 38). The fold

change of microglia activation in the Minocycline vehicle controls (0.969 ± 0.086) was not significantly different from sham controls. This suggests that even in the presence of Minocycline, there was still injury-specific microglia activation.

Following 2-week ligation, microglia proliferation was significantly different from sham (0.942 ± 0.584) at 2 weeks following ligation (3.528 ± 1.451) (Figure 31, 39). Significance was also observed 2 weeks after ligation with a 2-week Minocycline treatment (2.250 ± 0.775) (Figure 37). Unlike microglia activation following Minocycline treatment, the proliferation of microglia was significantly different between the two ligate injury animals (ligation with and without Minocycline).

Following 2-week ligation, astrocyte activation was significant from sham (1.108 ± 0.144) 2 weeks following ligation (1.567 ± 0.504) (Figure 33, 40). Significance was also observed 2 weeks after ligation, with a 2-week Minocycline treatment (1.450 ± 0.301) (Figure 38). Similar to microglia activation, astrocyte activation between the two ligate injury animals (without and with Minocycline) was not significant.

Two weeks following ligation, astrocyte proliferation was significant from sham at 2 weeks following ligation (Figure 34, 41). Unlike microglia proliferation, no significance in the fold change of astrocyte cell number was observed, following ligation and Minocycline treatment (Figure 39). There was a significance in astrocyte cell number between the standard 2-week ligation animal (2.164 ± 1.125) and the 2-Week ligate and Mino animal (1.349 ± 0.241).

An activation and proliferation of both glial cells was observed after the Minocycline treatment (See *Aim 2* for methods). Although the response after the

Minocycline was still significant from sham surgery controls, it was overall decreased when compared to the ligation animals (SA2) without the Minocycline treatment.

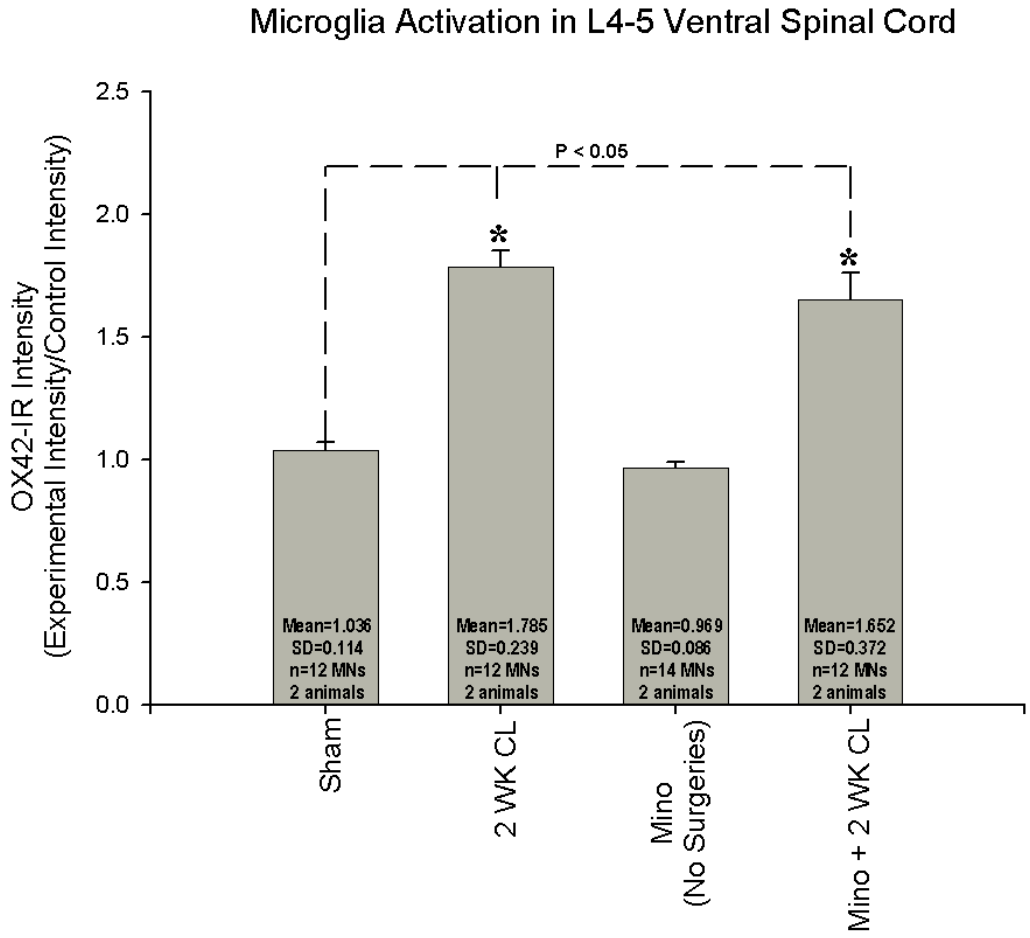
Microglia Activation in L4-5 Ventral Spinal Cord
OX42-IR Intensity
(Experimental Intensity/Control Intensity)
2.5
2.0
1.5
1.0
0.5
0.0
P < 0.05
*
*
Mean=1.036
SD=0.114
n=12 MNs
2 animals
Mean=1.785
SD=0.239
n=12 MNs
2 animals
Mean=0.969
SD=0.086
n=14 MNs
2 animals
Mean=1.652
SD=0.372
n=12 MNs
2 animals
Sham
2 WK CL
Mino
(No Surgeries)
Mino + 2 WK CL

Figure 36. Time course of microglia activation, indicated as OX42-IR intensity levels, in the L4-5 ventral horn of the rat spinal cord, following Minocycline treatments. The x-axis represents the time course following tibial n. injury. The y-axis signifies the fold change in microglia activation (calculated as experimental OX42-IR intensity/control OX42-IR intensity). A significant (indicated by black asterisks, $p<0.05$, t-test) increase in microglia activation was observed following a 2 week tibial n. ligation, and following Minocyline treatment plus 2 week ligation, when compared to sham surgery controls. A small decrease in microglia activation was observed following the Minocycline treatment plus ligation, in comparison to the 2 week ligation. The microglia activation in rats receiving Minocycline treatment but no ligation was insignificantly less than those of sham surgery controls.

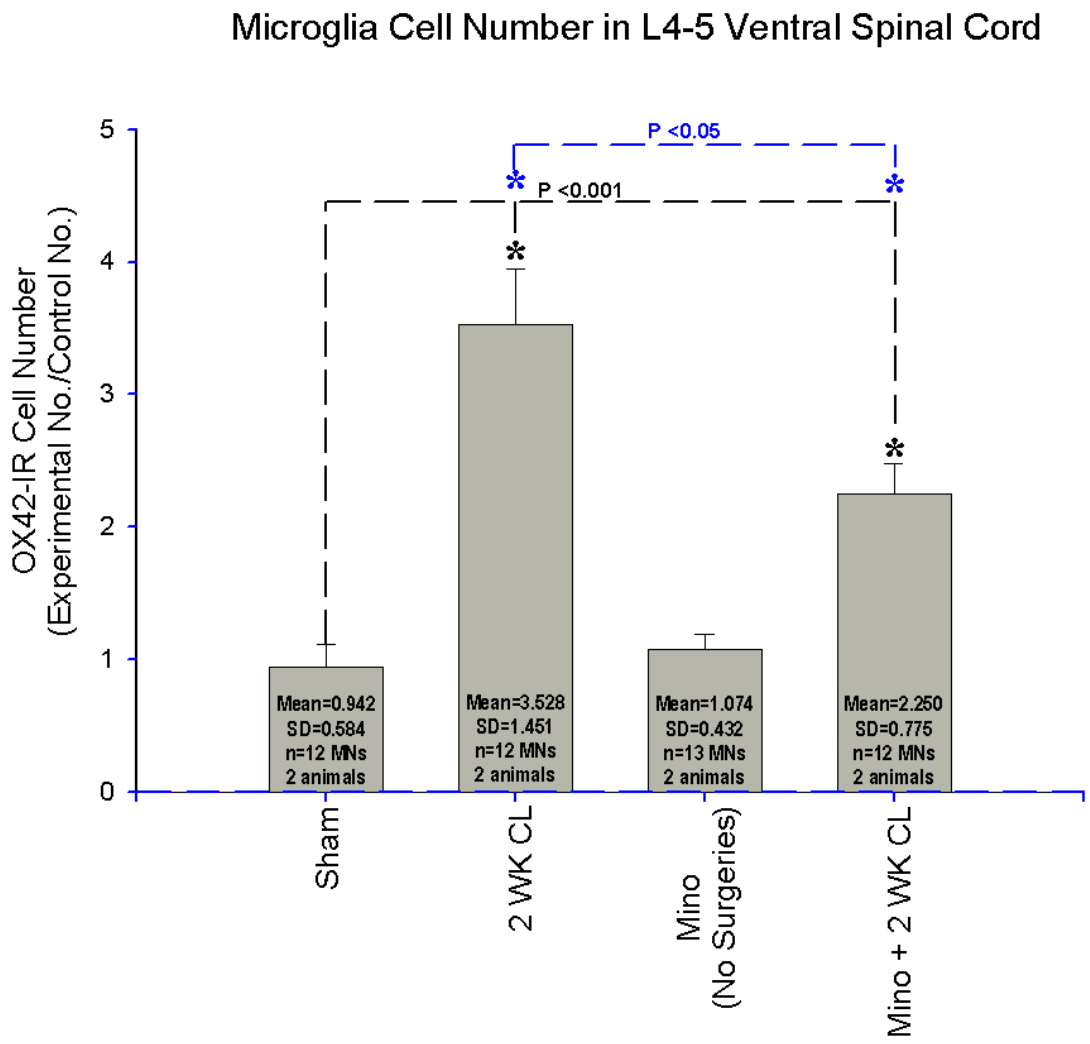
Microglia Cell Number in L4-5 Ventral Spinal Cord
OX42-IR Cell Number
(Experimental No./Control No.)
5
4
3
2
1
0
P <0.05
P <0.001
*
*
*
*
Mean=0.942
SD=0.584
n=12 MNs
2 animals
Mean=3.528
SD=1.451
n=12 MNs
2 animals
Mean=1.074
SD=0.432
n=13 MNs
2 animals
Mean=2.250
SD=0.775
n=12 MNs
2 animals
Sham
2 WK CL
Mino
(No Surgeries)
Mino + 2 WK CL

Figure 37. Time course of microglia proliferation, indicated as OX42-IR, in the L4-5 ventral horn of the rat spinal cord, following Minocycline treatments. The x-axis represents the differential experimental groups of rats. The y-axis signifies the fold change in OX42-IR cells (calculated as experimental cell number/control cell number). A significant increase (indicated by black asterisks; $p<0.001$, t-test) in the number of microglia, from sham surgery controls, was observed following a 2 week tibial nerve ligation, and following Minocycline plus 2 week ligation. The number of microglia cells observed, following Minocycline treatments plus a 2 week ligation, was significantly (indicated as blue asterisks, $p<0.05$, t-test) less than the number of microglia observed following a standard 2 week ligation. The number of microglia in the Minocycline only (no surgeries) group was insignificantly greater than those observed in the sham surgery control group.

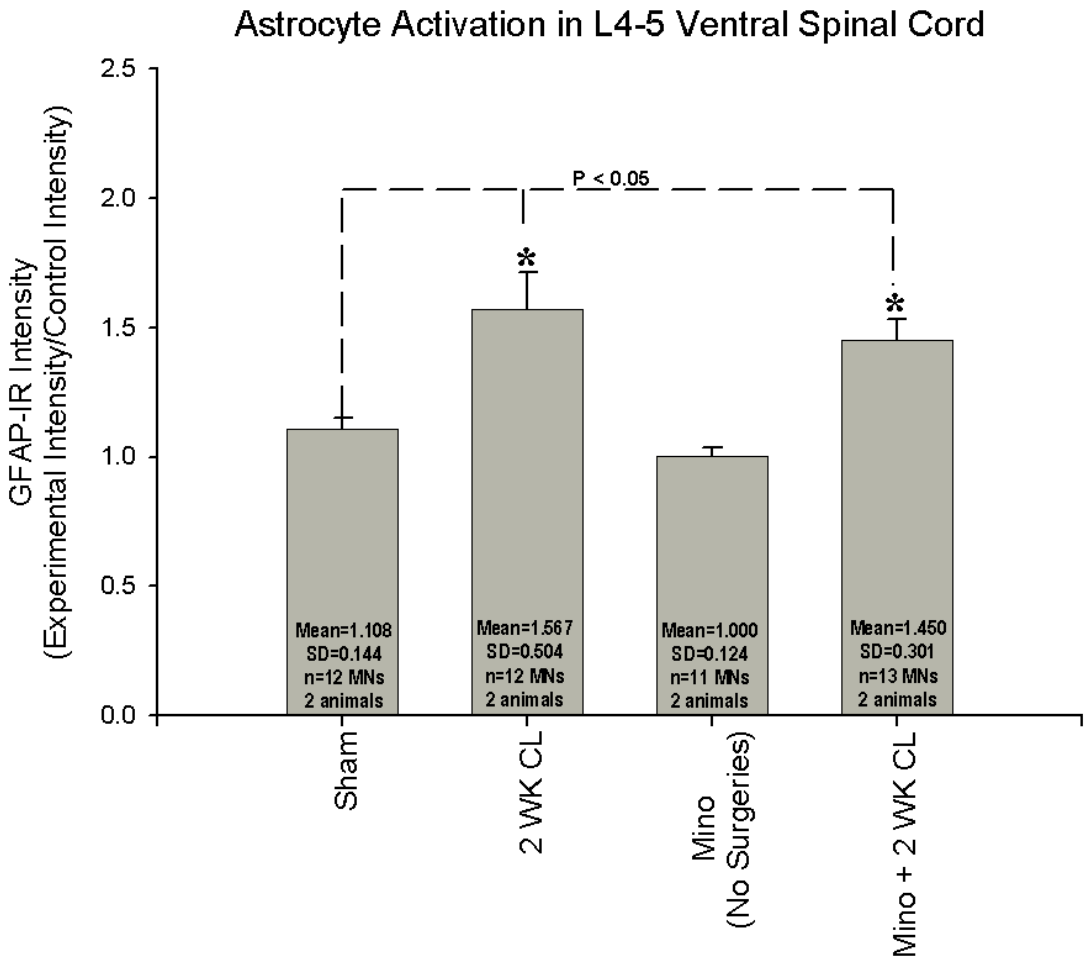
Astrocyte Activation in L4-5 Ventral Spinal Cord
GFAP-IR Intensity
(Experimental Intensity/Control Intensity)
2.5
2.0
1.5
1.0
0.5
0.0
P < 0.05
*
*
Mean=1.108
SD=0.144
n=12 MNs
2 animals
Mean=1.567
SD=0.504
n=12 MNs
2 animals
Mean=1.000
SD=0.124
n=11 MNs
2 animals
Mean=1.450
SD=0.301
n=13 MNs
2 animals
Sham
2 WK CL
Mino
(No Surgeries)
Mino + 2 WK CL

Figure 38. Time course of astrocyte activation, indicated as GFAP-IR intensity levels, in the L4-5 ventral horn of the rat spinal cord, following Minocycline treatments. The x-axis represents the time course following tibial n. injury. The y-axis signifies the fold change in astrocyte activation (calculated as experimental GFAP-IR intensity/control GFAP-IR intensity). A significant (indicated by black asterisks, $p<0.05$, t-test) increase in astrocyte activation was observed following a 2 week tibial n. ligation, and following Minocyline treatment plus 2 week ligation, when compared to sham surgery controls. A small decrease in astrocyte activation was observed following the Minocycline treatment plus ligation, in comparison to the 2 week ligation group. The astrocyte activation in rats receiving Minocycline treatment but no ligation was insignificantly less than those of sham surgery controls.

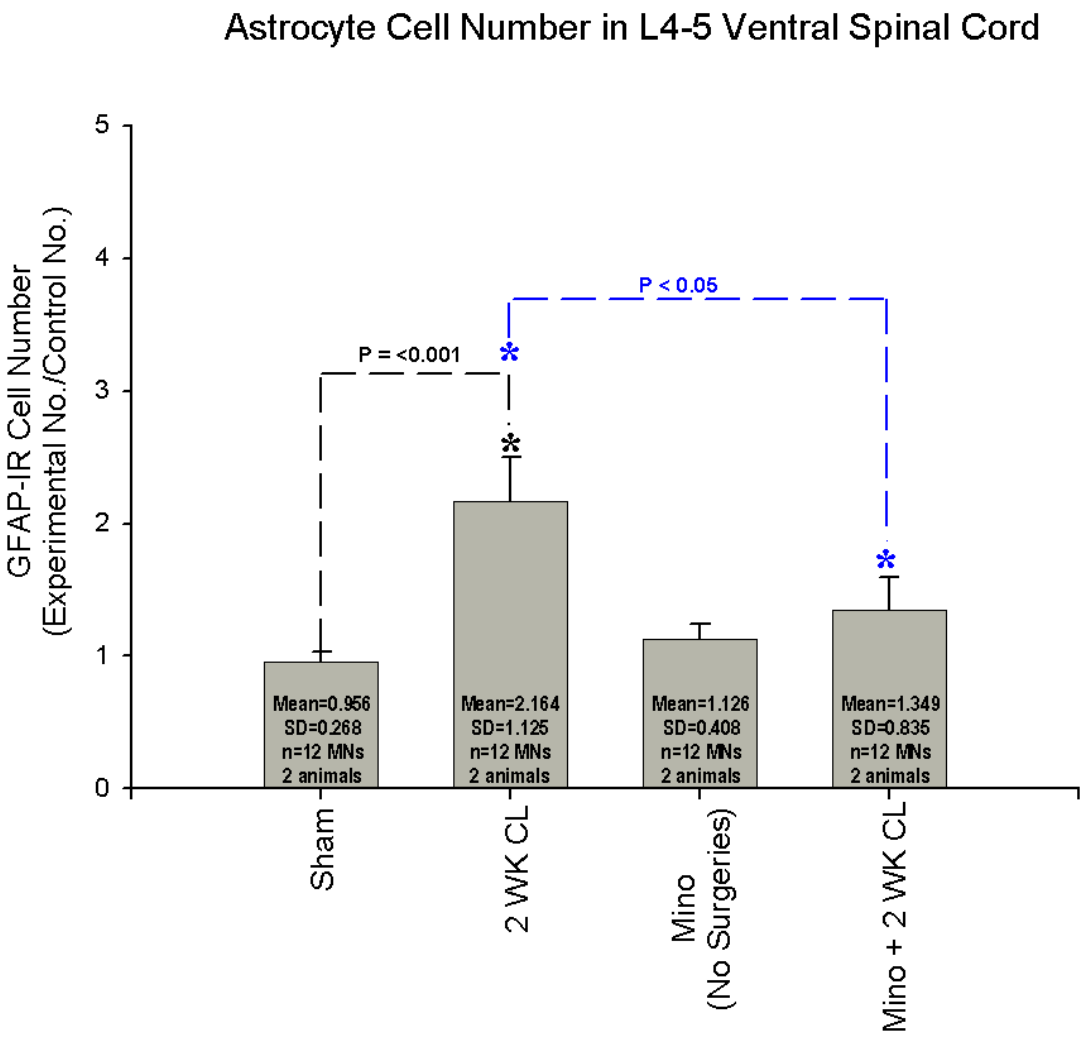
Astrocyte Cell Number in L4-5 Ventral Spinal Cord
GFAP-IR Cell Number
(Experimental No./Control No.)
5
4
3
2
1
0
P = <0.001
P < 0.05
*
*
*
Mean=0.956
SD=0.268
n=12 MNs
2 animals
Mean=2.164
SD=1.125
n=12 MNs
2 animals
Mean=1.126
SD=0.408
n=12 MNs
2 animals
Mean=1.349
SD=0.835
n=12 MNs
2 animals
Sham
2 WK CL
Mino
(No Surgeries)
Mino + 2 WK CL

Figure 39. Time course of astrocyte proliferation, indicated as GFAP-IR, in the L4-5 ventral horn of the rat spinal cord, following Minocycline treatments. The x-axis represents the differential experimental groups of rats. The y-axis signifies the fold change in GFAP-IR cells (calculated as experimental cell number/control cell number). A significant increase (indicated by black asterisks; $p<0.05$, t-test) in the number of astrocytes, from sham surgery controls, was observed following a 2 week tibial nerve ligation. The number of astrocytes cells following Minocycline treatments plus a 2 week ligation was significantly (indicated as blue asterisks, $p<0.05$, t-test) less than the number of astrocytes observed following a standard 2 week ligation. Both groups receiving Minocycline observed an insignificant increase in astrocytes, as compared to sham surgery controls.

C-Bouton Percent Membrane Coverage

The percent membrane coverage of C-boutons was also determined, using the same method described in Aim 1. A 48.269% ± 21.108 SD depletion of C-bouton membrane coverage was observed in the Minocycline vehicle control, as compared to sham controls (Figure 40). A 43.857% ± 19.198 SD depletion in C-bouton coverage was observed following a 2-week ligation and Minocycline treatment, as compared to sham controls.

C-Bouton Cluster Areas

The area of *en face* VAChT-IR clusters on retrograde CTB-labeled motoneurons was also determined (Figure 11). Following a standard 2-week tibial nerve ligation, a reduction in fold change in the area of *en face* VAChT-IR contacts is observed (8.761 ± 3.340), in comparison to sham controls (12.369 ± 4367) (Figure 41).

The average area of *en face* contacts on the Minocycline vehicle controls (6.179 ± 21.87) and the ligation plus Minocycline (6.149 ± 2.507) rats were significantly smaller than the VAChT-IR cluster areas of sham controls. Very minor differences between the two Minocycline-treated rats (vehicle control and ligate) were observed; however, almost a 50% fold change reduction was observed between the Minocycline-treated rats and sham controls. The cluster areas of these Minocycline-treated rats was also smaller than that of 2-week ligated animals receiving no Minocycline.

Minocycline Alters C-boutons

Unexpectedly, Minocycline alone dramatically affected the C-bouton percent coverage and cluster areas, even without the presence of injury. This dramatic effect

prevents us making any conclusions about the role of blocking glia activation on C-bouton stripping.

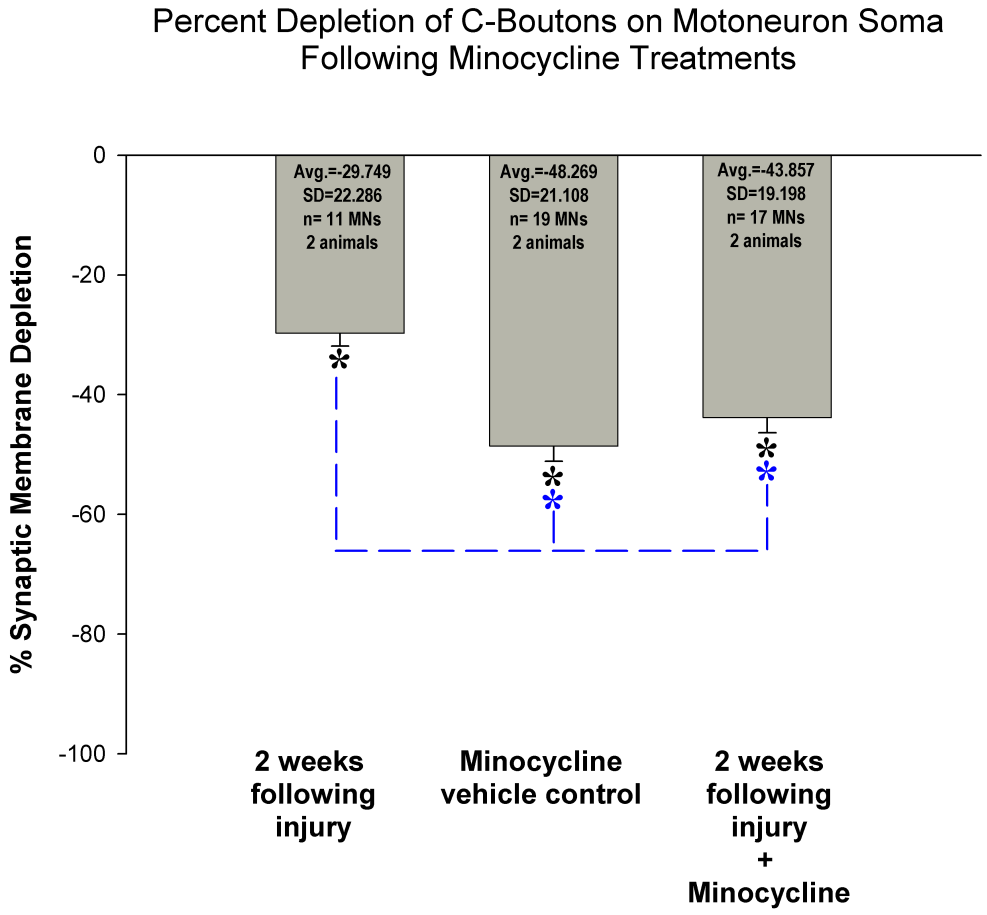
Percent Depletion of C-Boutons on Motoneuron Soma
Following Minocycline Treatments
% Synaptic Membrane Depletion
0
-20
-40
-60
-80
-100
Avg.=-29.749
SD=22.286
n= 11 MNs
2 animals
Avg.=-48.269
SD=21.108
n= 19 MNs
2 animals
Avg.=-43.857
SD=19.198
n= 17 MNs
2 animals
2 weeks following injury
Minocycline vehicle control
2 weeks following injury + Minocycline

Figure 40: Percent depletion of C-boutons on the soma of rat motoneurons in L4-5 following Minocycline treatments. The x-axis represents the different experimental groups. The y-axis represents the percent depletion of VAChT-IR membrane coverage, as compared to sham surgery controls**.** Minocycline significantly (indicated with blue asterisks, $p<0.001$, t-test) depleted the percent coverage of C-boutons on motoneurons, when compared to 2 week ligation. C-bouton percent coverage on motoneurons is significantly (indicated with black asterisks, $p<0.001$, t-test) depleted in all groups from sham surgery controls.

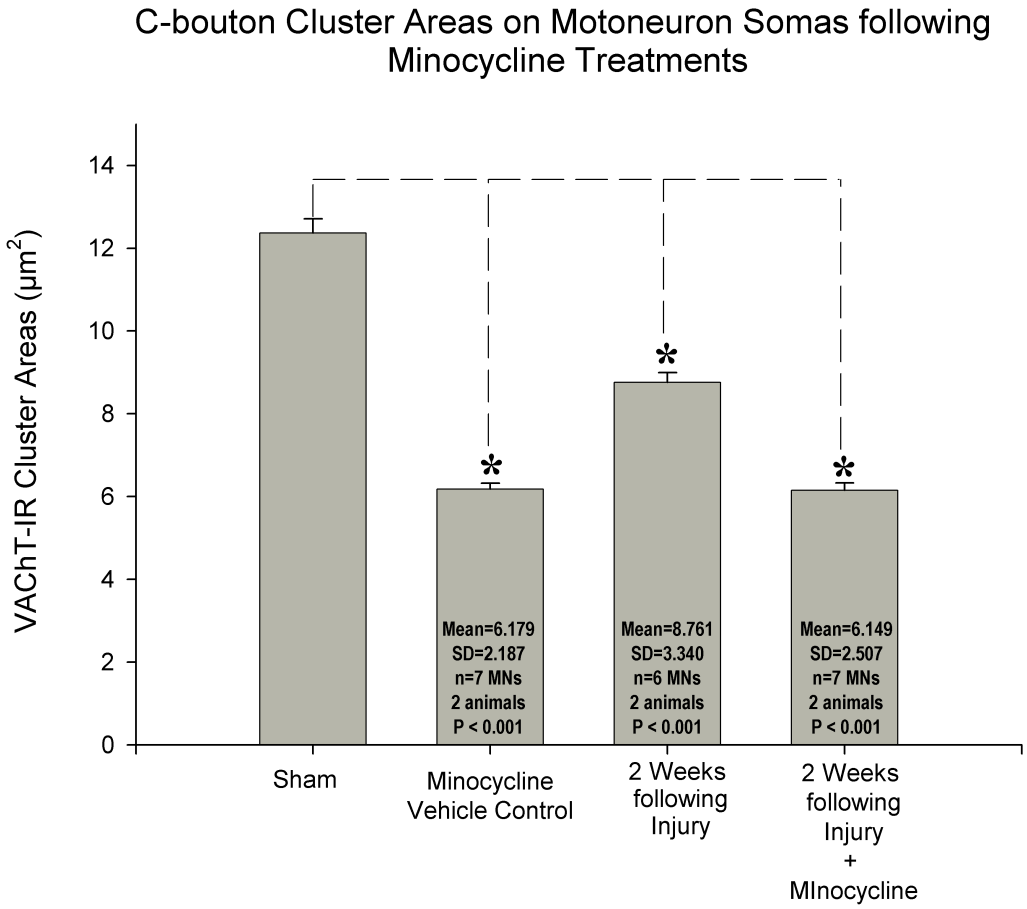
C-bouton Cluster Areas on Motoneuron Somas following Minocycline Treatments
VAChT-IR Cluster Areas (μm²)
14
12
10
8
6
4
2
0
Mean=6.179
SD=2.187
n=7 MNs
2 animals
P < 0.001
Mean=8.761
SD=3.340
n=6 MNs
2 animals
P < 0.001
Mean=6.149
SD=2.507
n=7 MNs
2 animals
P < 0.001
Sham
Minocycline Vehicle Control
2 Weeks following Injury
2 Weeks following Injury + MInocycline

Figure 41. C-bouton area clusters (indicated by VAChT-IR) following Minocycline treatments. The x-axis indicates the different experimental groups. The y-axis signifies the area of VAChT-IR clusters (μm^2). Minocycline decreased the area of C-bouton clusters, even in the absence of peripheral nerve ligation. The C-bouton cluster areas of all experimental groups were significantly (indicated with black asterisks, $p<0.001$, t-test) different, as compared to sham surgery controls.

VGLUT1 Synaptic Membrane Coverage

Another synapse has been well-characterized as stripping from motoneurons following tibial nerve injury. However, this synapse fully retracts from the MN in a different manner than what we observed in the C-bouton. This synapse is the VGLUT1-IR (Vesicular Glutamate Transporter) positive synapse that labels primary IA muscle afferents synapsing onto motoneurons. VGLUT1 synapses on motoneurons are lost after peripheral nerve injury and do not recover (Cope et al., 1993; Haftel et al., 2005; Maas et al., 2007; Alvarez et al., 2011). Since it appears that VGLUT1 synapses may strip in a different manner, we sought to determine the effects of Minocycline on VGLUT1 stripping in the same animals we examined for C-Bouton stripping.

Using the same methods described in SA1 we calculated percent membrane depletion of VGLUT1 synapses in tibial nerve ligation animals (no Minocycline), Minocycline-treated sham animals, and Minocycline-treated tibial nerve ligation animals. Following a 2 week tibial nerve ligation (no Minocycline) a 34.44% ± 44.471 SD depletion in VGLUT1 synapses on the motoneuron soma was observed, in comparison to sham controls (Figures 42, 43). These data are comparable to previously published VGLUT1 depletions (Alvarez et al, 2011). Unlike what was observed in the C-Bouton, Minocycline vehicle controls had no significant effect on VGLUT1 synapses with 1.778% ± 54.355 SD depletion observed. Following a 2-week tibial nerve ligation with Minocycline treatment, however, a 12.355% ± 56.4 SD increase in VGLUT1 synapses was observed on the membrane soma, compared to sham controls. Unlike what was observed for the C-bouton, we were able to prevent VGLUT1 synaptic stripping in 2

animals, with no significant variation between the two animals, following tibial nerve ligation.

Although we were only able to reduce the amount of glia proliferation following tibial nerve ligation and not eliminate it altogether, we clearly successfully blocked the mechanism that may give rise to VGLUT1 stripping. These data suggest that a different mechanism may underlie glia stripping of C-boutons than VGLUT1.

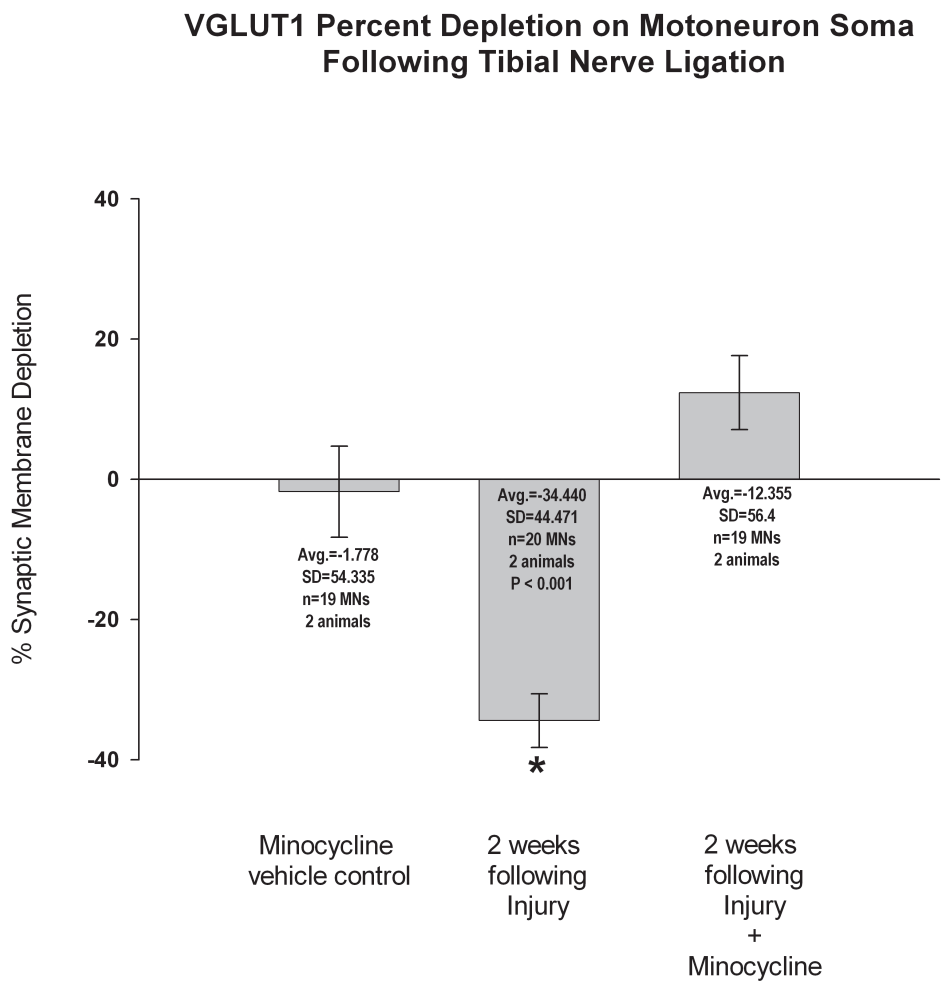
VGLUT1 Percent Depletion on Motoneuron Soma
Following Tibial Nerve Ligation
% Synaptic Membrane Depletion
40
20
0
-20
-40
Avg.=-1.778
SD=54.335
n=19 MNs
2 animals
Avg.=-34.440
SD=44.471
n=20 MNs
2 animals
P < 0.001
*
Avg.=-12.355
SD=56.4
n=19 MNs
2 animals
Minocycline
vehicle control
2 weeks
following
Injury
2 weeks
following
Injury
+
Minocycline

Figure 42: Percent Synaptic Depletion of VGLUT1 Somatic Coverage, following Minocycline treatments. The x-axis represents the different experimental groups. The y-axis indicates the percent membrane depletion of VGLUT1 somatic synapses, as compared to sham surgery controls. A significant (indicated by black asterisk, $p<0.001$, t-test) decrease in VGLUT1 synapses on the motoneuron soma is observed 2 weeks following tibial n. ligation, as compared to sham surgery controls. An small increase, insignificant from sham surgery and Minocycline control groups, is observed following Minocycline treatments plus 2 week following tibial n. ligation.

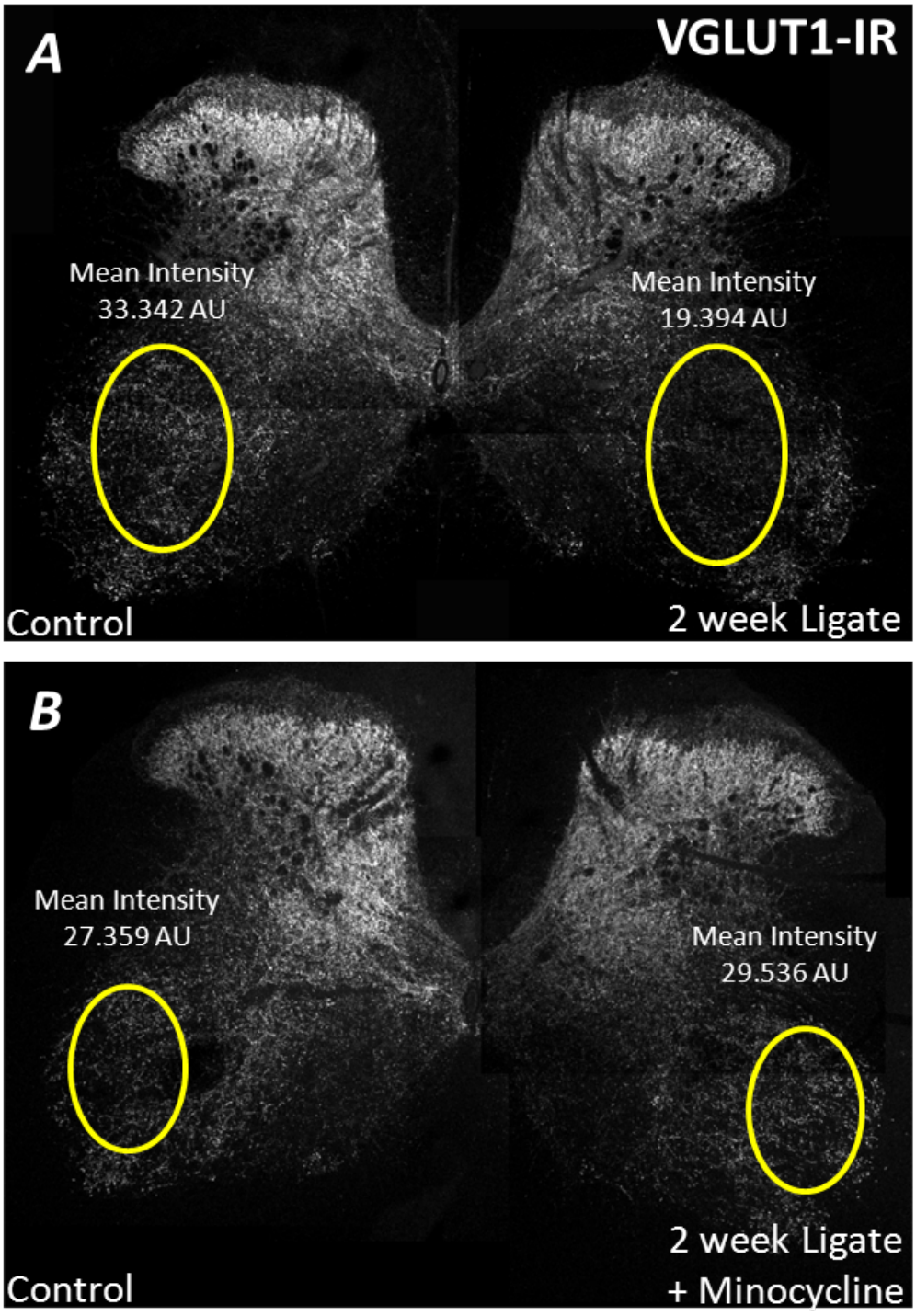
A
VGLUT1-IR
Mean Intensity
33.342 AU
Mean Intensity
19.394 AU
Control
2 week Ligate
B
Mean Intensity
27.359 AU
Mean Intensity
29.536 AU
Control
2 week Ligate
+ Minocycline

Figure 43: VGLUT1 synapses in L5 lumbar spinal cord *A)* 2 weeks following tibial nerve ligation and *B)* 2 weeks following tibial nerve ligation plus Minocycline treatments. VGLUT1 synapses in the ventral horn *A)* are lost after tibial nerve ligation but *B)* are not lost following Minocycline treatments, as compared to the contralateral control side. The mean intensity values of the outlined areas, on the injured *(right)* and control *(left)* sides of the ventral horn, are indicated. Image taken at 10X magnification (10 optical sections, at 2 μm z-steps) and montaged in CorelDRAW 12.

VI. Discussion

Peripheral nerve injury affects millions of people around the world, and can result in dysfunction or death of a neuron or neuronal circuit. One of the mechanisms that lead to dysfunction is the loss of synapses (Sumner and Sutherland, 1973; Sumner, 1975, 1976, 1979; Brannstrom and Kellerth, 1998, 1999; Alvarez et al, 2011; Bullinger et al, 2011). Microglia activation is part of the inflammatory response that occurs in the spinal cord following peripheral nerve injury, and is thought to be the major contributors to synaptic stripping. This study focuses on the stripping of the large synapse, the C-bouton and the role that glia activation may have in the loss of this synapse. **I hypothesize that glia activation following peripheral nerve injury correlates to the degree of depletion of the synaptic coverage of C-boutons.** Here, I present results that suggest that in injuries that produce lower amounts of glia activation and proliferation, there is less synaptic stripping than those injury types that produce more glia activation and proliferation (Figure 44). These data support the hypothesis and suggest that there is a correlation between glia activation and synaptic coverage of C-boutons.

A

Correlation Between C-Bouton Depletion and Neuroglia Proliferations

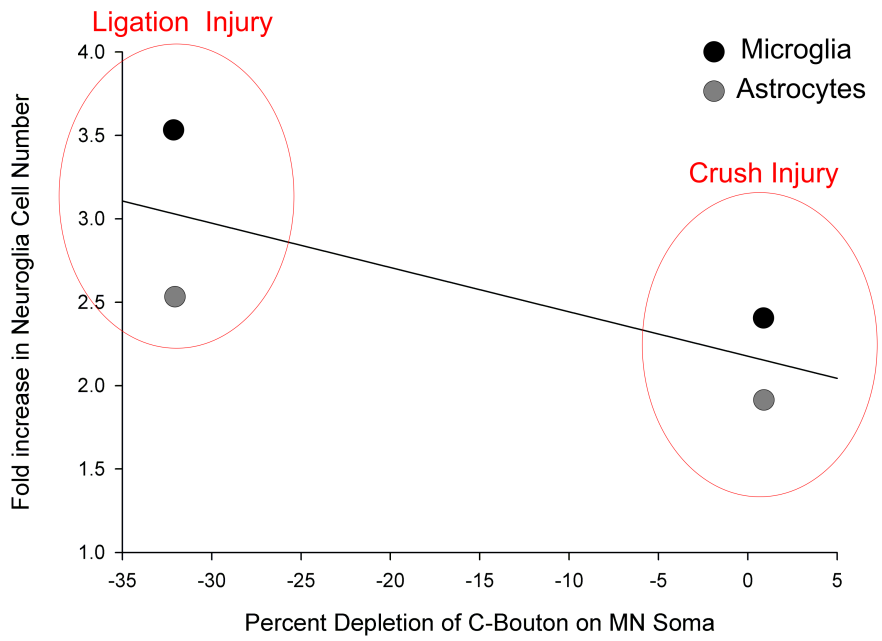

B

Correlation Between C-Bouton Depletion and Neuroglia Activation

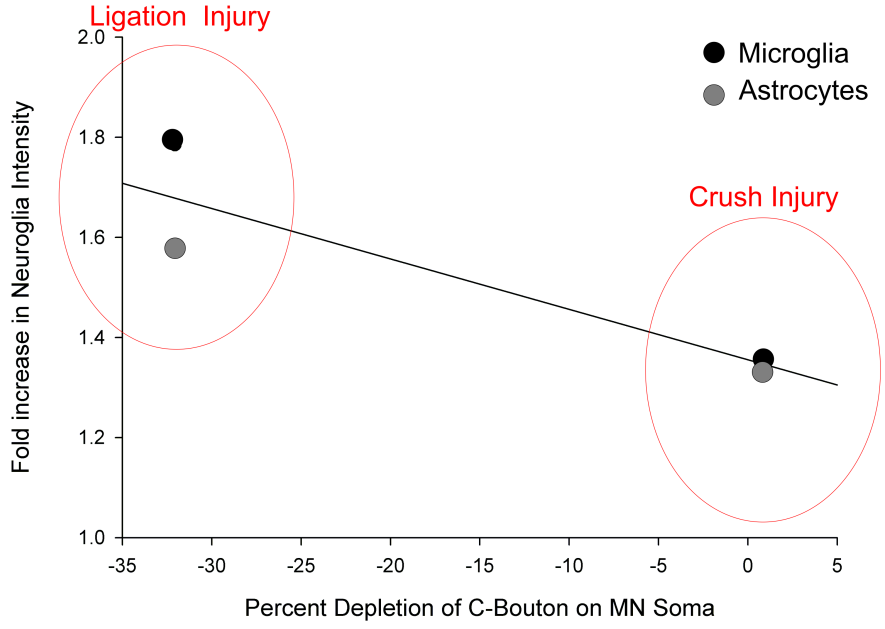

Figure 44: Correlation between C-bouton depletion and neuroglia *A)* proliferation and *B)* activation. The x-axis in *A* and *B* represents the percent depletion of C-boutons on the soma, as compared to sham surgery controls. The y-axis represents the fold change (experimental/control) in *A)* neuroglia proliferation and *B)* neuroglia activation. Microglia (black circle) and astrocytes (grey circle) were the two neuroglial cell types studied in this project. *A)* The percent depletion of C-boutons and the fold change of microglial (black circle) and astrocytic (grey circle) proliferation occur to a lesser degree 2 weeks following tibial nerve crush than ligation. *B)* The percent depletion of C-boutons and the fold change of microglial (black circle) and astrocytic (grey circle) activation occur to a lesser degree 2 weeks following tibial nerve crush than ligation.

A. Injury-Specific Differences

This project focused on two types of injury: tibial nerve crush, in which reinnervation is permitted, and tibial nerve ligation, in which reinnervation is inhibited. It is commonly thought that effects of a nerve crush resemble the effects of nerve ligation, with differences only arising after reinnervation or lack of reinnervation. Our data, however, show that differences beyond this exist. We see significant changes in the two types of injury before reinnervation occurs at approximately 4 weeks. There was not significant C-bouton stripping in the crush injury animals 2 weeks after injury, but there was significant stripping in the ligation injury. Preliminary data from our lab suggests at longer time periods after crush injury, C-bouton stripping is also trending to a decrease in percent somatic coverage, however, these data are not as significantly reduced following injury as that which is occurring following ligation injury (*Shannon Romer Pers. Comm)*. Furthermore, there was a general increase in glia activation in the ventral horn of the spinal cord following tibial nerve ligation than crush injury. Since glia are thought to underlie synaptic stripping, the difference in synaptic stripping between the two injury types is consistent with the difference in glia activation. Although these data support the hypothesis that glia activation correlates to the degree of C-bouton stripping, these data also disprove the common belief that similar responses exist in the two injury types.

B. Glial Response

Dorsal Horn

Inflammation is a common pathology associated with peripheral nerve injury. Inflammation is caused by the release of substances from the damaged nerve and from other molecules in the body. It is generally described as the activation of microglia and

other inflammatory cell types. In the CNS, inflammation is characterized by the activation of glia. This activation is often harmful, resulting in long-term detrimental effects. Glia activation can lead to the loss of synapses, the development of neurodegenerative diseases and neuropathic pain following injury, as well as other negative effects. The response of glia in the dorsal horn of the spinal cord has already been well characterized; therefore, I used this region to validate the response observed in the ventral horn.

In the dorsal horn, activated microglia are believed to act as the first line of defense following injury. As such, their response has been reported to begin within hours of the injury. Activated microglia upregulate immune receptors, including CD11b, Toll-like receptor 4 and the chemokine receptor CCR2 (Svensson et al., 1993; Suter et al., 2007; Wen et al., 2007; Ji et al., 2008), making these receptors effective markers for studying microglia activation. Peak activation of microglia has been reported to occur 3 days to 2 weeks following injury, depending on the marker used, time course of the study and the injury type. A decline in activation typically occurs by 1 or 2 weeks following injury and basal levels of activation have been reported after 1-2 months following injury (Svensson et al., 1993; Tanga et al., 2004; Echeverry et al., 2007). Our data in the dorsal horn has been very consistent with these published data (Figures 9-16).

Moreover, in the dorsal horn, astrocytes play a large role with the changes accompanying peripheral nerve injury, and are believed to be activated by microglia (Svensoon et al., 1993; Ji et al., 2008). Glial fibrillary acidic protein (GFAP) is the primary identifying marker of reactive astrocytes. It is the major protein component of the glial intermediate filaments making up astrocytes (Eng et al., 1971; Bignami et al.,

1972; Graeber and Kreutzberg 1986). The most common observation reported after injury is an up regulation of GFAP in the ipsilateral side of the injury during the first phase of the astrocytic reaction, which lasts up to 3 weeks. Although microglial proliferation is initially much greater in the dorsal horn, an increase in GFAP expression in the dorsal horn has been reported by day 1 post-axotomy in several experiments (Graeber and Kreutzberg, 1988; Eriksson et al., 1993; Eriksson et al., 1997; Hajos et al., 1997) and by 2-4 days in other studies (Gilmore et al., 1990). Peaks in GFAP levels have been reported to occur between 1 and 3 weeks post-injury (Graeber and Kreutzberg, 1988; Tsuda et al., 2011).

In my study, the greatest increases in astrocyte cell number were observed at the same time points in which astrocyte activation was observed in each of the injury animals. The most significant proliferation of astrocytes was observed at 2 weeks post-crush, and at 1 week post-ligation. The increase in cell number at 1 week post-ligation was much greater than at any of the other time points, with more than a 2-fold increase over sham. Much debate surrounds the proliferation of astrocytes. Some studies have reported a proliferation only after ligation (reviewed in Eddleston and Mucke, 1993; Svensson et al., 2008; Tsuda et al., 2011), while others have observed an astrocytic proliferation following ligation and crush injuries (Wohl et al., 2009). Our data supports the proliferation of astrocytes following crush and ligation. Our data in the dorsal horn have been very consistent with these published data (Figures 9-16).

In conclusion, our data regarding the response of microglia and astrocytes in the dorsal horn are consistent with published literature. Although the exact role of these cells following peripheral nerve injury is unknown, the early and robust response of microglia

and astrocytes following nerve injury indicates that they play an important role following nerve injury.

Ventral Horn

The presence of microglia and astrocytes has been observed surrounding motoneurons in the ventral horn; however, the response of glia in the ventral horn has not been well characterized. Microglia are believed to migrate down from the dorsal horn into the ventral horn, and make transient contact with motoneurons, before being replaced by astrocytes (Graeber and Kreutzberg, 1988; Svensson et al., 1993). Microglia were once believed to play a role in removing synaptic terminals from motoneurons. Later studies, however, have shown that, except for a possible transient association, microglia never actually make contact with the motoneuron. Instead, lamellar processes of astrocytes intervene between the synapse and the motoneuron, and ensheathe the motoneuron soma (Sumner and Sutherland, 1973; Graeber and Kreutzberg, 1988; Svensson et al., 1993; Ji et al., 2007; Aldskogius et al., 1999).

In general, our data is consistent with the literature discussing the possible roles of microglia and astrocytes in the ventral horn, following a peripheral injury. In our data, the peak response of microglia was observed at 1 or 2 weeks following injury, while the peak response of astrocytes occurred at 2 weeks in nearly all observations. The activation of astrocytes was observed at 1 week following nerve crush (Figure 21), however, the peak at 1 week post-crush was only slightly greater than that at 2 weeks. Furthermore, our data also confirmed the return to sham levels by 3 months post-axotomy. This data strongly supports the belief that the microglia move into the ventral horn and surround

motoneurons, first, and astrocytes move in later to replace them, as indicated in the literature.

C. Minocycline Effects on Glia Activation

Minocycline has been used to block microglia in many studies focusing on neuropathic pain. Following tibial nerve ligation and a 2-week treatment of Minocycline, significant activation and proliferation of microglia and astrocytes, as compared to sham controls, were clearly observed in the dorsal and ventral horns. Although we were unable to fully block glia activation with Minocycline treatment, the extent of activation and proliferation after the Minocycline treatment was reduced when compared to ligation studies in the absence of Minocycline treatment.

D. Different Mechanisms of Synaptic Stripping

Inhibitory synapses are more resistant to synaptic stripping than excitatory synapses. Differences in the loss and recovery of excitatory synapses, however, have also been reported (Linda et al., 2000; Novikov et al., 2000). VGlut1 synapses are removed and retracted from the motoneuron membrane following peripheral nerve injury, while work in this thesis suggests that C-boutons appear to not be removed from the membrane, just smaller in size. The two types of synapses appear to strip in different manners. Whether or not the C-bouton is functional following injury is unknown. Electron microscopy data suggests that astrocytes stick a process into the synaptic cleft between C-boutons and the motoneuron, rendering the synapse silent (Sumner, 1975). Further support that these synapses may strip with different mechanisms is evident in our Minocycline experiments in this study. Minocycline alone had a profound effect on C-boutons that prevented me from testing my hypothesis about the role of glia activation in

C-Bouton stripping. However, Minocycline appeared to inhibit the stripping of VGluT1-IR+ synapses, a synapse that is permanently loss following injury leading to permanent loss of the 1A stretch reflex (Bullinger et al., 2011). These data suggest that the mechanisms blocked by Minocycline may have a role in VGlut1 stripping, but does not have a role in C-bouton stripping. The effect of Minocycline on the C-bouton was not expected. Perhaps the effect is a compensatory reaction to modulate motoneuron output, since clinically motor deficits are not associated with Minocycline treatments. If the effect of Minocycline on the C-bouton is reversible once the drug is removed, Minocycline could be therapeutically used following peripheral nerve injury to prevent the permanent loss of 1A afferent reflexes following peripheral nerve injury.

E. Conclusion

In conclusion, C-bouton stripping following peripheral nerve injury appears to be caused by a decrease in the size of the C-bouton contacts, and not by a decrease in the number of C-boutons synapsing onto the soma. The activation and proliferation of microglia and astrocytes in the ventral horn following peripheral injury correlate with the degree of synaptic loss onto motoneurons following injury. By partially blocking glia activation with the FDA approved antibiotic Minocycline, our data suggests that different stripping mechanisms may underlie C-bouton stripping from other VGLUT1-IR+ excitatory synapses. Preventing the stripping of VGLUT1 synapses following peripheral nerve injury, a synapse that is permanently lost, using Minocycline would be a major advancement in the clinical world and has the potential to improve the lives of millions of people.

References

Aldskogius H (2001). Microglia in Neuroregeneration. *Microsc Res Tech* **54**, 40-46.

Aldskogius H, Liu L, and Svensson M (1999). Glial responses to synaptic damage and plasticity. *J Neurosci Res* **58**, 33-31.

Allen NJ and Barres AB (2009). Glia—more than just brain glue. *Nature* **457,** 65-677.

Alvarez FJ, Titus-Mitchell HE, Bullinger KL, Kraspulski M, Nardelli P, and Cope TC (2011). Permanent central synaptic disconnection of proprioceptors after nerve injury and regeneration. I. Loss of VGLUT1/IA synapses on motoneurons. *J Neurophysiol* **106**, 2450-2470.

Amor S, Puentes F, Baker D and van der Valk P (2010). Inflammation in neurodegenerative diseases. *Immunology* **129**, 154-169.

Barres B (1991). New roles for glia. *J Neurosci* **11**, 3685-3694.

Bichler EK, Carrasco DI, Rich MM, Cope TC, and Pinter MJ (2007). Rat motoneuron properties recover following reinnervation in the absence of muscle activity and evoked acetylcholine release. J Physiol, **585.1**, 47-56.

Blinzinger K and Kreutzberg G (1968). Displacement of synaptic terminals from regenerating motoneurons by microglial cells. *Zeitschrift fur Zellforschung* **85**, 145-157.

Brannstrom T and Kellerth (1998). Changes in synaptology of adult cat spinal α-motoneurons after axotomy. *Exp Brain Res* **118**, 1-13.

Brannstrom T and Kellerth (1999). Recovery of synapses in axotomized adult cat spinal motoneurons after reinnervation into muscle. *Exp Brain Res* **125**, 19-27.

Brannstrom T (1993). Quantitative synaptology of functionally different types of cat medial gastrocnemius alpha-motoneurons. *J Comp Neurol* **330,** 439-454.

Bomze HM et al. (2001). Spinal axon regeneration evoked by replacing two growth cone proteins in adult neurons. *Nat Neurosci* **4**, 38-43.

Boyd JG and Gordon T (2003). Neurotrophic factors and their receptors in axonal regeneration and functional recovery after peripheral nerve injury. *Mol Neurobiol* **27,** 277-324.

Bunge MB (2001). Bridging areas of injury in the spinal cord. *Neuroscientist* **7**, 325-339.

Bullinger KL, Nardelli P, Pinter MJ, Alvarez FJ, and Cope TC (2011). Permanent central synaptic disconnection of proprioceptors after nerve injury and regeneration. II. Loss of functional connectivity with motoneurons. *J Neurophysiol* **106**, 2471-2485.

Burnett MG and Zager EL (2004). Pathophysiology of Peripheral Nerve Injury: A Brief Review. *Neurological FOCUS*, 16 (5), E1-E11.

Calvo M, Zhu N, Tsantoulas C, Zhenzhong Ma, Grist J, Loeb J, and Bennett DLH (2010). Neuregulin-ErbB Signaling Promotes Microglial Proliferation and Chemotaxis Contributing to Microgliosis and Pain after Peripheral Nerve Injury. *J Neurosci* **30**, 5437-5450.

Conradi S (1969). Ultrastructure and distribution of neuronal and glial elements on the surface of the proximal part of a motoneuron dendrite, as analyzed by serial sections. *Acta physiologica Scandinavica Supplementum* **332,** 49-64.

Conradi S, Kellerth JO and Berthold CH (1979). Electron microscopic studies of serially sectioned cat spinal alpha-motoneurons. II. A method for the description of

architecture and synaptology of the cell body and proximal dendritic segments. *J Comp Neurol* **184,** 741-754.

Conradi S and Skoglund S (1969). Observations on the ultrastruture and distribution of neuronal and glial elements on the motoneuron surface in the lumbosacral spinal cord of the cat during postnatal development. *Acta physiologica Scandinavica Supplementum* **333,** 5-52.

Corbett A, McGowin A, Sieber S, Tiffany F, and Sibbit B (2012). A method for reliable voluntary oral administration of a fixed dosage (mg/kg) of chronic daily medication to rats. *Lab Animals* **46**, 1-7.

Dai C, Kanoh N, Li K, and Wang, Z (2000). Study on Facial Motoneuronal Death After Proximal or Distal Facial Nerve Transection. *Am Journal Otol* **21**, 115-118.

Destombes J, Horcholle-Bossavit G, Thiesson D & Jami L (1992). Alpha and gamma motoneurons in the peroneal nuclei of the cat spinal cord: an ultrastructural study. *J Comp Neurol* **317,** 79-90.

Deardorff AS, Romer SH, Deng Z, Bullinger KL, Nardelli P, Cope TC, and Fyffe REW

Eddleston M and Mucke L (1993). Molecular profile of reactive astrocytes - Implications in their role in neurologic disease. *Neurosci* **54**, 15-36.

Engstrom H, Wersall J (1958). The ultrastructural organization of the organ of Corti and of the vestibular sensory epithelia. *Exp Cell Res* **14** (5), 460-492.

Eriksson PS, Nilsson M, Wågberg M, Hansson E, Rönnbäck L (1993). Kappa-opioid receptors on astrocytes stimulate L-type Ca^{2+} channels. *Neurosci* **54**, 401-407.

Eriksson NP, Persson JK, Aldskogius H, Svensson M (1997). A quantitative analysis of the glial cell reaction in primary sensory termination areas following sciatic nerve

injury and treatment with nerve growth factor in the adult rat. *Exp Brain Res* **114**, 393-404.

Evans, RD (2001). Peripheral Nerve Injury: A Review and Approach to Tissue Engineered Constructs. *The Anatomical Record* **263**, 396-404.

Filbin MT (1996). The Muddle with MAG. *Mol Cell Neurosci* **8**, 84-92.

Filbin MT (1995). Myelin-associated glycoprotein: a role in myelination and in the inhibition of axonal regeneration? *Curr Opin Neurobiol*, **5** 588-595.

Fisher SK and Goldman K (1975). Subsurface cisterns in the vertebrate retina. *Cell Tissue Res*. **164**, 473-480.

Fouad K, Dietz V and Schwab ME. (2001). Improving axonal growth and functional recovery after experimental spinal cord injury by neutralizing myelin associated inhibitons. *Brain Res Brain Res Rev* **36**, 204-212.

Foehring RC, Sypert GW, and Munson JB (1986). Properties of self-reinnervated motor units of medial gastrocnemius of cat. I. Long-term reinnervation. *J Neurophysiol* **55**, 931-946.

Foehring RC, Sypert GW, and Munson JB (1986). Properties of self-reinnervated motor units of medial gastrocnemius of cat. II. Axotomized motoneurons and time course of recovery. *J Neurophysiol* **55**, 947-965.

Fugleholm K, Schmalbruch H, and Krarup C (1994). Early Peripheral Nerve Regeneration after Crushing, Sectioning, and Freeze Studied by Implanted Electrodes in the Cat. *J Neurosci* **14**, 2659-2673.

George R and Griffin JW (1994). Delayed macrophage responses and myelin clearance during Wallerian degeneration in the central nervous system: the dorsal radiculotomy model. *Exp Neurol* **129**, 225-236.

George EB, Glass JD and Griffin JW (1995). Axotomy-induced axonal degeneration is mediated by calcium influx through ion-specific channels. *J Neuroscience* **15**, 6445-6452.

Gilmore SA, Sims TJ and Leiting JE (1990). Astrocytic Reactions in Spinal Gray Matter Following Sciatic Axotomy. *GLIA* **3**, 342-349.

Graeber MB and Kreutzberg GW (1988). Delayed astrocyte reaction following facial nerve axotomy. *J Neurocytol* **17**, 209-220.

Graeber MB and Kretuzberg GW (1986). Astrocytes increase in glial fibrillary acidic protein during retrograde changes of facial motor neurons. J Neurocytol 15, 363-373.

Gustafsson B and Pinter MJ (1984). Relations among passive electrical properties of lumbar α-motoneurones of the cat. *J Physiol* **356**, 401-431.

Gustafsson B and Pinter MJ. (1984). Effects of axotomy on the distribution of passive electrical properties of cat otoneurones. *J Physiol* **356**, 433-442.

Hajós F, Jancsik V, Sótonyi P (1996). Remote astroglial response associated with synaptic degeneration results in a net increase of perisynaptic glial fibrillary acidic protein. *Acta Biol Hung* **47**, 173-179

Hellstrom J, Oliveira AL, Meister B & Cullheim S (2003). Large cholinergic nerve terminals on subsets of motoneurons and their relation to muscarinic receptor type 2. *J Comp Neurol* **460,** 476-486.

Horner PJ, Gage FH (2000). Regenerating the damaged central nervous system. *Nature* **407**, 963-970.

Igarashi M, Li WW, Sudo Y, Fishman MC (1995). Ligand-induced growth cone collapse: amplification and blockade by variant GAP 43 peptides. *J Neurosci* **15**, 5660-5667.

Ikeda H, Kiritoshi T and Murase Kazuyuki (2011). Contribution of microglia and astrocytes to the central sensitization, inflammatory and neuropathic pain in the juvenile rat. *Molec Pain* **8**:43.

Johnson IP (1986). A quantitative ultrastructural comparison of alpha and gamma motoneurons in the thoracic region of the spinal cord of the adult cat. *J of Anatomy* **147,** 55-72.

Ji and Suter (2007). p38 MAPK, microglial signaling, and neuropathic pain. *Molec Pain* 3:33.

Ji R, Kawasaki Y, Zhuang Z, Wen Y, and Decosterd I (2006). Possible role of spinal astrocytes in maintaining chronic pain sensitization: review of current evidence with focus on bFGF/JNK pathway. *Neuron Glia Biol* **2**, 259-269.

Jinno S and Yamada J (2011). Using comparative anatomy in the axotomy model to identify distinct roles for microglia and astrocytes in synaptic stripping. *Neuron Glia Biol* 1-12.

Klusman I, Schwab ME (2003). Axonal regeneration in the central nervous system of mammals. *Neuroglia.*

Kuno M, Miyata Y and Munoz-Martinez, EJ (1974). Properties of fast and slow alpha motoneurones following motor reinnervation. *J Physiol* **242**, 273-288.

Lagerback PA (1983). An ultrastructural study of serially sectioned Renshaw cells. III. Quantitative distribution of synaptic boutons. *Brain Res* **264,** 215-223.

Lagerback PA, Cullheim S & Ulfhake B (1986). Electron microscopic observations on the synaptology of cat sciatic gamma-motoneurons after intracellular staining with horseradish peroxidase. *Neurosci Lett* **70,** 23-27.

Li W, Ochalski PA, Brimijoin S, Jordan LM & Nagy JI (1995). C-terminals on motoneurons: electron microscope localization of cholinergic markers in adult rats and antibody-induced depletion in neonates. *Neurosci* **65,** 879-891.

Lui W, Lin C, Hsiao M, and Gean P (2011). Minocycline inhibits the growth of glioma by inducing autophagy. *Autophagy* **7**, 166-175.

Madison RD, Archibald SJ and Brushart TM (1996). Reinnervation Accuracy of the Rat Femoral Nerve by Motor and Sensory Neurons. *J Physiol* **16**, 5698-5703.

Miles GB, Hartley R, Todd AJ & Brownstone RM (2007). Spinal cholinergic interneurons regulate the excitability of motoneurons during locomotion. *Pro Natl Acad Sci U S A* **104,** 2448-2453.

Muennich EA & Fyffe RE (2004). Focal aggregation of voltage-gated, Kv2.1 subunit-containing, potassium channels at synaptic sites in rat spinal motoneurones. *J Physiol* **554**, 673-685.

Nagy JI, Yamamoto T & Jordan LM (1993). Evidence for the cholinergic nature of C-terminals associated with subsurface cisterns in alpha-motoneurons of rat. *Synapse* **15,** 17-32.

Ornung G, Ottersen OP, Cullheim S & Ulfhake B (1998). Distribution of glutamate-, glycine- and GABA-immunoreactive nerve terminals on dendrites in the cat

spinal motor nucleus. *Experimental Brain Research Experimentelle Hirnforschung Experimentation Cerebrale* **118,** 517-532.

Ornung G, Shupliakov O, Linda H, Ottersen OP, Storm-Mathisen J, Ulfhake B & Cullheim S (1996). Qualitative and quantitative analysis of glycine- and GABA-immunoreactive nerve terminals on motoneuron cell bodies in the cat spinal cord: a postembedding electron microscopic study. J Comp Neurol **365,** 413-426.

Paino, CL, Fernandez-Valle C, Bates ML, Bunge MB (1994). Regrowth of axons in lesioned adult rat spinal cord: promotion by implants of cultured Schwann cells. *J Neurocytol* **23**, 433-452.

Perry VH and O'Connor V (2010). The role of microglia in synaptic stripping and synaptic degeneration: a revised perspective. *ASN Neuro* **5**, 281-291.

Raghavendra V, Flobert T and Deleo JA (2003). Inhibition of Microglial Activation Attenuates the Development but Not Existing Hypersensitvity in a Rat Model of Neuropathy. *J Pharmacology and Experimental Therapeutics* **306**, 624-630.

Reisert I, Wildemann G, Grab D, Pilgrim C (1984). The glial reaction in the course of axon regeneration: a stereological study in the rat hypoglossal nucleus. *J Comp Neurol* **229**, 121-128.

Rose PK & Neuber-Hess M (1991). Morphology and frequency of axon terminals on the somata, proximal dendrites, and distal dendrites of dorsal neck motoneurons in the cat. *J Comp Neurol* **307,** 259-280.

Rosenbluth J (1962). Subsurface cisterns and their relationship to the neuronal plasma membrane. J Cell Biol 13, 405-420.

Schlaepfer WW and Bunge RP (1973). Effects of calcium ion concentration on the degeneration of amputated axons in tissue culture. *J Cell Biol* **59**, 456-470.

Strittmatter SM, Igrashi M, Fishman MC (1994). GAP-43 amino terminal peptides modulate growth cone morphology and neurite outgrowth. *J Neuroscience* **15**, 5503-5513.

Stoll G and Muller HW (1999). Nerve Injury, Axonal Degeneration and Neural Regeneration: Basic Insights. *Brain Pathology* **9**, 313-325.

Sumner BEH (1975). A Quantitative Analysis of the Response of Presynaptic Boutons to Postsynaptic Motor Neuron Axotomy. *Experimental Neurology* 46, 605-615.

Sumner BEH (1975). A Quantitative Study of Subsurface Cisterns and their Relationships in Normal and Axotomized Hypoglossal Neurones. *Exp Brain Res* **22**, 175-183.

Sumner BEH (1976). Quantitative Ultrastructural Observations on the Inhibited Recovery of the Hypoglossal Nucleus from the Axotomy Response when Regeneration of the Hypoglossal Nerve is Prevented. Exp Brain Res **26**, 141-150.

Sumner BEH (1977). Responses in the Hypoglossal Nucleus to Delayed Regeneration of the Transected Hypoglossal Nerve, a Quantitative Ultrastructural Study. *Exp Brain Res* **29**, 219-231.

Sumner BEH (1979). Ultrastructural Data, with Special Reference to Bouton/Glia Relationships, from the Hypoglossal Nucleus after a Second Axotomy of the Hypoglossal Nerve. *Exp Brain Res* **36**, 107-118.

Sumner BEH and Sutherland FI (1973). Quantitative electron microscopy on the injured hypoglossal nucleus in the rat. *J Neurocytology* **2**, 315-328.

Sun D, Lye-Barthel M, Masland RH, Jakobs TC. (2010). Structural remodeling of fibrous astrocytes after axonal injury.

Suter MR, Wen Y, Decosterd I, and Ji R (2007). Do glial cells control pain? *Neuron Glia Biol* **3**, 255-268.

Svensson M et al. (1993). The response of central glia to peripheral nerve injury. *Brain Research Bulletin* **30**, 499-506.

Tang S et al. (1997). Soluble myelin-associated glycoprotein (MAG) found in vivo inhibits axonal regeneration. *Mol Cell Neurosci* **9**, 333-346.

Tanga FY, Raghavendra V, DeLeo, JA (2004). Quantitative real-time PCR assessment of spinal microglial and astrocytic activation markers in a rat model of neuropathic pain. *Neurochemistry International* **45**, 397-407.

Tikka T, Fiebich BL, Goldsteins G, Keinanen R, and Koistinkaho J (2001). Minocycline, a tetracycline derivative, is neuroprotective against excitotoxicity by inhibiting activation and proliferation of microglia. *J Neurosci* **21**, 2580-2588.

Tsuda M et. al. (2011). JAK-STAT3 pathway regulates spinal astrocyte proliferation and neuropathic pain maintenance in rats. *Brain* **134**, 1127-1139.

Waller A (1850). Experiments on the section of the glossopharyngeal and hypoglossal nerves of the frog, and observations of the alterations produced thereby in the structure of their primitive fibers . *Phil Transact Royal Soc London*, **140**, 423-429.

Wen Y, Suter MR, Kawaski Y, Huang J, Pertin M, Kohono Tatsuro, Berde CB, Decosterd Isabelle, and Ji R. Nerve conduction blockade in the sciatic nerve prevents but does not reverse the activation of p38 Mitogen-activated protein

kinase in spinal microglia in the rat spared nerve injury model (2007). *Anesthesiology* **107**, 312-321.

Wilson JM, Rempel J & Brownstone RM (2004). Postnatal development of cholinergic synapses on mouse spinal motoneurons. *J Comp Neurol* **474**, 13-23.

Wohl SG, Schmeer CW, Kretz A, Witte OW, and Isenmann S (2009). Optic nerve lesion increases cell proliferation and nestin expression in the adult mouse eye in vivo. *Experimental Neurology* **219,** 175-186.

Xie W, Strong JA and Zhang JM.(2009). Early blockade of injured primary sensory afferents reduces glial cell activation in two rat neuropathic pain models. *Neuroscience* **160**, 847-857.

Zagoraiou L, Akay T, Martin JF, Brownstone RM, Jessell TM & Miles GB (2009). A cluster of cholinergic premotor interneurons modulates mouse locomotor activity. *Neuron* **64,** 645-662.